POLITECNICO DI MILANO

Scuola di Ingegneria Civile, Ambientale e Territoriale
Corso di Laurea Magistrale in Ingegneria Civile

EXPERIMENTAL INVESTIGATION OF THE BEHAVIOUR OF BEAM AND BLOCK SLABS RETROFITTED WITH LIGHTWEIGHT CONCRETE TOPPING

Supervisor: Prof. Ing. LIBERATO FERRARA (Politecnico di Milano)

M.Sc. Thesis in Civil
Engineering major Structures

By: VICENTE SANCHIS GARCÍA
Matr. n. 836607

Academic Year 2015/2016

ACKNOWLEDGEMENTS

I would like to thank Professor Ferrara, supervisor of this thesis, for his availability, dedication and kindness shown and for all the help provided during the realization of this document.

I would also acknowledge the laboratory technicians Andrea De Steffani and Marco Antico for their assistance during all laboratory tests.

And finally, also, acknowledge Laterlite Leca S.P.A. for the supplied material, essential to the fulfilment of this thesis.

VICENTE SANCHIS GARCÍA: I will always be grateful to my parents and friends for their support and encouragement through all this years. All these things will help me and make me more confident in the future.

ABSTRACT

One of the main issues found in the current Italian construction activities is the recovery of existing buildings, which nowadays is still extremely delicate and complex. The current trend in the construction market shows how the attention is geared towards the interventions of consolidation, both for economic reasons and for the necessity of a more efficient use of the resources.

The interventions of consolidation should have, as a primary issue, to efficiently increase the performance of the buildings from a structural safety point of view, for example with reference to seismic actions. This can be accomplished by means of a careful analysis of the needs and performance and a complete diagnosis of the existing constraints and state of work, to ensure the requirements, priorities and objectives of the project.

Different approaches may be adopted with different technical solutions and with the use of reliable and durable materials as well as compatible with the existing building object of the interventions of restructuration.

In this experimental work an investigation will be carried out about the efficiency of a “cooperating topping slab”, consolidation technique for floor slabs. It consists of the realization of a new cooperating slab, herein made of lightweight concrete, connected with the existing slab by the use of a two-component epoxy adhesive (connector "Centro Storico Chimico" by Leca system).

The purpose of this investigation is to verify the improvement of the mechanical performance of floor slabs, through loading tests on consolidated and non – consolidated mock-ups.

The most significant aspects of the experimentally investigated structure will also be analysed in a design – oriented perspective.

KEYWORDS: consolidation of floor slabs; the composite cooperating topping slab technique; beam and block floor slab “SAP”; full scale load tests.

INDEX

1

INTRODUCTION

In building renewal activity the need to retrofit floor slabs frequently occurs, which can be of several different types; the retrofitting can be performed using different techniques in relation to the type of floor slab, to its constraints and to its geometric characteristics.

The consolidation of existing floor slabs can be included, depending on the case, in adjustment operations, improvement or "local" repairs, suitable to increase the technical characteristics of the elements, as well as to yield an effective performance increase of the entire building in terms of safety, structural stability and seismic behaviour increase.

The Italian existing building stock, including heritage buildings, consists of a countless number of floors slabs, different from each other because of building technologies and construction periods. These important structural elements can be grouped into six different categories:

1. Wooden floor slabs
2. Steel floor slabs
3. Beam and block floor slabs (such as e.g. "SAP" slabs)
4. Prefabricated floor slabs
5. Cast in place reinforced concrete floor slabs
6. Arched and vaulted floor slabs

Regardless of the type of floor slab, any work on such structures implies the complete and detailed knowledge of their current state; as a matter of fact, this affects the reliability and the probability of success of the retrofitting design and subsequent execution of the consolidation and reinforcement.
On each structural element it is therefore necessary to perform an assessment, which essentially consist of three phases:

1. Visual inspection to detect defects, anomalies or alterations made over time.
2. Instrumental analysis, with particular reference to inaccessible parts of the structure, through non-destructive diagnostic techniques applied "in situ".
3. Analysis of the results in which is detailed the type of the floor slab, its constructive “stratigraphy” and an estimation of the mechanical performance.

The results of this survey will be essential to assess which operations of consolidation and reinforcing implementation should be used.

In this work the effectiveness will be investigated of a consolidation technique that involves the construction of a lightweight concrete topping 40 mm thick, cast after the application, on the floor slab substrate to be consolidated, of an epoxy resin.
In detail, beam and block reinforced concrete slabs have been investigated with an initial height equal to 120 mm or 160 mm. Both non – consolidated and consolidated slabs have been experimentally tested up to failure. The employed consolidation technique resulted quite efficient and easy to use.

The present study will illustrate, through the analysis of laboratory tests, not only the differences in behaviour between consolidated and non - consolidated floors slabs, but also the advantages and the structural benefits that such consolidation technique brings to the structural element.

2

THE ITALIAN EXISTING BUILDING STOCK

According to surveys carried out in the first months of 2012 by CRESME (Centro Ricerche Economiche Sociali di Mercato per l'Edilizia e il Territorio), the Italian existing building stock is the oldest in Europe: about 25% of the buildings have never been subjected to redevelopment, 5% require urgent action, while 40% require special maintenance measures. It is estimated that there are about 2.5 million buildings in a state of bad or mediocre conservation (Figure 1).

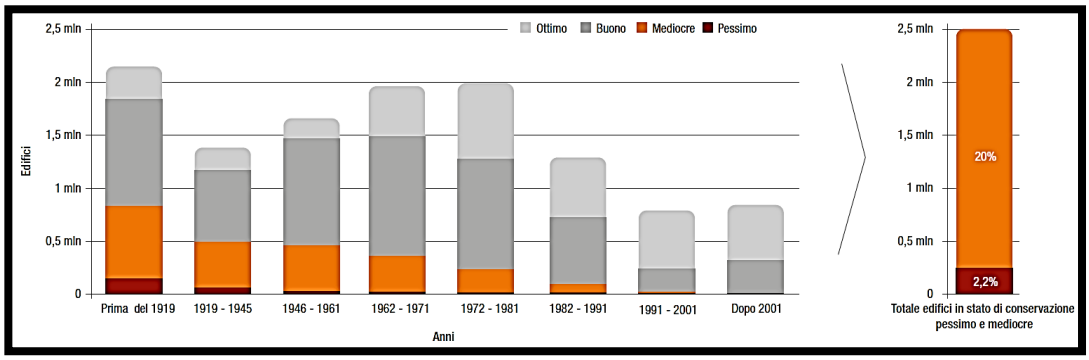

Figure 1. State of preservation of existing buildings at 31/12/12 (Source: CRESME)

These data remind us of the importance of developing actions aimed at the preservation of the value and efficiency of the buildings: the obsolescence of "in-structure" properties requires corrective maintenance, in order to restore an acceptable level of

performance or even bringing the structure to a performance level higher than what originally planned (valuing in this case the same property).
Currently the theme of building rehabilitation proposes different systems and constructive solutions, applying several different new technologies to existing systems, in order to bring them back to the required levels of technical and structural safety, with particular reference to the behaviour under seismic actions, also as enforced by current codes.

2.1 Engineering problem

Over the past century, since the 1908 earthquake of Messina and Reggio Calabria, the seismic classification of the Italian territory was continuously updated, making it mandatory, in the most vulnerable areas, the compliance with specific design and construction rules for buildings. In 2003, a year after the earthquake in Puglia and Molise, the Order of the President of the Ministers Council n.3274 was issued that reclassifies the whole country in four different hazard zones, removing the "unclassified" areas. The D.M. 14/01/2008 (Norme Tecniche per le Costruzioni), entered in force on July 1, 2009 as a result of the L'Aquila earthquake, has introduced a new, more comprehensive and detailed methodology to determine the seismic hazard of a site. Today, therefore, all the Italian regions, except for a few areas of Piemonte and Sardegna, are prone to earthquakes. The need to make existing buildings compliant with the new required safety levels, even partially, makes the retrofitting and upgrading interventions of paramount importance.

2.2 Consolidation of floor slabs

The analysis of the Italian heritage building stock clearly highlights, as a priority, the redevelopment of existing buildings, in order to enhance their performance. The design and implementation of a retrofitting / upgrading intervention requires much more effort and technical skills than designing and building a new structure, because of the existing constraints.
The subject investigated in the present work, that is the consolidation of floor slabs, relates to a widespread type of intervention, and of particular importance, that shows the structural recovery of existing floors with consolidation techniques in composite sections. This system is recognized by the standards as a suitable system for earthquake safety purposes.

2.3 Categories of floor slabs

The beam and block floor slabs category, which has been herein experimentally investigated, will be described in the forthcoming section.
A brief mention is given hereafter also of the different types of floor slabs which can be found in the existing Italian heritage building stock.

2.3.1 Wooden floor slabs

Always very popular and of great historical value, the wooden floors are the oldest existing models of floor slabs for buildings. They represent the first solution adopted for the floor slabs in multi-storey buildings. The supporting structure consists of wooden beams with circular section (used for poorer construction) or square (most valuable). The beams are covered on top, in correspondence of the extrados, by a plank (or planks) of brick tiles or by a screed for the enticement of the pavement. At the intrados of the floors, instead, countertops can be placed (made in some cases by real fabric) which hides the structure.
The wooden floors are often subjected to consolidation, as for example through the technique of “cooperating composite wood-concrete slab" and are generally grouped into two types:

1. One - way floor slabs: consist of a series of beams arranged to cover spans of 3 to 4 m. The upper "mould", used to cover the gap between the beams can be made with a wooden plank or bricks (Figure 2).
2. Two - way floor slabs: consist of series of main beams arranged at centre distances of 2 to 4 m, in accordance with the minor dimension of the space to be covered; on top of them, orthogonally to the main beams, a series of shorter secondary beams is arranged. The upper "mould" covering the gap between the beams can be made with a wooden or brick planks (Figure 3).

Figure 2. One – way floor slabs with one frame with wooden plank. (Source: Leca)

Figure 3. Two – way floor slabs with both wooden and brick plank. (Source: Leca)

2.3.2 Steel floor slabs

The steel floor slab structure is the same as of the wooden floor slabs. Instead of the wooden support beams, however, supporting steel beams (commonly called girders) are used. Depending on the element placed between the lower or upper wings of the metal elements, three types of steel floors can be distinguished:

1. Steel vaults floor slabs: still present in buildings, these floors are characterized by bricks placed between the wings of the steel beams. The vaults can be curved or flat. The arch effect is ensured by specially shaped blocks called "Volterrane" (Figure 4).
2. Steel-brick floor slabs: represent a more modern version of the steel vaults floor slabs and are often used for the retrofitting of masonry buildings. Brick planks are used to fill the spaces where the steel beams are used (Figure 5a).
3. Trapezoidal sheet floor slabs: consist of a principal steel frame (often accompanied by a secondary) topped with connectors that are banned to the ribbed sheets positioned on the extrados, guaranteeing the collaboration between the steel structure and the cast in place concrete slabs. These floors are mostly found in steel - frame buildings. Aside from other types of slabs, this kind of slabs is generally made of materials featuring good performance and therefore they are not generally subjected to retrofitting interventions (Figure 5b).

Figure 4. Steel vaults floor slabs (left) and curved vaults “Volterrane” (right). (Source: Leca)

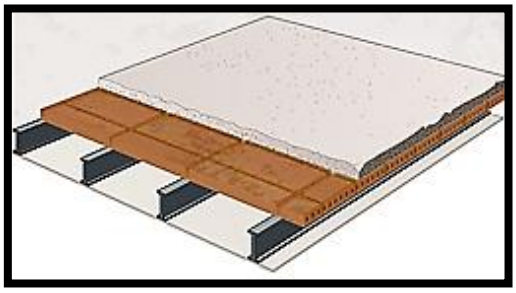

Figure 5a. Steel-brick slab with cast concrete floor slab. (Source: Leca)

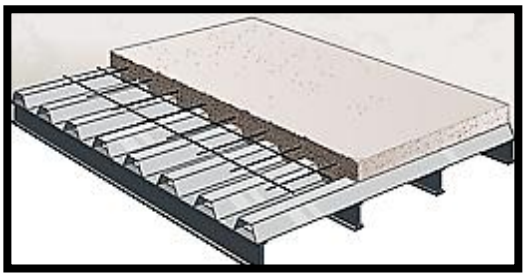

*Figure 5b. T*rapezoidal sheet floor slab. (Source: Leca)

2.3.3 Prefabricated floor slabs

The prefabricated floor slabs, made since the 70s of last century, are a fairly recent construction system and are characterized by good construction quality, reduced installation time and easy build up. They can be categorized into three different types:

1. Hollow core floor slabs: consist of prefabricated slabs made of pre-stressed concrete, used mainly in prefabricated buildings. The slabs feature hollows with tube form with the purpose of lighten the weight and save material. Generally they do not require interventions of consolidation and reinforcement (Figure 6).
2. Prefabricated panels floor slabs: are made by assembling bricks and reinforced concrete beams. They are characterized by a quick execution and require provisional support and reduced cast finishing. It is not frequent the use of consolidation or reinforcement (Figure 7).
3. Floor slabs consisting of precast R / C slab and "lightening" blocks: are characterized by prefabricated reinforced concrete slabs that are placed between supports of the bearing structure. On them "lightening" blocks are placed spaced each other to allow the casting of reinforced concrete slabs by means of the finishing casting. This kind of slabs features a fast execution and generally does not need consolidation (Figure 8).

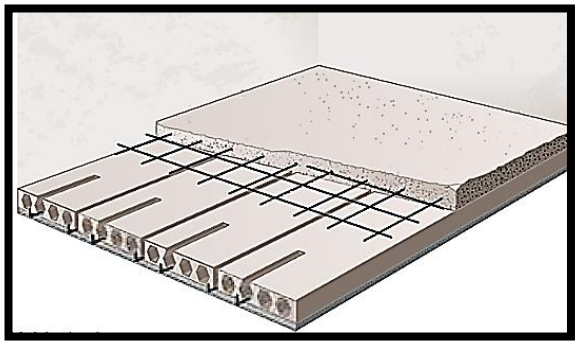

Figure 6. Hollow core floor slab. (Source: Leca)

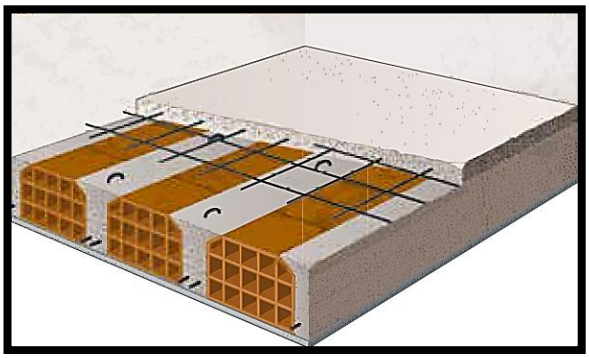

Figure 7. Prefabricated panels floor slabs. (Source: Leca)

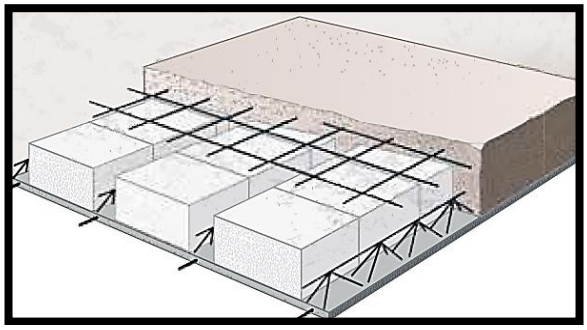

Figure 8. Floor slabs consisting of precast R/C slab and "lightening" blocks. (Source: Leca)

2.3.4 Reinforced floor slabs

The reinforced concrete floors slabs are a fairly recent construction system. They can be prestressed or not and flat or curved. Rarely do they require consolidation and reinforcement, as due to the intrinsic constructive nature and performance as well as to the use of materials with good mechanical characteristics (Figure 9).
Recently the use of fibre reinforced concrete for this type of slabs has also been proposed which would reduce the need for conventional steel reinforcement. (e.g. only to anti – progressive collapse one).

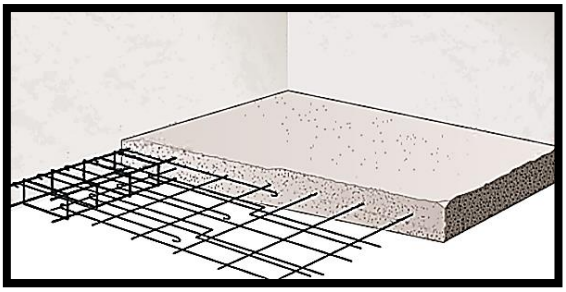

Figure 9. Reinforced floor slabs. (Source: Leca)

2.3.5 Arched and vaulted floor slabs

The arched and vaulted floor slabs represent, together with the wooden ones, the earliest solutions adopted for the realization of floors in multi-storey buildings. The arched structures support the loads by a combination of compression and bending. In order to keep a horizontal surface, debris fillers (called “abutments”) were made; the debris fillers, although constituting a "dead weight" added to the bearing structure, improved the stability of the vaults, limiting the stresses on them exclusively to compression stresses. The arched vaults may require consolidation and retrofitting, which generally employ tailored solutions (Figure 10).

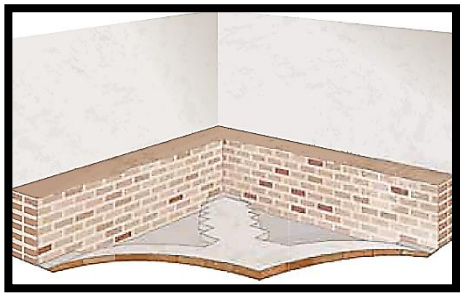

Figure 10. Arched vaulted floor slabs. (Source: Leca)

3

THE EXPERIMENTAL CAMPAIGN

In this section the type of floor slab which has been experimentally investigated will be described. The definition of the necessary measures to improve the performance will be presented together with the entailed benefits. Finally, the planning and execution of the laboratory tests will be described.

3.1 "Beam and block" floor slabs, "SAP"

The most common types of this category of slabs are listed hereafter:

1. Cast in place floor slabs: belongs to a quite old construction technique and are made by placing the bricks on a wooden plank at a distance such as to allow the realization of the beams by means of the arrangement of the reinforcing bars and the subsequent concrete casting. Once the proper concrete curing age is reached, the wooden plank can be dismantled (Figure 11).
2. "Varese" floor slabs: consist of prefabricated beams of reinforced concrete with interposed hollow flat clay bricks arranged to form an air chamber and with the aim of making a monolithic structure. These type of floor slabs, was widely employed in the mid-40s to replace the wooden floor slabs.
3. Prefabricated beams and block floor slabs: they are characterized by a bearing structure (beams) which can be prefabricated or cast in place and does not require provisional supporting structures during the execution. This kind of floor slabs features quicker realization. A wide range of this kind of floor slabs was employed, differing from each other for the different prefabricated beams which have been used. Also these floors slabs have become popular since the 40s.

4. **<u>"SAP" floor slabs (Senza armatura provvisoria)</u>:** this kind of floor slabs has been herein experimentally investigated. This category was introduced in Italy in 1930's and today represents one of the most commonly found in the Italian existing buildings.
   The "SAP" floor slab consists of reinforced brick beams assembled in place inserting reinforced bars (usually smooth and with small diameter) in holes specially crafted on the bricks and sealed with mortar.
   The reinforced brick beams are spaced from each other by clay blocks and are cast in place. In correspondence, at the intrados, generally only the bricks are visible. Usually the concrete topping is provided (Figure 12).
   This type of floor slabs features a good speed execution, but over the years several critical problems were highlighted. In particular, plaster chipping and flaking of bricks often occurred with outcrop of reinforcing bars, which were further subjected to oxidation due to the very low concrete cover. These critical issues, therefore, often require an improvement of the slab performance in terms of bearing capacity, but, because of the inherent constructive nature, the interventions of consolidation and reinforcement are difficult to enforce, with complex technical realization and demanding design analysis.

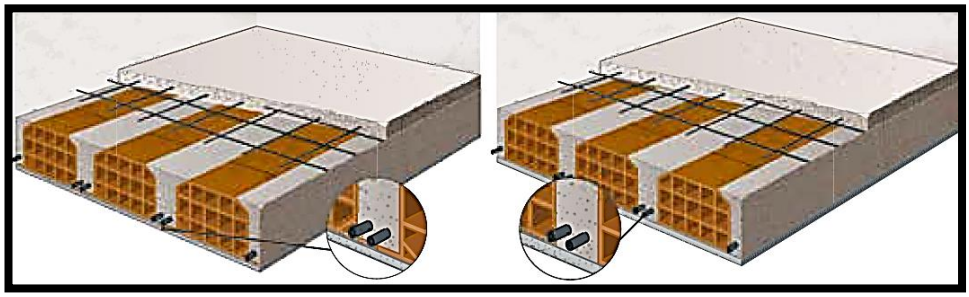

Figure 11. Cast in place floor slabs (Source: Leca)

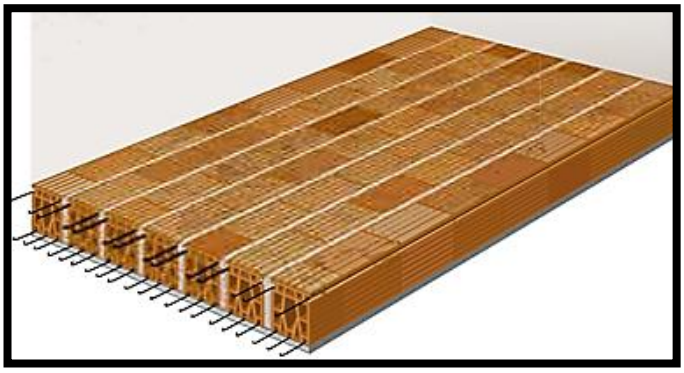

Figure 12. "SAP" floor slab. (Source: Leca)

3.2 Structural consolidation intervention applied to the "SAP" floor slabs

The following sections will discuss the motivation and techniques which have been used to improve the performance of the "SAP" floor slabs:

3.2.1 The reasons of the consolidation

The consolidation and reinforcement performed should be fully integrated with the existing slab and continue to exploit the bearing capacity of the floor. The need for intervention occurs when the structural element does not any longer perform the functions for which it was designed: failure to withstand higher loads, excessive flexural deformability, low stiffness, etc.

3.2.2 The composite cooperating topping slab technique (chemical interconnection)

The technique of the composite floor slab, analysed in the present work, as previously mentioned, in addition to being easy to use, has been widely employed for several years.

The new cooperating slab, herein made of lightweight concrete, must be perfectly interconnected with the existing floor by the use of connectors, which can be of chemical or mechanical type. The "composite section" (formed by the original floor and the cooperating topping slab) is able to increase the resistance and the flexural stiffness of the floor, to withstand the action of vertical loads and to further stiffen the floor also in its plane (rigid diaphragm effect), allowing a correct transmission and distribution of seismic actions to the lateral load resisting walls.

The connection between the topping slab and the older floor slab is crucial. If this is not secured by connectors, the union between the two elements would works as a mechanical parallel coupling with the consequent mutual delamination in the horizontal plane. The topping, in this case, represents a permanent load acting on the original slab that, although strengthened, would not be stiff enough and would feature significant deformation and deflection (Figure 13).

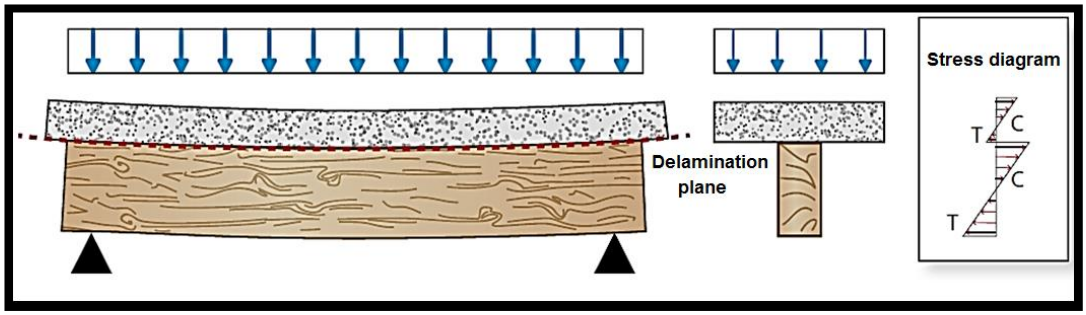

Figure 13. Diagram of a non - connected slab. (Source: Leca)

If instead there is a strong and reliable connection, a real topping - composite structure with effective structural continuity will be created. The connector then has the function of preventing the mutual delamination between the existing floor and the topping slab: it works to take over the anticipated shear actions and creates a single entity subjected to the anticipated actions, so as to ensure a substantial increase in terms of strength and stiffness of the structure.

As it can be appreciated from the stress diagram in Figure 14, the structural use of the material topping is also likely to be optimized:

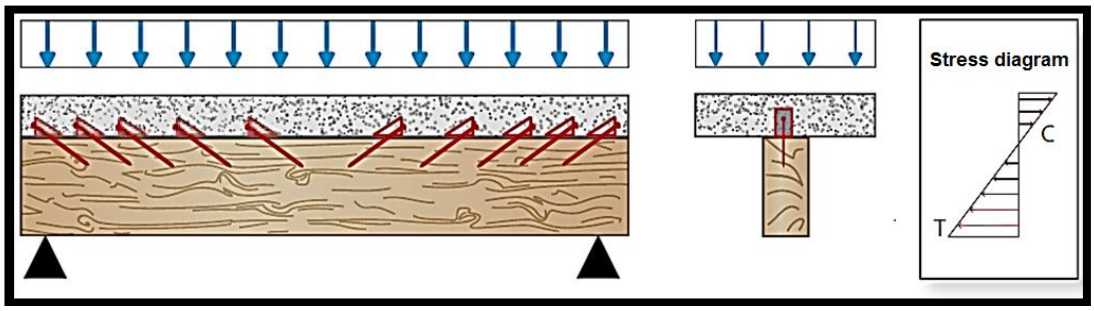

Figure 14. Diagram of a structure well connected slabs. (Source: Leca)

The consolidation of the floors herein investigated was carried out through a chemical type connection. In particular, the connector "Centro Storico Chimico" Leca system, a two-component epoxy adhesive, was used. The product provides an excellent and robust adhesion between the hardened concrete of the subgrade and the freshly cast concrete of the topping slab allowing to obtain a monolithic structure composed of the two elements to be connected; the performance system, in compliance with the instructions of installation, is certified.

The system has already been verified experimentally in order to determine the maximum level of shear resistance in a previous project, the main results of which will be summarized hereafter.

As a matter of fact, the chemical connector has some advantages compared to traditionally used solutions, such as riveting:

- The in place installation process is simplified.
- A continuous interface is created, without the typical stress concentrations from discontinued mechanical connectors.

The strength of elements consolidated with the chemical connector, can be evaluated starting from the assumed shear performance of elements without transverse reinforcement (stirrups).

In this framework the glue interface should not be "the weak link" in the chain of the resistant shear mechanisms. In other words, the shear strength of the interface must not be lower than the maximum shear expected at that position where and when the consolidated element as a whole will develop its full shear strength. The maximum shear that can be transmitted to the interface of an element without transversal reinforcement, can be evaluated by the following expression:

$$V_{INT} = \tau_d \cdot bw \cdot z$$

Where

- τ_d is the design shear strength limit guaranteed by gluing
- b_w is the minimum section width
- z is the lever arm, equal to 0.9d, with d as the effective depth of the section.

The experimental tests of characterization of the maximum shear stress sustainable by the resin were carried out on "T" samples, verifying the capacity of the resin for different values of "glued surface".

A summary table is hereafter reported with the experimental results for the characterization program performed, considering specimens with a glued width equal to 80 and 120 mm:

Specimen	τ_d (MPa)	τ_k (MPa)	τ_{av} (MPa)
CC – 80	**1,52**	**1,57**	**2,04**
CC – 120	**0,72**	**0,9**	**1,50**

Table 1. Values of the shear stress for the resin in “T” specimens 80 and 120 mm wide (Source: Previous project of shear stress sustainability of the resin)

On the other hand, Figure 15 shows the distribution of the experimental data corresponding to a glued width of 80 and 120 mm, from which were the mean ($\boldsymbol{\tau_{av}}$), characteristic ($\boldsymbol{\tau_k}$) and design ($\boldsymbol{\tau_d}$) values of shear stress, respectively calculated as the lower fractile 5% and 0.5% of the related experimental results:

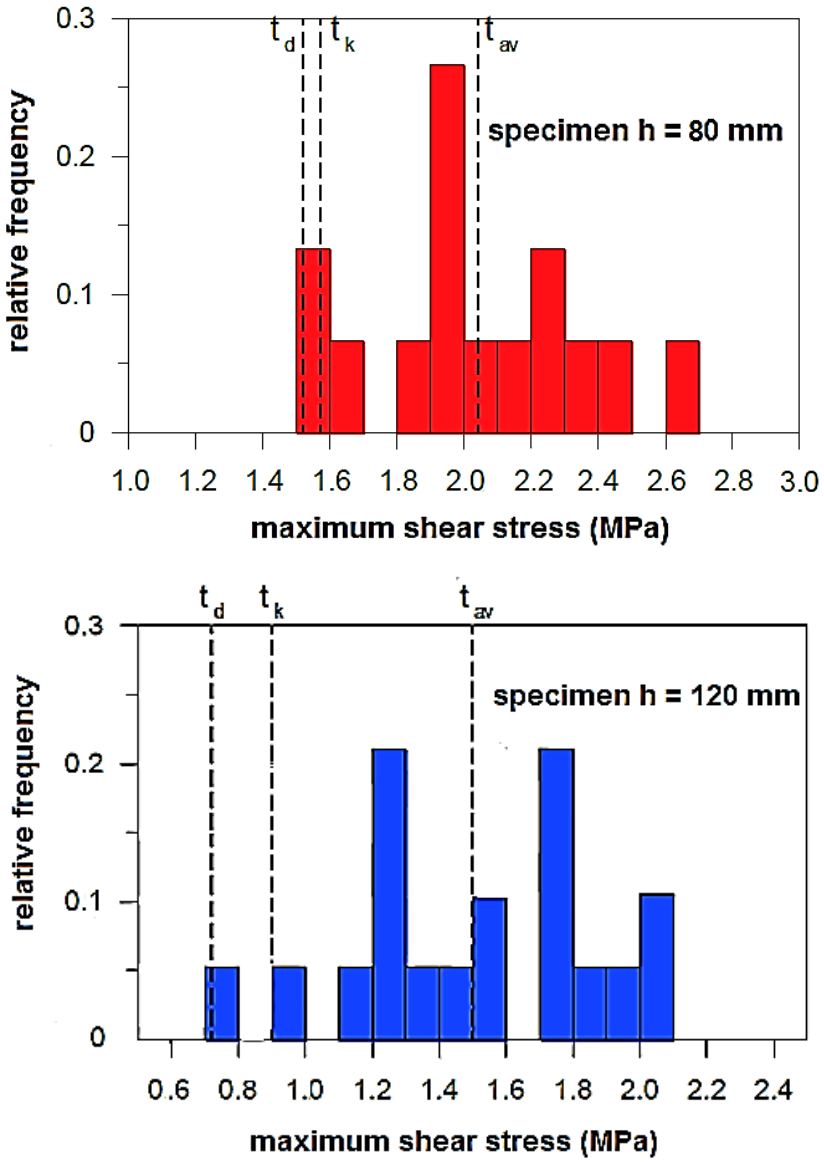

Figure 15. Values of the shear stress for the resin in "T" specimens 80 and 120 mm wide (Source: Previous project of shear stress sustainability of the resin)

A decrease of the nominal shear strength with increasing "glued" width is observed, as coherent with size effects in brittle material mechanics.

The experimental investigation has shown that the employed epoxy resin:

- Is able to ensure, when it is used for the consolidation of existing floors made even with modest / low – quality concrete, the tangential stress values at the interface between the existing floor and the consolidation slab and the shear stress values of adhesion concrete-concrete fully compatible with the expected structural applications.
- The shear bond stress values obtained are comparable for both concrete – concrete and for brick – concrete interface adherence.

The experimental campaign herein reported has been conceived and planned in order to check, at the true scale, the performance of the consolidation technique as from the preliminary test on the subassemblies.

The main improvements that may be observed by employing the (Light weight aggregate concrete "LWAC") topping slab + epoxy using consolidation technologies are:

1. Improvement of the seismic behaviour: the creation of a new slab of lightweight reinforced concrete, interconnected to the floor and the walls, can improve the seismic behaviour of the entire building. The diaphragm action capacity, thus achieved by the retrofitted slab, will make it possible to transfer horizontal actions to seismic resistant to shear walls, tying the deformation outside the plane of the walls and making the collapse mechanism of the structure, to obey the anticipated design predictions. This aspect is not negligible since local collapse mechanisms represent one of the main sources of vulnerability for the entire building.
2. Increase of the load – bearing capacity of the floor in case of change of use destination: the change of use of a property is a frequent situation that may imply an increase of loads transferred to the floor. For this reason both a structural reinforcement of the slab and the strengthening of the whole structure are needed. The use of structural lightweight concrete helps to a further increase of the live load capacity with reduced increase of dead loads that act on the existing structure.
3. Improvement of slab flexural behaviour: the decks of the buildings often undergo high flexural deformation with an obvious mid span "deflection", being generally designed for lower live loads than those required by current regulations or having structural elements which have suffered static and environmental degradation over time. A greater stiffness is thus required, both to avoid floor damage and to improve the living comfort. The intervention of

consolidation results in a substantial improvement of the flexural stiffness of the structures, also contributing to the overall structural stiffness.

4. Recovery of the top part of the floor slab for elevation: for the recovery of the slabs is necessary to check the overall structural compatibility of the building. For the intervention of renovation of the property, and in particular of the floor slabs, it is used a new cooperating slab as light as possible to reduce to the maximum dead loads.

Other significant benefits in the behaviour of the floor slabs can be: a good sound insulation, through the use of specific sound - proof mats; a better thermal insulation, thanks to the use of lightweight solutions with low thermal conductivity, and a fire protection due to the presence of one full layer of incombustible insulating material.

3.2.3 The benefits of using lightweight concrete

For the creation of the new cooperating topping slab, both for the case at issue and in the case of common interventions, the proposed solutions with lightweight structural high-performance concrete are used.
The main feature of the lightweight concrete is the favourable resistance / weight ratio, which makes this material suitable in different circumstances:

1. Structures where the self - weight outweighs the live loads: weight reduction involves the reduction of all sections.
2. Large structures characterized by great heights and important spans, in which each section reduction involves benefits from the economic point of view.
3. Interventions on soils with limited bearing capacity, in which each weight reduction results in significant savings in foundation costs.
4. Several applications in renovation, in which the reduction of the self - weight makes the structure prone to carry higher live loads.
5. Structures subject to relevant horizontal actions (for example, seismic actions), for which a reduction of the masses is equivalent to a reduction of the earthquake induced loads.
6. Structures in which the good heat resistance of the lightweight concrete will be exploited, opposed to a traditional concrete, with minor insulating characteristics.
7. Structures in which it is possible to obtain reduced concrete sections with smaller thickness of the concrete cover and with improved fire behaviour because of the lightweight concrete.
8. Floor slabs in which it becomes possible to make full castings, even with small thickness, reducing the need for intermediate supporting beams.

3.3 Experimental "set up"

In the following paragraphs the characteristics of the tested slabs will be described together with the experimental set up and the procedures employed to characterize their behaviour.

3.3.1 Design and characteristics of the floor slabs.

In this study both non – consolidated and consolidated slabs have been investigated. Non – consolidated slabs of two different cross section heights respectively equal to 120 and 160 mm have been considered as a reference.
Moreover, for each of the two aforementioned slab heights, consolidated slabs with a 50 mm thick LWAC topping have been also investigated. Two slabs for each type have been tested, summing up to eight slabs.

The mock – ups have been built to the purpose of this research project, deriving their geometrical and statical features from "old" design tables since this kind of slabs are no longer industrially manufactured.

48 — SOLAI — SAP — 49

SOLAIO SAP

H Altezza solaio	Peso laterizi	Peso travi	Conglomerato	Peso solaio in opera	Momenti massimi di servizio riferiti alla striscia di solaio larga 1 m M_{max}				h Altezza utile	CARATTERISTICHE DELLA SEZIONE FARZIALIZZATA LARGA 1 METRO										Sezione tutta reagente			Resistenze termiche	
										Asse neutro	Mom. d'inerzia	Momenti resistenti di compr.	Momenti resistenti di tens.	Asse neutro	Mom. d'inerzia	Momenti resistenti di compr.	Momenti resistenti di tens.	Asse neutro	Mom. d'inerzia	Momenti resistenti di compr.	Momenti resistenti di tens.	Distanza asse baricentrico	Area sezione	Mom. d'inerzia baricentrico	Calore dall'alto al basso	Calore dal basso all'alto
cm	Kg/m²	Kg/ml	l/m²	Kg/m²	Kgm				cm	cm	cm⁴	cm³	cm³	cm	cm⁴	cm³	cm³	cm	cm⁴	cm³	cm³	cm	cm²	cm⁴	m³ h °C / Kcal	
8	50	14	7	85	230	290	405	—	7	1,12	409	365	6,95	1,46	683	469	12,35	1,81	990	547	19,1	2,17	1332	614	27,60	4,05	445	3400	0,20	0,17
8 + 3	50	14	37	160	360	490	685	—	10	1,35	865	641	10	1,76	1460	829	17,70	2,15	2150	1000	27,4	2,52	2910	1155	36,95	4,61	745	8955	0,22	0,19
12	70	18	11	110	385	540	755	—	11	1,43	1059	739	11,05	1,94	1793	924	19,80	2,44	2653	1089	31,0	2,94	3815	1230	44,80	5,60	930	10000	0,33	0,30
12 + 3	70	18	41	185	510	750	945	—	14	1,61	1744	1085	14,10	2,12	2972	1400	25,10	2,60	4415	1698	38,7	3,05	6045	1983	55,20	6,23	700	20105	0,35	0,32
16	80	20	15	130	540	720	960	1290	15	1,72	2015	1170	15,20	2,36	3443	1462	27,30	3	5150	1720	43	3,55	7105	2000	62,10	7,75	750	21800	0,40	0,37
16 + 3	80	20	45	205	650	1000	1274	1654	18	1,84	2947	1602	18,25	2,42	5037	2080	32,40	2,98	7555	2528	50,4	3,52	10340	2940	71,50	8,10	1050	40155	0,42	0,39
20	95	22	30	175	700	1070	1430	1890	19	1,98	3300	1670	19,40	2,71	5650	2080	34,80	3,40	8485	2490	54,4	4,03	11685	2890	78	9,50	975	40400	0,45	0,42
20 + 3	95	22	60	250	800	1235	1637	2144	22	2,05	4462	2180	22,40	2,70	7620	2844	38,80	3,32	11520	3470	61,9	3,92	15900	4050	88,10	9,91	1275	68232	0,47	0,44
Armature					3Ø5	3Ø4	3Ø5	3Ø6		3 ⌀ 3				3 ⌀ 4				3 ⌀ 5				3 ⌀ 6				Numero e diametro dei tondini inferiori per ogni travetto			
σ_{fs} Kg/mmq					70	60	55	50	Limite elastico al 2‰ dell'acc. trafilato che si impiega nei travetti prefabbricati dalla RDB																			

(4)

Table 2. Dimensions of the section of SAP slab for 1 m length. (Source: "Old design tables")

In this respect, test on non – consolidated beam mock – ups are intended, besides a reference to evaluate the effectiveness of the employed consolidation technique, also as a validation of the purposedly cast specimens and of the achieved goal in reproducing the anticipated load – bearing capacity, as designed through "historical" design charts.

The geometrical characteristics of the tested slabs are shown in Figure 16 and 17 and summarized in Tables 3 and 4.

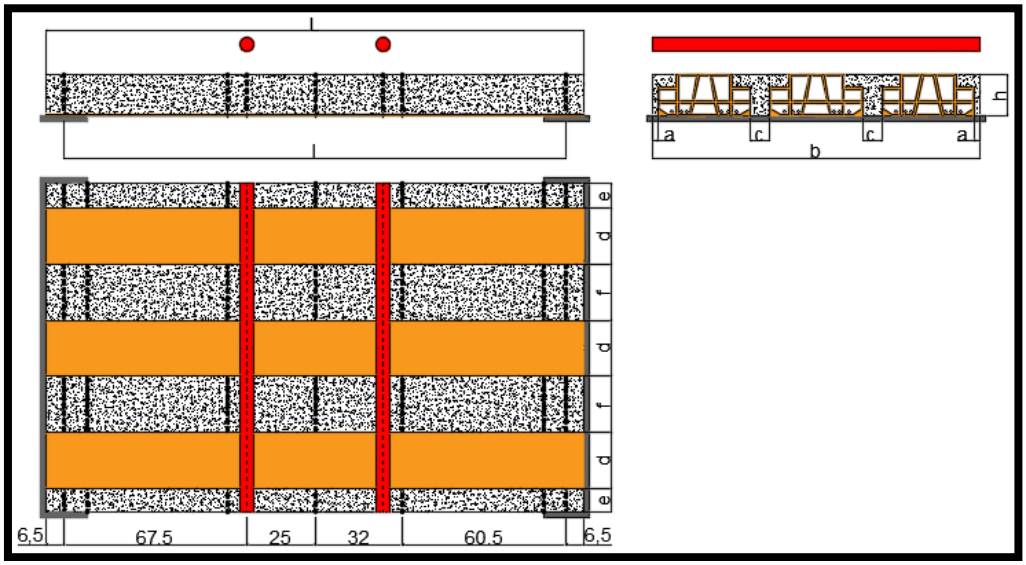

Figure 16. Design of the dimensions of the non - consolidated floor slab. (Source: Own design)

SAP 12	SAP 16
a = 0,06 m	**a = 0,07 m**
b = 1,2 m	**b = 1,2 m**
c = 0,08 m	**c = 0,1 m**
d = 0,27 m	**d = 0,25 m**
e = 0,08 m	**e = 0,09 m**
f = 0,12 m	**f = 0,14 m**
h = 0,12 m	**h = 0,16 m**
l = 1,85 m	**l = 1,85 m**
L = 2,0 m	**L = 2,0 m**

Table 3. Dimensions of the non - consolidated floor slab. (Source: Own design)

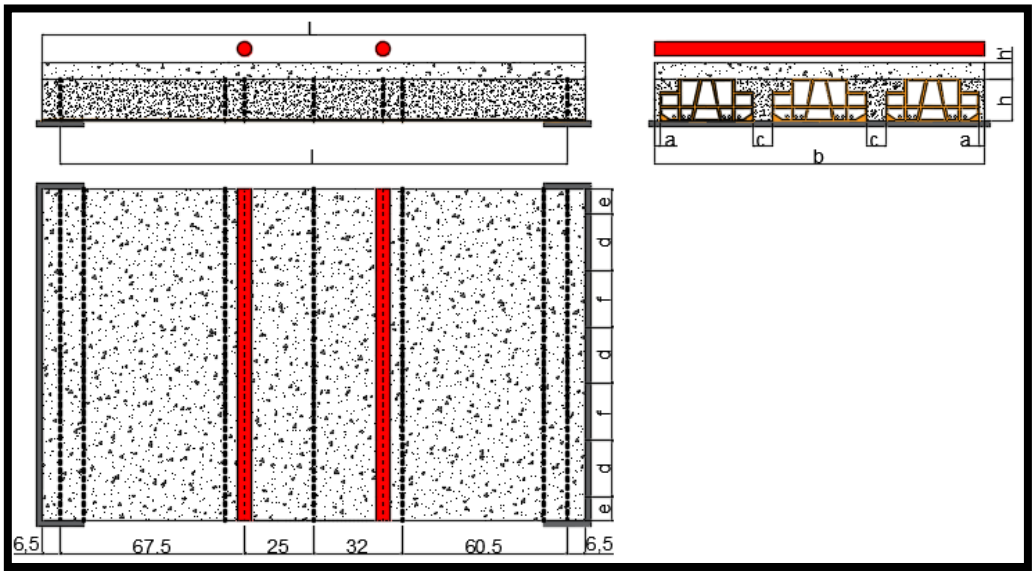

Figure 17. Design of the dimensions of the consolidated floor slab. (Source: Own design)

SAP 12 + 5 cm	SAP 16 + 5 cm
a = 0,06 m	**a = 0,07 m**
b = 1,2 m	**b = 1,2 m**
c = 0,08 m	**c = 0,1 m**
d = 0,27 m	**d = 0,25 m**
e = 0,08 m	**e = 0,09 m**
f = 0,12 m	**f = 0,14 m**
h = 0,12 m	**h = 0,16 m**
h' = 0,05 m	**h' = 0,05 m**
l = 1,85 m	**l = 1,85 m**
L = 2,0 m	**L = 2,0 m**

Table 4. Dimensions of the consolidated floor slabs. (Source: Own design)

The slabs were made with a C 16 / 20 concrete whose properties are listed hereafter:

- Characteristic cubic strength: $\mathbf{R_{ck} = 20\ MPa}$
- Characteristic cylindrical strength: $\mathbf{f_{ck} = 16\ MPa}$
- Compressive strength for design: $\mathbf{f_{cd}} = \mathbf{0,85} * \frac{fck}{1,5} = \mathbf{9,07\ MPa}$
- Average cylindrical strength: $\mathbf{f_{cm} = f_{ck} + 8 = 24\ MPa}$
- Average tensile strength: $\mathbf{f_{ctm}} = \mathbf{0,3} * \sqrt[3]{\mathbf{fck^2}} = \mathbf{1,91\ MPa}$
- Average flexural tensile strength:
  $\mathbf{f_{ctm,fl}}$ = max (1,6 - $\frac{h\,(mm)}{1000}$ * f_{ctm}; f_{ctm})= **2,82 MPa**
- Elastic modulus of concrete: $\mathbf{E_c} = \mathbf{22.000} * \left(\frac{\mathbf{fcm}}{\mathbf{10}}\right)^{\mathbf{0,3}} = \mathbf{28.600\ MPa}$

For the topping LWAC class C 18 / 22 was employed: this kind of LWAC has been specifically conceived to this purpose, representing a good compromise between strength and weight.

- Characteristic cubic strength: $\mathbf{R_{ck} = 22\ MPa}$
- Characteristic cylindrical strength: $\mathbf{f_{ck} = 18\ MPa}$
- Compressive strength for design: $\mathbf{f_{cd}} = \mathbf{0,85} * \frac{fck}{1,5} = \mathbf{10,20\ MPa}$
- Characteristic cylindrical average: $\mathbf{f_{cm} = f_{ck} + 8 = 26\ MPa}$
- Reduction factor for lightweight concrete: $\boldsymbol{\eta} = \left(\frac{\rho}{2.200}\right)^2 = \mathbf{0,405}, \boldsymbol{\rho} = \mathbf{1400}$
- Simple tensile strength: $\mathbf{f_{ctm}} = \mathbf{0,3} * \boldsymbol{\eta} * \sqrt[3]{\mathbf{fck^2}} = \mathbf{0,77\ MPa}$
- Flexural tensile strength: $\mathbf{f_{ctm,fl}}$ = max (1,6 - $\frac{h\,(mm)}{1000}$ * f_{ctm}; f_{ctm})= **1,1 MPa**
- Elastic modulus of concrete: $\mathbf{E_c} = \boldsymbol{\eta}\ \mathbf{*22.000} * \left(\frac{\mathbf{fcm}}{\mathbf{10}}\right)^{\mathbf{0,3}} = \mathbf{11.868\ MPa}$

In order to "mimic" as close as possible an existing slab (dating back up to the 60's or 70's of the last century) steel FeB 32K (as in old Italian standards) was used as reinforcement:

- Concrete cover: $\mathbf{d' = 0,02\ m}$
- Lower reinforcement for SAP12 and SAP12+5: $\mathbf{As = 471,24 * 10^{-6}\ m^2}$ (2ϕ8+2ϕ6 each module)
- Lower reinforcement for SAP16 and SAP16+5: $\mathbf{As = 508,94 * 10^{-6}\ m^2}$ (6ϕ6 each module)
- Upper reinforcement: $\mathbf{As' = 84,82 * 10^{-6}\ m^2}$ (1ϕ6 each modulus)
- Characteristic yield stress: $\mathbf{f_{yk} = 320\ MPa}$
- Design resistance: $\mathbf{f_{yd}} = \frac{\mathbf{fyk}}{\mathbf{1,15}} = \mathbf{274\ MPa}$
- Average expected yield stress: $\mathbf{f_{ym}} = \mathbf{1,35} * \mathbf{fyk} = \mathbf{425,25\ MPa}$
- Elastic modulus of the steel: $\mathbf{Es = 206.000\ MPa}$

3.3.2 Experimental test equipment and design.

Figure 18 shows a typical employed test set up. It consists of the following components:

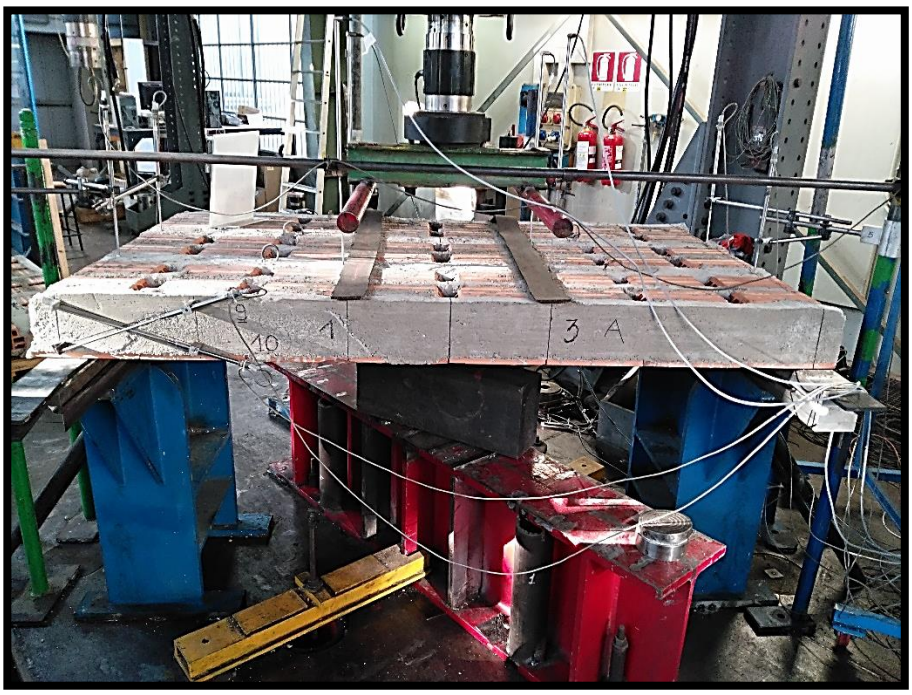

Figure 18. Distribution of the equipment. (Source: Laboratory image)

1. **Oleo - dynamic actuator**: used to apply the load to the test sample. The oleo - dynamic actuators are generally used for the application of heavy loads. They have a heavier and non – solid construction compared to pneumatic pistons, because the operating pressure is high (100-300 bar), and allow a very precise positioning of loads (± 0.01 mm). This instrument consists of two basic parts:

    - The load cell, which provides the force to be transmitted to the sample;
    - The transducer, which measures, through appropriate instruments, the displacement of the actuator.

    The load is transmitted to the sample through two steel blades, placed parallel to the short side and at a distance of 250 mm from the mid span (Figure 19).

Figure 19. Oleo - dynamic actuator (Source: Laboratory image)

2. **Deflectometers "LVDTs" (Linear Variable Differential Transducer)**: used to detect the test element behaviour during loading and unloading. They have a length of about 20 cm and are free to extend and shorten; they have a precision of thousandth of millimetre (μm). They were numbered and placed in the positions where it was of interest to the deformation of the sample and they were connected to two receiver units (Spider 8), which were controlled by a computer that receives and processes through software all the data to be analysed (Figure 20).

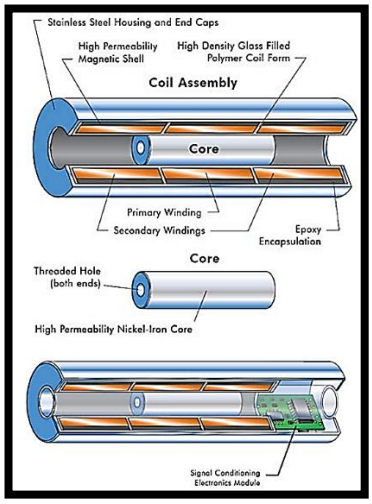

Figure 20. Linear Variable Differential Transducer scheme. (Source: Laboratory image)

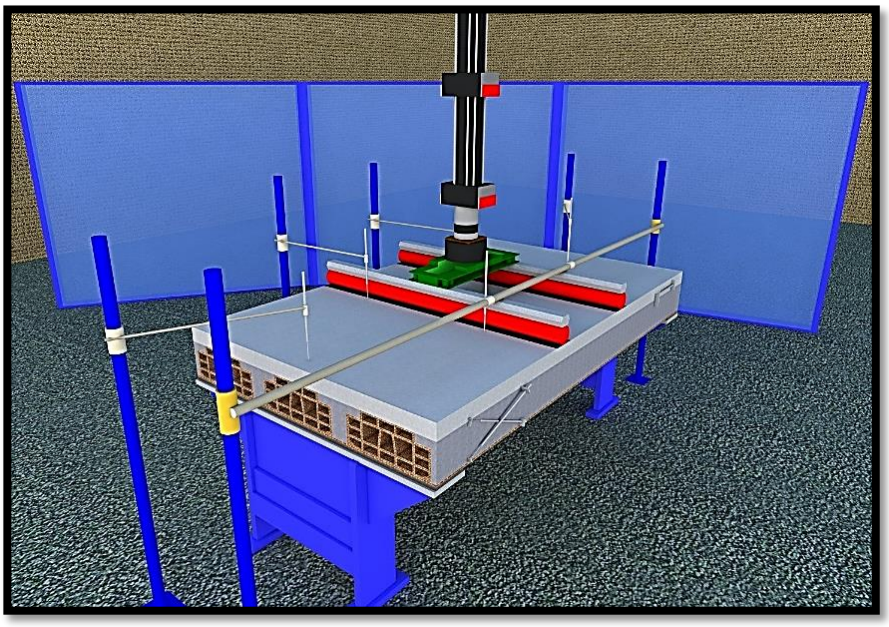

Figure 21. 3D detail of the scheme of the LVDTs distribution. (Source: Own design)

The deflectometers that were used to measure the vertical displacement were placed on the top of the floor slab as in Figure 21 and Figure 22.

The deflectometers which measured the shear deformation were arranged in an "X" pattern on the side surface of the slab, in the vicinity of the supports. These LVDTs were placed with an inclination of 1:2. (Figure 23).

Finally (on the consolidated floor slabs) deflectometers were also used to measure the delamination between the beam and block floor slab and the lightweight concrete topping slab as shown in Figure 24.

Figure 22. Instruments to measure the deflection. (Source: Laboratory image)

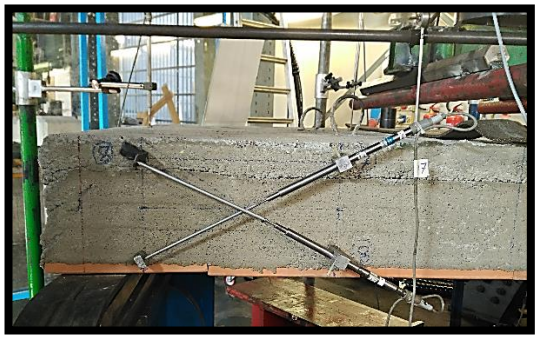

Figure 23. Instruments to measure the shear. (Source: Laboratory image)

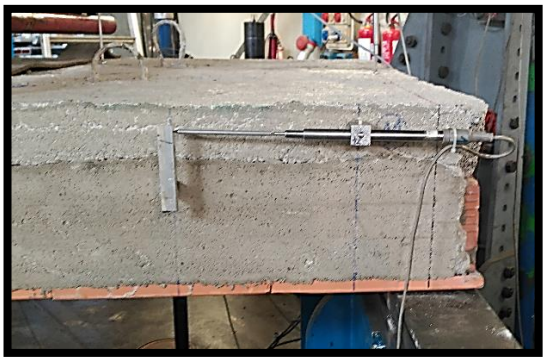

Figure 24. Instrument to measure the delamination between the two floor slab parts. (Source: Laboratory image)

3. **<u>Hardware and Software:</u>** two computers were used connected to two receptors (Spider 8). One of them was used to control the applied load and displacement steps and the other recorded the values of the vertical and horizontal displacements and the shear deformation (Figure 25).

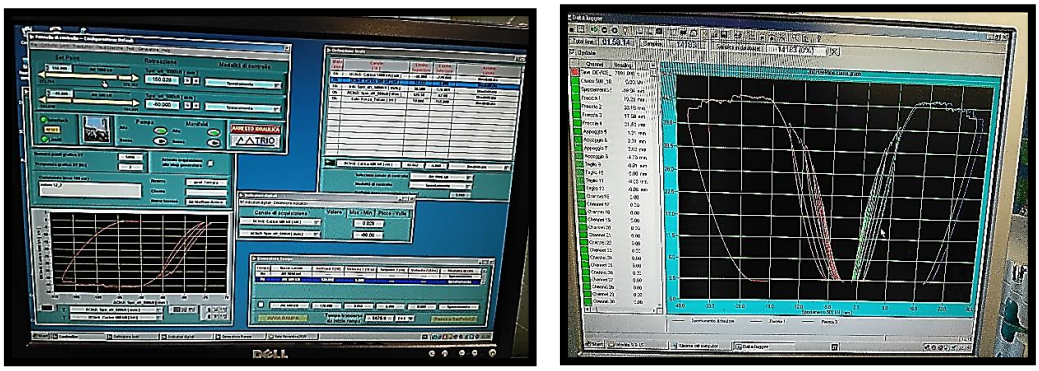

Figure 25. Results of the computers for the second test. (Source: Laboratory image)

3.3.3 Steps of the laboratory test

Slab mock ups were moved by an overhead crane equipped with hooks and chains. The crane allows the raising and movement of the floor slabs, in which were pre - installed suitable lifting hooks, safely allowing ease and precise movements of the floor slab (Figure 26).

Finally, the specimens were placed on a lift truck which allowed the positioning on the supports of the test set up (Figure 27). The same procedure in the opposite way was used to remove the specimens at the end of the loading tests.

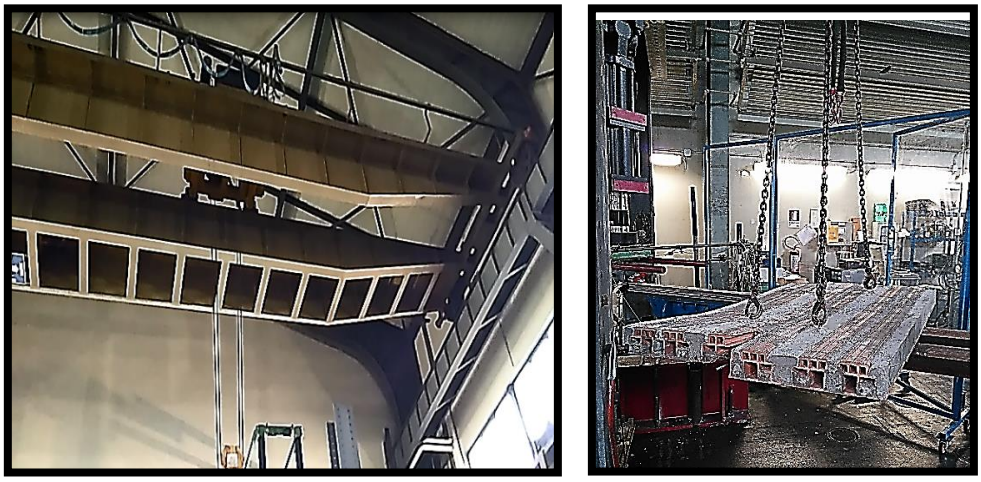

Figure 26. Crane and hooks to lift the slab. (Source: Laboratory image)

Figure 27. Lift truck to place the slab in the correct position. (Source: Laboratory image)

A detailed experimental load path has been planned, along the different test stages that were performed in order to analyse the structural performance of each specimen, as summarized hereafter in Table 5:

		NON – CONSOLIDATED SLABS		CONSOLIDATED SLABS	
		H = 12 cm	H = 16 cm	H = 12 + 5 cm	H = 16 + 5 cm
STAGE 1 LOAD CONTROL	LOADING UNLOADING VELOCITY	0,1 KN / s 0,2 KN / s	0,1 KN / s 0,2 KN / s	0,1 KN / s 0,2 KN / s	0,1 KN / s 0,2 KN / s
	Nº CYCLES & LOAD	3 CYC: 0 – 5 KN 3 CYC: 0 – 10 KN	3 CYC: 0 – 5 KN 3 CYC: 0 – 10 KN 3 CYC: 0 – 20 KN	3 CYC: 0 – 10 KN	3 CYC: 0 – 15 KN
STAGE 2 DISPLACEMENT CONTROL	LOADING UNLOADING VELOCITY	0,015 mm / s 0,030 mm / s	0,0,15 mm / s 0,030 mm / s	0,0,15 mm / s 0,030 mm / s	0,0,15 mm / s 0,030 mm / s
	Nº CYCLES & LOAD	3 CYC: 0 – 20 KN 1 CYC: 0 – 25 KN	3 CYC: 0 – 25 KN	3 CYC: 0 – 25 KN	3 CYC: 0 – 30 KN
STAGE 3 DISPLACEMENT CONTROL	LOADING UNLOADING VELOCITY	0,025 mm / s 0,050 mm / s	0,025 mm / s 0,050 mm / s	0,025 mm / s 0,050 mm / s	0,025 mm / s 0,050 mm / s
	Nº CYCLES & LOAD	1 CYC: 0 – 30 KN 1 CYC: 0 – 35 KN 1 CYC: 0 – 40 KN	3 CYC: 0 – 30 KN 3 CYC: 0 – 35 KN 3 CYC: 0 – 40 KN	3 CYC: 0 – 30 KN 3 CYC: 0 – 40 KN 3 CYC: 0 – 50 KN	3 CYC: 0 – 40 KN 3 CYC: 0 – 50 KN 3 CYC: 0 – 75 KN
MONOTONICAL LOAD PATH UNTIL REACH FAILURE		SLAB 1: 47 KN SLAB 2: 46 KN	SLAB 3: 73 KN SLAB 4: 75 KN	SLAB 5: 99 KN SLAB 6: 99 KN	SLAB 7: 125 KN SLAB 8: 116 KN

Table 5. Details of the experimental load paths for each floor slab. (Source: Own design)

Once the slabs were carefully placed on the testing supports as describe above, they were tested in 4 – point bending over a span of 1,85 m.

1. First of all, as it was defined before, the test samples were placed on two metal hinges (supports), making use of the crane and the lift truck, with a span of 185 cm between them; then the deflectometers were positioned at the points of interest and they were numbered and named according to the relevant position.
2. The following action was to prepare the oleo – dynamic actuator which had to apply the load along the two steel blades which were spaced 50 cm from each other symmetrically located with respect to the mid span..
   To ensure a uniform load distribution a neoprene pad was used.
3. The connection between the deflectometers and the computers was then checked and reset to zero was performed in order to avoid previous readings.
4. Finally, the last part consisted in defining the different steps which were used to test the slab. As the total heights of the tested floor slabs were different, the consolidated ones having higher resistance than the non – consolidated ones, the applied load steps were different for each type of slabs.

   - The test was based on loading and unloading cycles, also called hysteresis loops, at a speed set according to the needs: for the first few cycles the test was performed in load control, at a speed of the order of $KN/s * 10^{-1}$. As the load was increased, it was shifted to displacement control in order to obtain more stable control and to avoid sudden failure and detect also “softening curves” (for example in the case of shear failure), or have a more reliability and precise information on the ductile behaviour as related to an expected bending failure.
   - For the first few cycles it is natural to expect a linear behaviour of the load-deflection curve (linear elastic behaviour), until the yield strength is reached. When the test reaches this load, the curve shows a "sharp bend" and will not grow linearly any more. During the test, at each load increment, on each slab the cracks were highlighted.

4

EXPERIMENTAL RESULTS

The results will be presented and analysed of experimental tests performed on non – consolidated and consolidated slabs, with the purpose of highlighting peculiar features of their behaviour as well as assessing the reliability of predicting formulas and design approaches for the load bearing capacity.

4.1 Detailed description of the laboratory results

The following paragraphs define specifically each test performed in the laboratory for each specimen:

4.1.1 Floor Slab Nº1. Non – consolidated. H = 12 cm

The first non – consolidated floor slab of h = 12 cm had the following dimensions: L = 2 m; l = 1,85 m; b = 1,2 m; h = 12 cm.
The specimen was subjected to three cycles of loading - unloading in load control up to 5 KN and 10 KN with a loading speed equal to 0,1 KN / s and an unloading speed of 0.2 KN / s.
Subsequently, the slab underwent three loading - unloading cycles up to 20 KN and one of 25 KN in displacement control, with a loading speed equal to 0,015 mm / s and an unloading speed of 0,03 mm / s.
For the following cycles of loading and unloading up to 30 KN, 35 KN and 40 KN in displacement control the rate of loading and unloading speed was increased respectively to 0.025 mm / s and 0.05 mm / s.

Finally the slab was subjected to a last monotonic load path until it reached the failure. In this case, the specimen presented its first crack at a load of 35 KN in the vicinity of the loading blades and it reached the failure at 47 KN also in the central part due to bending, which was the expected failure mode (Figure 28).

Figure 28. Failure of the first non – consolidated floor slab of h = 12 cm.
(Source: Laboratory image)

4.1.2 Floor Slab Nº2. Non – consolidated. H = 12 cm

The second non – consolidated floor slab of h = 12 cm had the same characteristics as the first one and underwent the same test protocol unless for the last stage of loading. In the last part of the cycles, the specimen presented its first crack at a load of 30 KN; it started to yield at 40 KN and finally it reached the failure at 46 KN. The first crack appeared in the vicinity of the blades due to the bending stress; the failure was also reached in the central part due to bending which was the expected failure. During the failure of the floor slab, a centre piece of the brick part was broken and fell down to the floor (Figure 29).

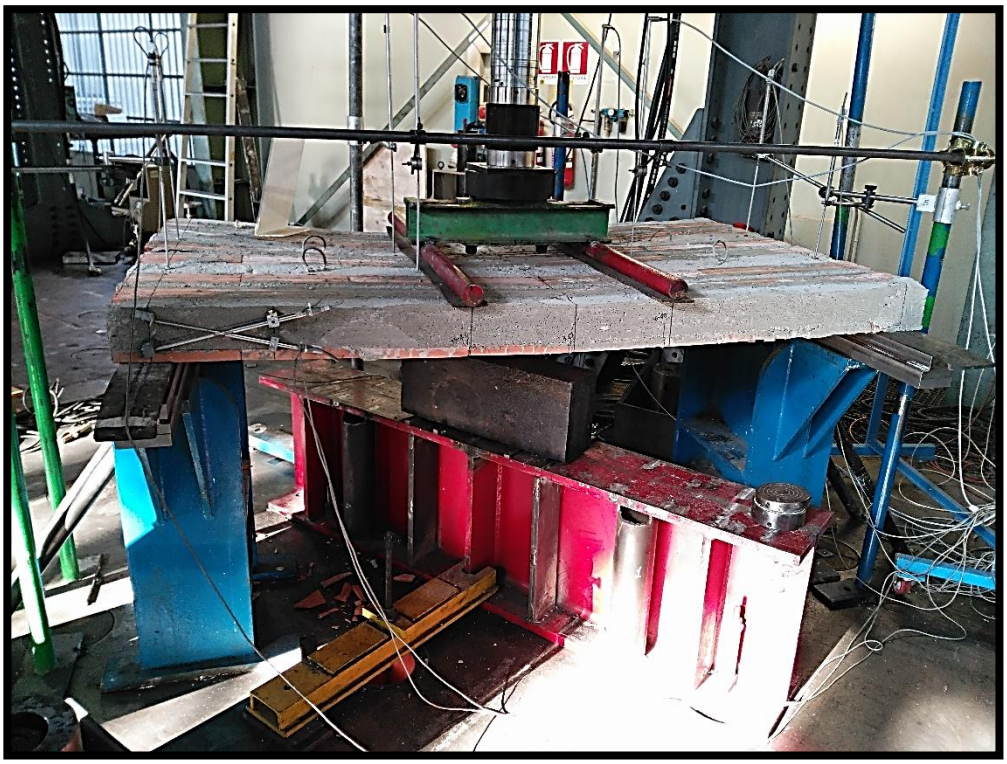

Figure 29. Failure of the second non – consolidated floor slab of h = 12 cm.
(Source: Laboratory image)

4.1.3 Floor Slab Nº1. Non – consolidated. H = 16 cm

The first non – consolidated floor slab of h = 16 cm had the following dimensions: L = 2 m; l = 1,85 m; b = 1,2 m; h = 16 cm.

The test protocol was similar as for the two previous slabs, adding three more cycles for load control, unless for the last stage of loading.

In the last part of the load path, the specimen presented its first crack at a load of 40 KN, then it started to yield at 50 KN and finally it reached the failure at 73 KN.

The first crack appeared in the vicinity of the blades due to bending stress and at the end of the test an inclined crack appeared near the support at 45º, which meant a failure due to shear, and caused the total failure of the specimen. This was an unexpected behaviour, most probably due to defects in the test specimen manufacturing. Luckily the crack appeared on the side where the shear deflectometers were placed and the crack opening values were recorded but the crack did not properly cross the LVDTs (Figure 30).

Figure 30. Failure of the first non – consolidated floor slab of h = 16 cm. (Source: Laboratory image)

4.1.4 Floor Slab Nº2. Non – consolidated. H = 16 cm

The second non – consolidated floor slab of h = 16 cm had the same characteristics and underwent the same test protocol as for the previous slab unless for the last stage of loading.

In the last part of the load path, the specimen presented its first crack at a load of 45 KN; it started to yield at 50 KN and finally it reached the failure at 72 KN. The first crack appeared in the vicinity of the blades due to bending stress and the failure was reached also in the central part due to bending, as for the specimens of h = 12 cm (Figure 31).

Figure 31. Failure of the second non – consolidated floor slab of h = 16 cm. (Source: Laboratory image)

4.1.5 Floor Slab Nº1. Consolidated. H = 12 + 5 cm

The first consolidated floor slab of h = 12 + 5 cm had the following dimensions: L = 2 m; l = 1,85 m; b = 1,2 m; h = 12 cm and h' = 5 cm as the new layer of lightweight concrete.

The specimen was subjected to three cycles of loading - unloading in load control up to 10 KN with a load speed equal to 0,1 KN / s and an unloading speed of 0.2 KN / s. Subsequently, the slab underwent three cycles of loading - unloading up to 25 KN in displacement control, with a load speed equal to 0,015 mm / s and an unloading speed of 0,03 mm / s.

For the following cycles of loading and unloading up to 30 KN, 40 KN and 50 KN in displacement control the rate of loading and unloading speed was increased respectively to 0.025 mm / s and 0.05 mm / s.

In the last part of the load path, the specimen showed its first crack at a load of 40 KN and reached the failure at 99 KN due to shear stresses.

The first crack appeared in the vicinity of the blades due to bending stress. Nearly at the end of the test an inclined crack appeared near to the support at 45º, which meant a failure due to shear, and caused the total failure of the specimen. Unfortunately it appeared on the side where the shear deflectometer was not placed and the values were not received on the Spider 8.

It can be argued that, because of the consolidation, the moment capacity was increased so that the shear failure became critical as it will be after explained.

Close to failure, significant delamination was observed between the existing floor slab and the new cooperating slab (topping) (Figure 32).

Figure 32. Failure of the first consolidated floor slab of h = 12 + 5 cm.
(Source: Laboratory image)

4.1.6 Floor Slab Nº2. Consolidated. H = 12 + 5 cm

The second consolidated floor slab of h = 12 cm had a similar geometry as the first one and underwent the same test protocol.

The specimen presented its first crack at a load of 30 KN and then other cracks appeared at 40 and 50 KN; finally it reached the failure at 99 KN due to shear.

The first crack appeared in the vicinity of the loading blades due to bending stress and at the end of the test an inclined crack appeared near to the support at 45º, which meant a failure due to shear, and caused the total failure of the specimen. Same as before for delamination. In this case the instruments recorded the crack due to shear actions (Figure 33).

Figure 33. Failure of the second consolidated floor slab of h = 12 + 5 cm.
(Source: Laboratory image)

4.1.7 Floor Slab Nº1. Consolidated. H = 16 + 5 cm

The first consolidated floor slab of h = 16 cm had the following dimensions: L = 2 m; l = 1,85 m; b = 1,2 m; h = 16 cm and h' = 5 cm as the new layer of lightweight concrete. The specimen was subjected to three cycles of loading - unloading in load control up to 15 KN with a load speed equal to 0,1 KN / s and an unloading speed of 0.2 KN / s. Subsequently, the slab underwent three cycles of loading - unloading up to 25 KN in displacement control, with a load speed equal to 0,015 mm / s and an unloading speed of 0,03 mm / s.

For the following cycles of loading and unloading up to 40 KN, 50 KN and 75 KN in displacement control the rate of loading and unloading speed was increased respectively to 0.025 mm / s and 0.05 mm / s.

The specimen presented its first crack at a load of 50 KN and then successive cracks at 75 KN, reaching finally the failure at 125 KN due to a mix of bending, shear and delamination.

The first crack appeared in the vicinity of the blades due to bending stress at the end of the test an inclined crack appeared near to the support at 45º, which meant a failure due to shear, and caused the total failure of the specimen. A significant delamination was also observed starting at 75 KN and it was recorded by the instruments (Figure 34).

Figure 34. Failure of the first consolidated floor slab of h = 12 + 5 cm.
(Source: Laboratory image)

4.1.8 Floor Slab Nº2. Consolidated. H = 16 + 5 cm

The second consolidated floor slab of h = 16 cm had the same dimensions and underwent the same test protocol as its companion slabs described before. It also showed a similar failure.

The specimen presented its first crack at a load of 75 KN reaching finally the failure at 116 KN due to shear stresses.

The first crack appeared in the vicinity of the blades due to bending stress to and at the very end of the test an inclined crack suddenly appeared near to the support at 45º, which meant a failure due to shear, and caused the total failure of the specimen. Same as before for delamination behaviour (Figure 35).

Figure 35. Failure of the second consolidated floor slab of h = 16 + 5 cm.
(Source: Laboratory image)

4.2 Load vs Vertical Deflection curves

As it was defined in the introduction of the section 4, different graphs are going to be used to show the behaviour for both non – consolidated and consolidated floor slabs. This first part shows the diagram of load – vertical deflection.

4.2.1 Non - consolidated floor slab results

In Figure 36 the load vs average vertical deflection curves are shown for the four tested non – consolidated slabs.

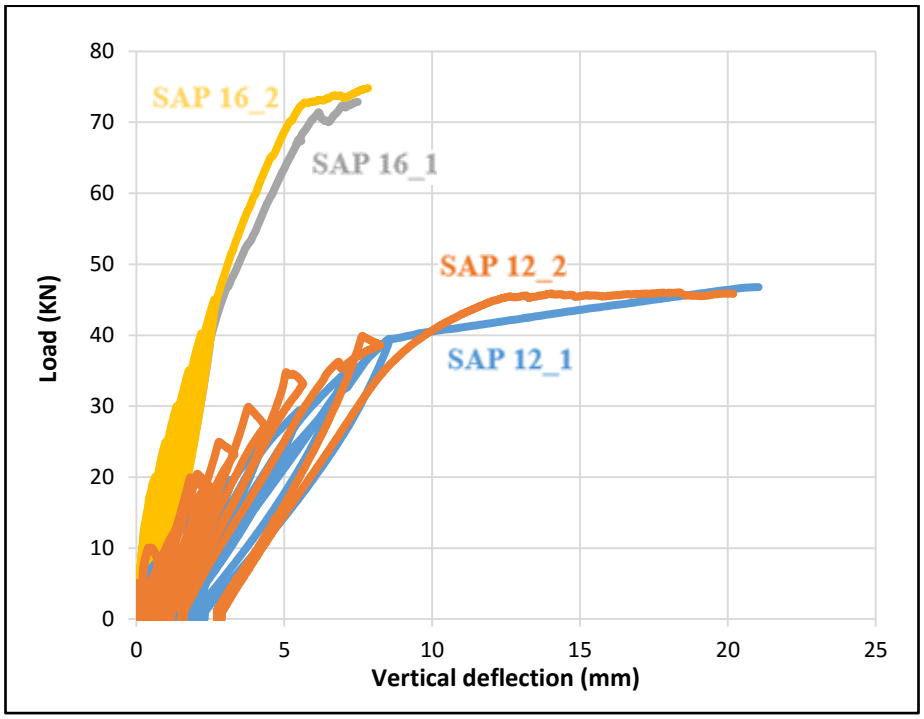

Figure 36. Graph of the load – deflection average of the non – consolidated floor slabs. (Source: Own design)

The specimens had a linear behaviour up to the yielding strength, equal to approximately 40 KN for the two floor slabs with h = 12 cm and 70 KN for the two of h = 16 cm. In all four tests vertical cracks appeared due to bending in the central part; in particular the SAP16_1 sample also developed a shear crack, most likely due to some random scattering of material properties and accidental errors in specimen manufacturing. The specimens reached the failure for loads approximately equal to 46-47 KN for the two floors of h = 12 cm and 72 KN for the two of h = 16 cm.

As it can be observed from Figure 36, the first two specimens had a higher ductility than the second pair of slabs, which failed just after the yielding. This is due to the steel reinforcement ratio $\rho_s = \frac{A_s}{b*d}$, which is higher for the specimens of h = 12 cm, so they experimented a better contribution of the reinforcement, leading to a better ductility.

4.2.2 Consolidated floor slab results

Figure 37 shows the load vs average vertical deflection curves for the four tested consolidated slabs.

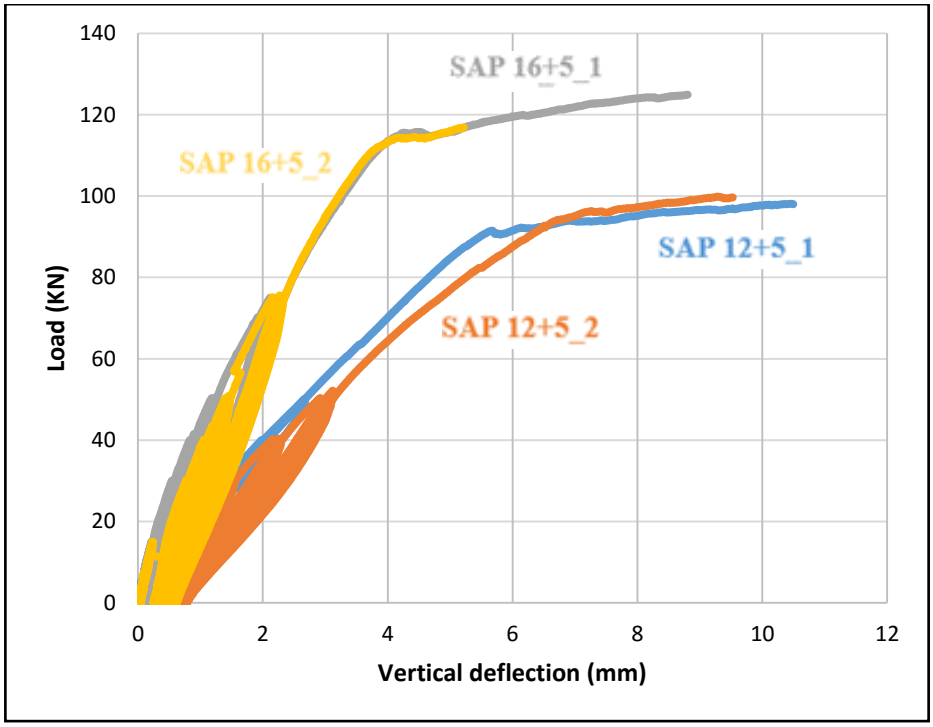

Figure 37. Graph of the load – deflection average of the consolidated floor slabs. (Source: Own design)

Similarly to the previous specimens, the consolidated slabs showed a linear behaviour up to the yielding strength, equal to approximately 90 KN and 110 KN respectively. In this case the behaviour until the failure reached by the two pairs was similar, which was around 100 KN for the pair of h = 12 + 5 cm and 125 – 116 KN for the pair of h = 16 + 5 cm.

In this case, the ductility was lower as a matter of fact, the addition of the topping reduces the overall reinforcement ratio. It is worth remarking that these specimens suffered also failure due to shear and delamination.

4.2.3 Comparison between consolidated and non – consolidated floor slabs

In Figures 38 and 39 the relative load vs average vertical deflection curves are compared.

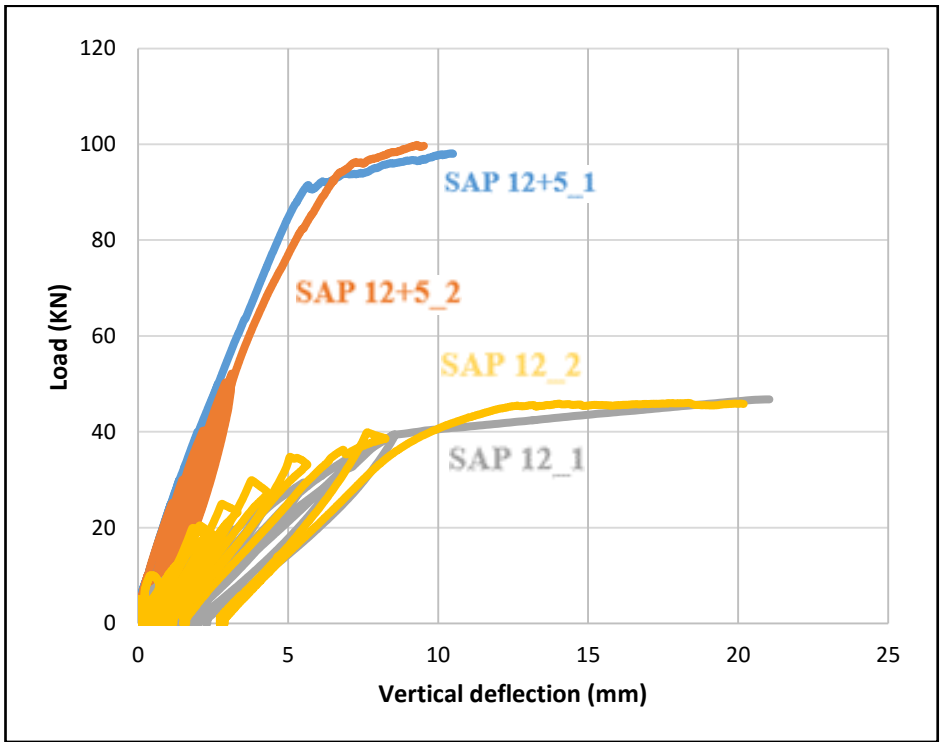

Figure 38. Comparative graph of the load – deflection average of the consolidated and non – consolidated floor slabs of h = 12 cm and h = 12+5 cm. (Source: Own design)

As it can be observed, the employed retrofitting technique provided good results, increasing the resistance of the consolidated slabs by about 100 % for the 12 cm high slabs (from about 50 KN to about 100 KN) and by nearly 70 % for the 16 cm high slabs (from about 70 KN to about 120 KN).

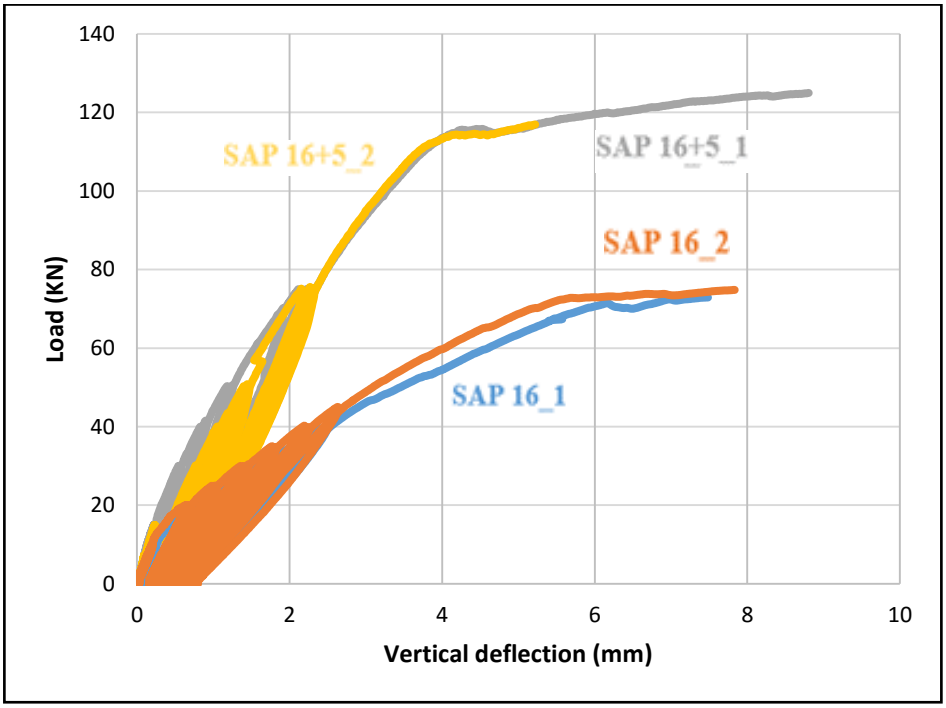

Figure 39. Comparative graph of the load – deflection average of the consolidated and non – consolidated floor slabs of h = 16 cm and h = 16+5 cm. (Source: Own design)

4.3 Shear load vs shear deformation curves

In this second part the results will be shown in terms of shear load vs shear deformation diagrams; since some of the specimens, and most of the consolidated ones, failed in shear, it will be of interest to analyse also this kind of results.
As it was explained before, the deflectometers which measured the shear deformation were arranged in an "X" pattern on the side surface of the slab, in the vicinity of the supports. These LVDTs were placed with an inclination of 1:2, so shear deformation has been calculated as the ratio of the absolute value of the elongation of the two instruments which form the "X" cross ($\delta 1$ & $\delta 2$) divided by the length "L" of the diagonal, as it can be seen in Figure 40:

$$\gamma_{TOT} = \frac{\|\delta 1 + \delta 2\|}{L}$$

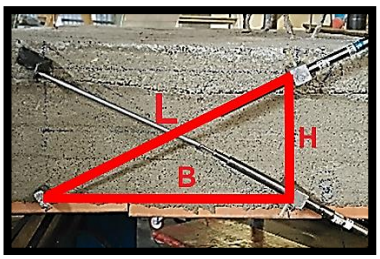

Figure 40. Disposition of the instruments to measure the elongation due to shear. (Source: Own design)

An example is introduced hereafter of the results of shear deformation for the second test, being "Taglio 9" & "Taglio 10" for example, a pair of instruments which formed the "X" cross and for whose diagonal "L" is computed the total elongation "γ_{TOT}":

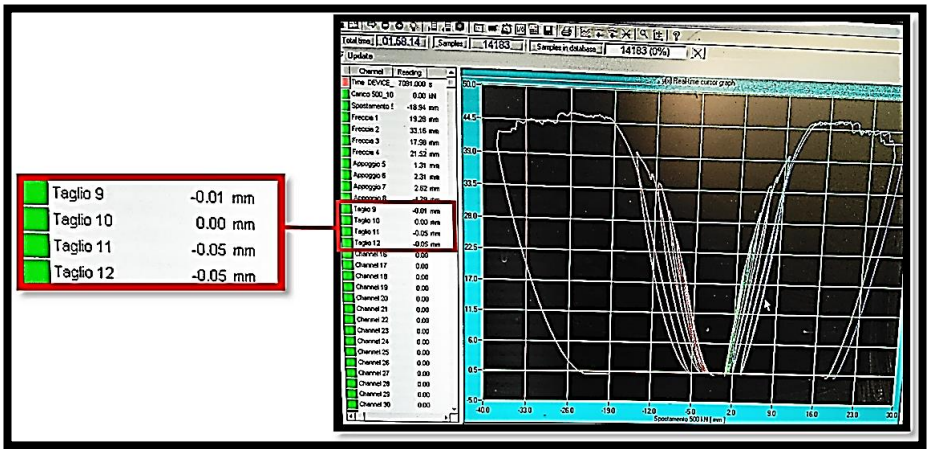

Figure 41. Results of the elongation due to shear from the laboratory computers for the second test. (Source: Own design)

4.3.1 Non - consolidated floor slab results

FLOOR SLAB Nº 1. NON - CONSOLIDATED. H= 12 cm

Figure 42 shows the relation between the shear load and the shear deformation "γ_{TOT}", calculated as above.

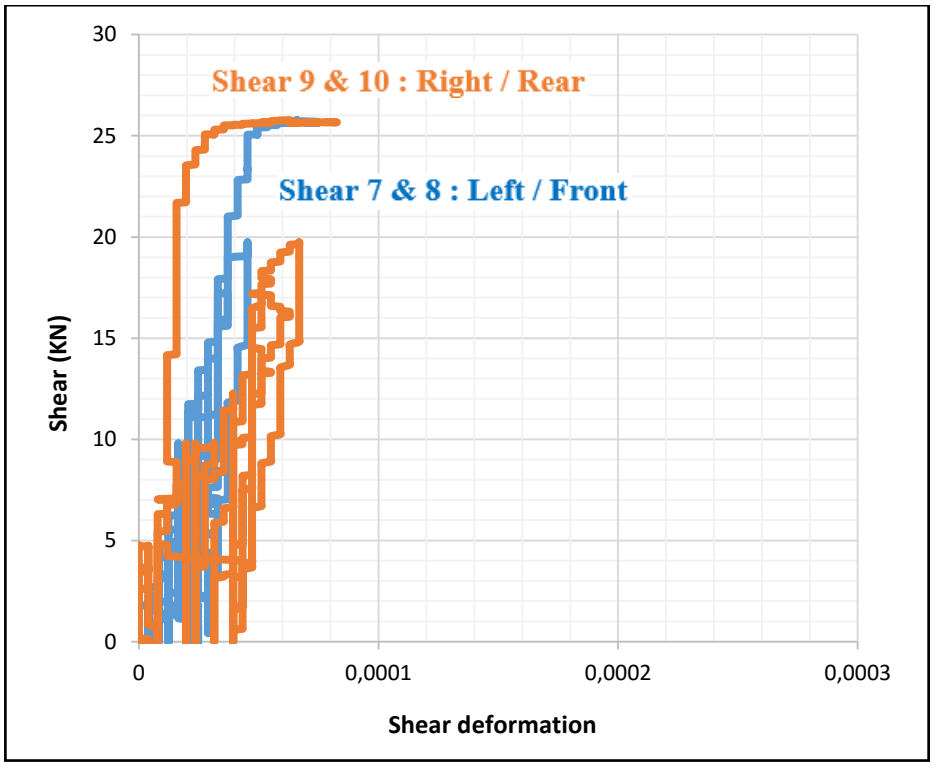

Figure 42. Graph of the shear load vs shear deformation for the first floor slab of h = 12 cm. (Source: Own design)

As it can be appreciated from the graph, for this first specimen the values recorded by the instruments show that the shear deformation is negligible almost up to failure.

FLOOR SLAB Nº 2. NON - CONSOLIDATED. H= 12 cm

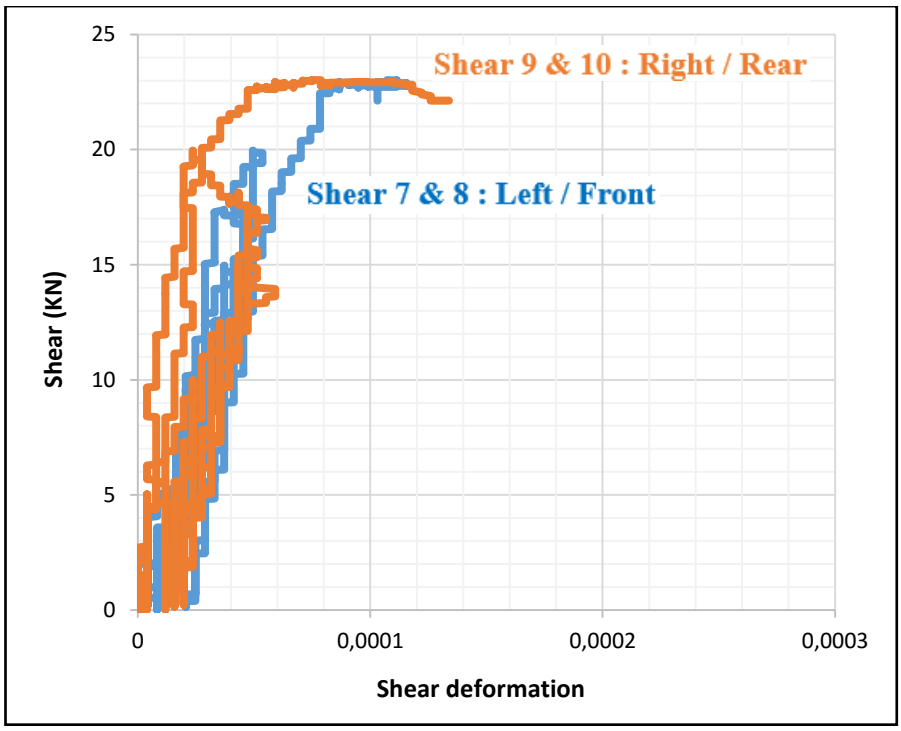

Figure 43. Graph of the shear load vs shear deformation for the second floor slab of h = 12 cm. (Source: Own design)

In Figure 43, it can be observed that the shear deformation recorded by the instruments for the second specimen of h = 12 cm is also negligible.
Only really close to the peak load some increase of the measured shear deformation has been detected. Actually the specimen failed in bending.

FLOOR SLAB Nº 1. NON - CONSOLIDATED. H= 16 cm

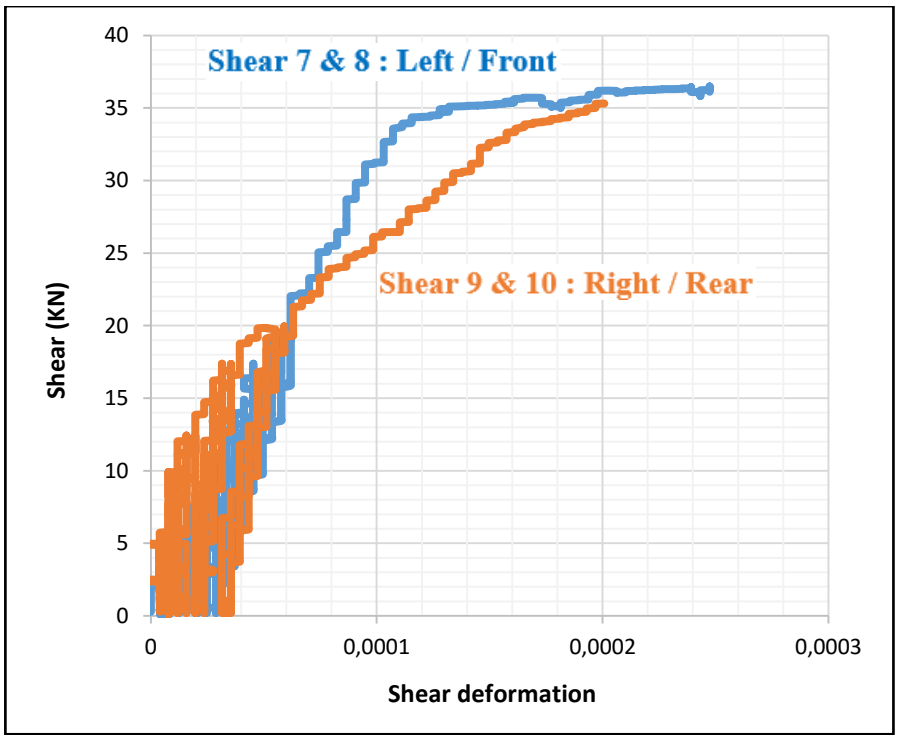

Figure 44. Graph of the shear load vs shear deformation for the first floor slab of h = 16 cm. (Source: Own design)

Figure 44 shows the results recorded by the instruments for the first specimen of h = 16 cm. As it can be appreciated from the graph, in this case the specimen reached the failure due shear deformation. A distinction also appears between an initial elastic stage, a post elastic stage and a "plastic" one.

The values of the measured shear deformation were higher than for the previous slabs, but they remain quite low, since the crack mostly propagated outside of the recording LVDTs.

FLOOR SLAB Nº 2. NON - CONSOLIDATED. H= 16 cm

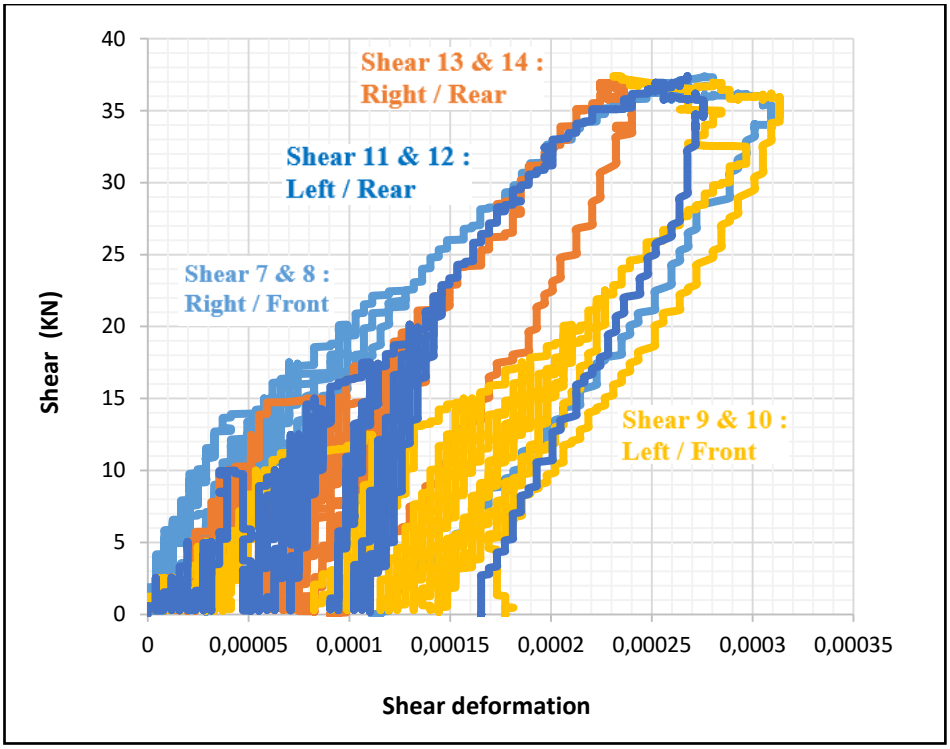

Figure 45. Graph shear load vs shear deformation
for the second floor slab of h = 16 cm. (Source: Own design)

Since the first specimen of h = 16 cm reached the failure due to shear stresses, two pair of instruments were added in order to receive the information of the shear failure in the four corners of the floor slab.

In this case the slab reached the failure in bending although the values measured of the shear deformation were significant.

4.3.2 Consolidated floor slab results

FLOOR SLAB Nº 1. CONSOLIDATED. H= 12 + 5 cm

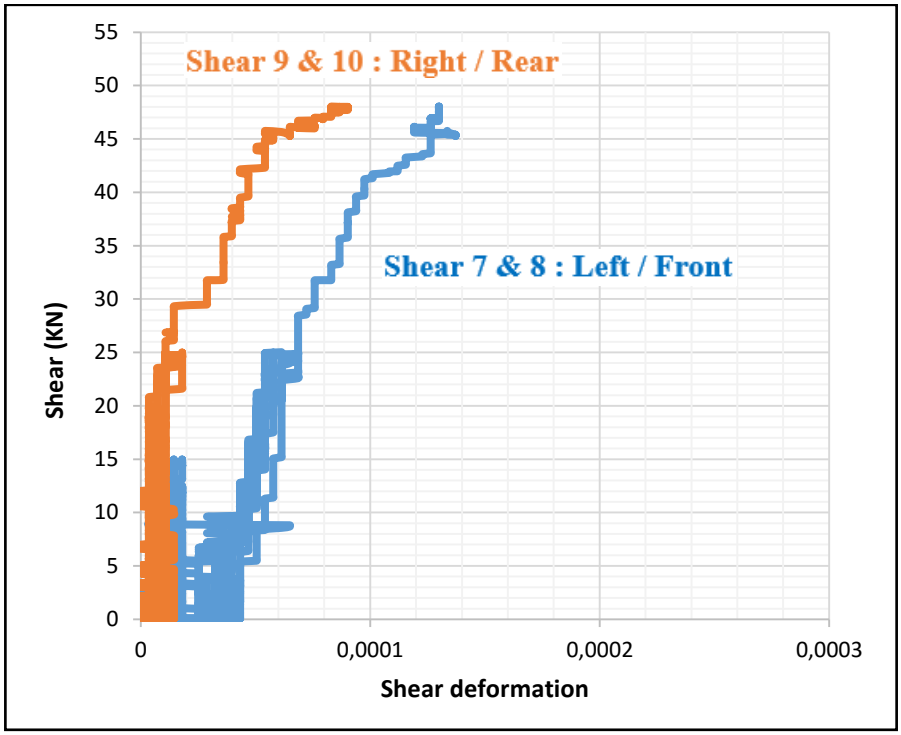

Figure 46. Graph shear load vs shear deformation
for the first floor slab of h = 12 + 5 cm. (Source: Own design)

In this first specimen of h = 12+ 5 cm the failure was due to shear as it can be clearly seen from Figure 32 in the section 4.1.5, but the instruments were placed in the other corner with respect to the one where the shear crack formed so the graph shows lower values of deformation due to shear actions.

FLOOR SLAB Nº 2. CONSOLIDATED. H= 12 + 5 cm

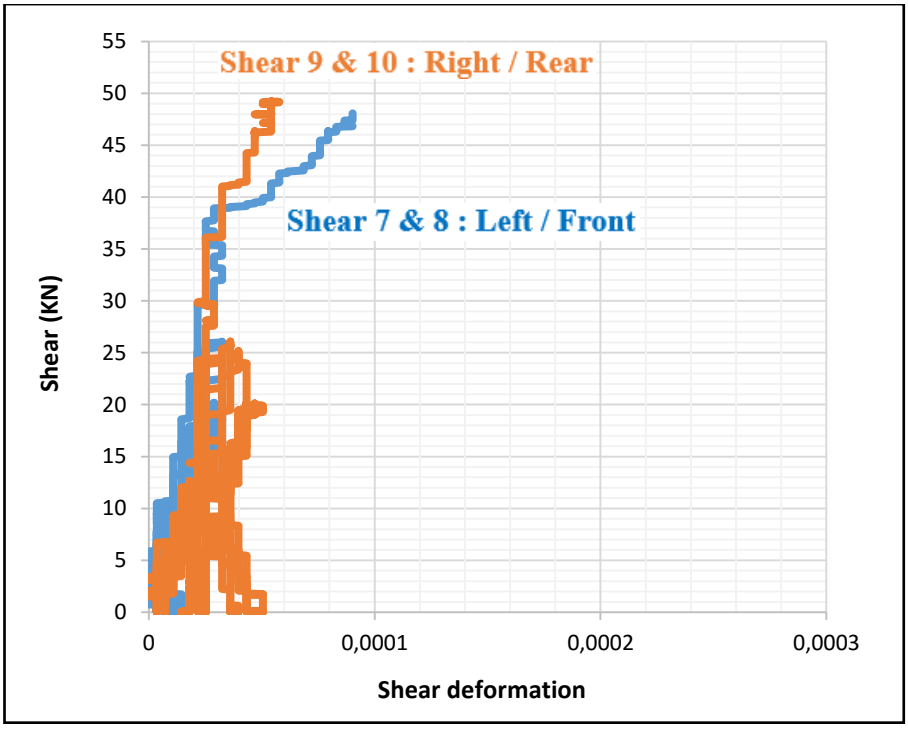

Figure 47. Graph shear load vs shear deformation
for the second floor slab of h = 12 + 5 cm. (Source: Own design)

In this case the failure was due to shear stresses also but in this case it was recorded by the instruments as shown in Figure 33 in the section 4.1.6.

It can be observed after an initial elastic stage up to about 40 KN shear (80 KN total load), the shear deformation start to increase as soon as the shear crack started propagating.

FLOOR SLAB Nº 1. CONSOLIDATED. H= 16 + 5 cm

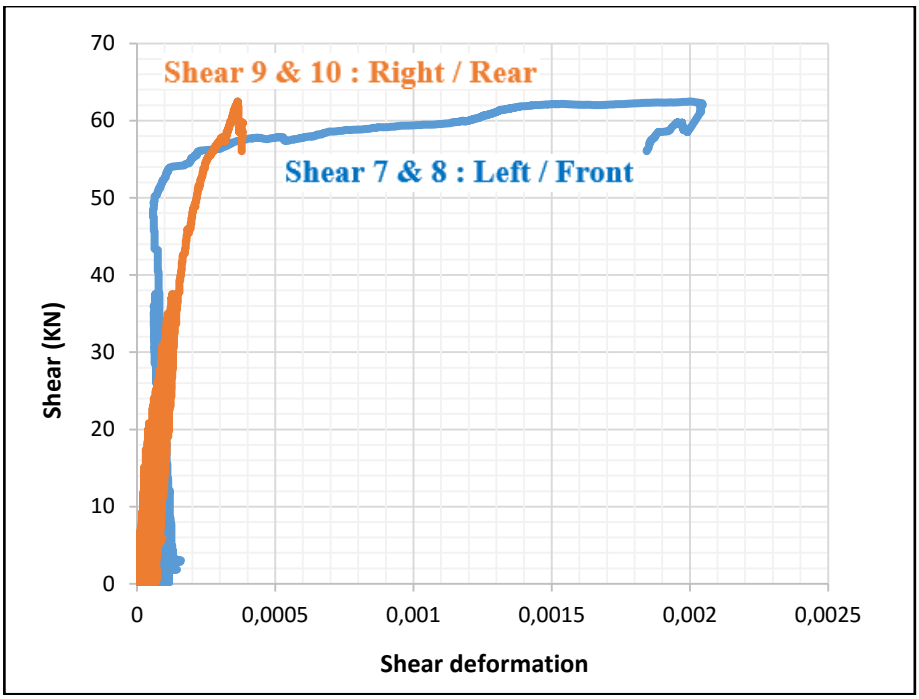

Figure 48. Graph shear load vs shear deformation
for the first floor slab of h = 16 + 5 cm. (Source: Own design)

For this first specimen of h = 16 + 5 cm failure was due to a mix of bending, shear and delamination, the delamination being the most critical behaviour.

In Figure 48 can be clearly observed the strong increase in shear deformation in the last stage of the test, corresponding to the progressive opening of the diagonal crack, which reaches values one order of magnitude higher than those measured in all other tested samples.

FLOOR SLAB Nº 2. CONSOLIDATED. H= 16 + 5 cm

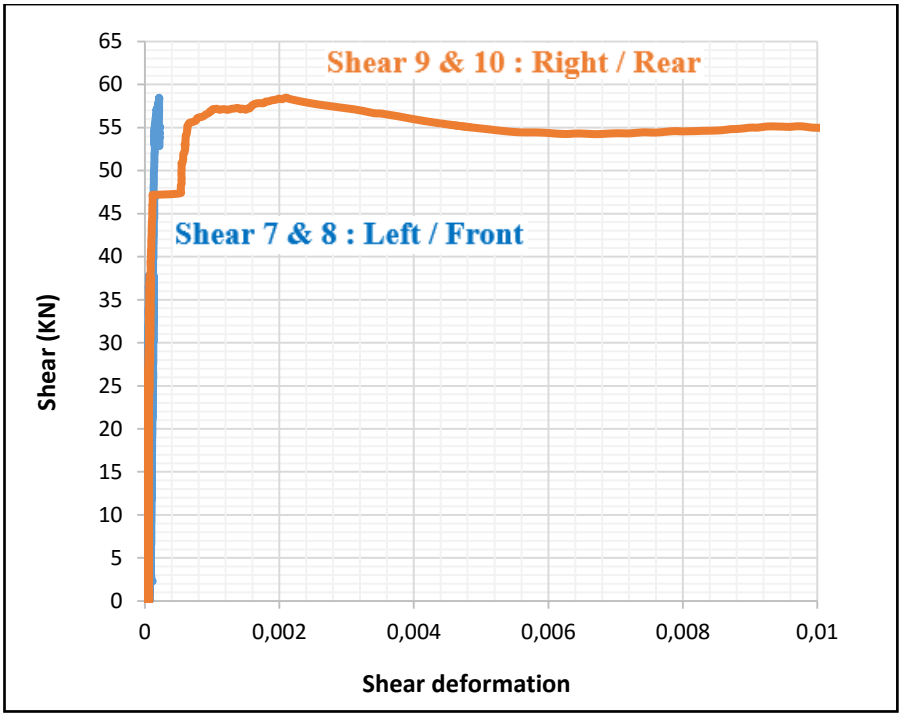

Figure 49. Graph shear load vs shear deformation
for the second floor slab of h = 16 + 5 cm. (Source: Own design)

Finally in this last consolidated specimen, similarly to the previous one, the failure was due to a mix of bending, shear and delamination. As it can be seen in the graph, a similar value of the shear deformation was measured as for the first specimen of h = 16 + 5 cm.

It anyway appears, as expectable due to the absence of any shear reinforcement, that the inclined shear crack started forming close to the maximum load and rapidly propagated, the slab retaining not any significant further shear resistance hence after.

Also in this case the measured shear deformation is one, and ever up to two orders of magnitude higher than deformation measured in other non – consolidated and h = 12 +5 cm consolidated samples.

4.4 Diagram of Load – Delamination of the different layers in the consolidated slabs

In the following section the behaviour will be explained of the floor slabs with respect to the delamination of the two layers, the reinforced concrete "original" one and the lightweight concrete in the top of the consolidated floor slabs. The occurrence of this effect depends on the quality of the connection through the chemical adhesive defined previously in the section 3 of this document.

FLOOR SLAB Nº 1. CONSOLIDATED. H= 12 + 5 cm

Figure 50 shows the relation between the load applied by the actuator and the delamination between the two layers of concrete which has been measured by the two deflectometers located at opposite corners of the specimen as it was explained in the description of the experimental activity.

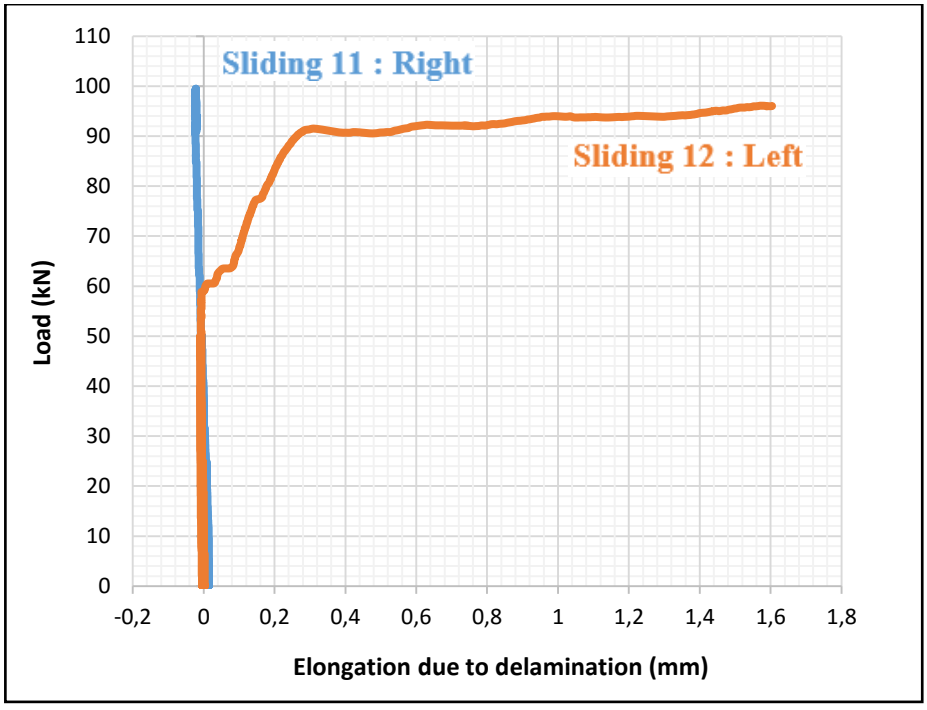

Figure 50. Graph of the load – elongation due to delamination for the first floor slab of h = 12 + 5 cm. (Source: Own design)

For this first specimen of h = 12 + 5 cm the crack appeared in the side where the instruments to measure the delamination were placed; delamination started at a total applied load of about 60 KN and then gradually progressed until catastrophic propagation in correspondence of failure maximum measured deformation was equal to 1,6 mm.

FLOOR SLAB Nº 2. CONSOLIDATED. H= 12 + 5 cm

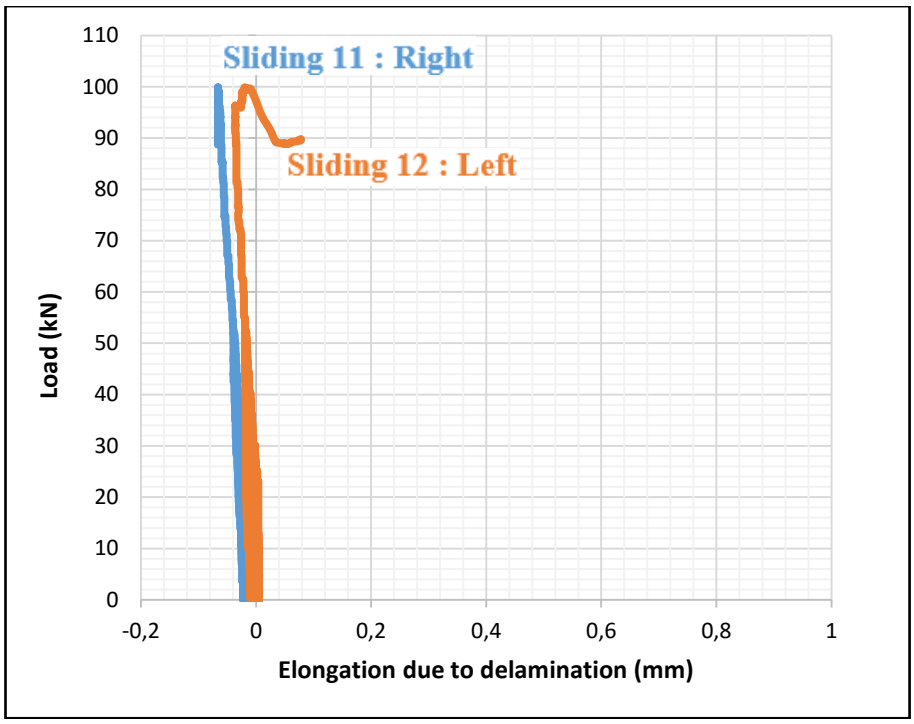

Figure 51. Graph of the load – elongation due to delamination for the second floor slab of h = 12 + 5 cm. (Source: Own design)

In this case, the delamination crack also appeared on the side were measuring instruments were located. The interlayer delamination deformation was negligible most likely due to randomness of local efficacy of the chemical connection.

FLOOR SLAB Nº 1. CONSOLIDATED. H= 16 + 5 cm

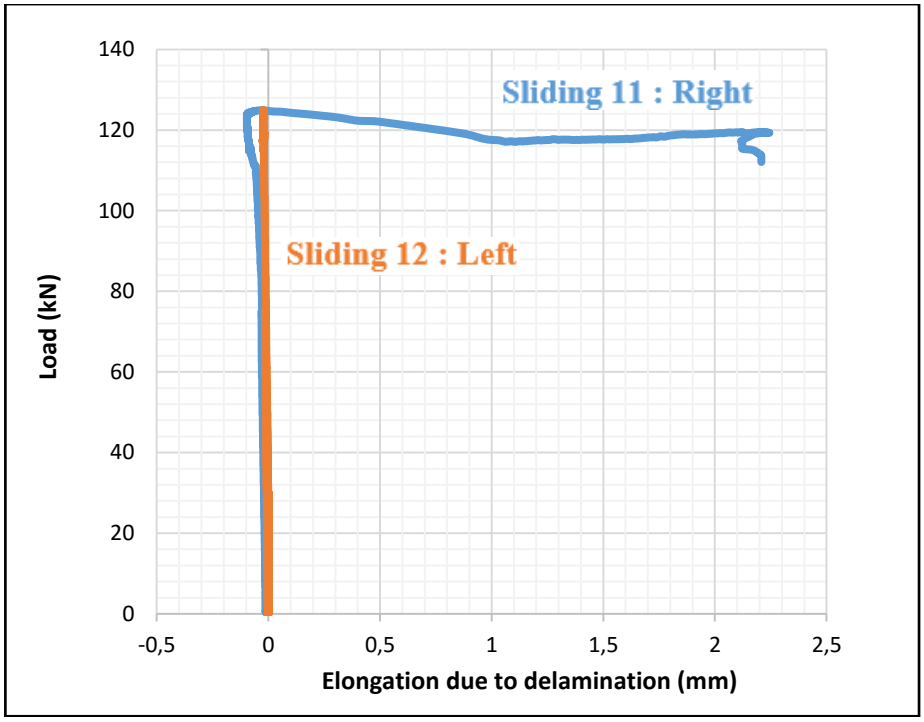

Figure 52. Graph of the load – elongation due to delamination for the first floor slab of h = 16 + 5 cm. (Source: Own design)

As for the previously examined h = 12 + 5 cm consolidated slab, delamination started close to the failure load and underwent abrupt propagation, up to similar maximum values.

FLOOR SLAB Nº 2. CONSOLIDATED. H= 16 + 5 cm

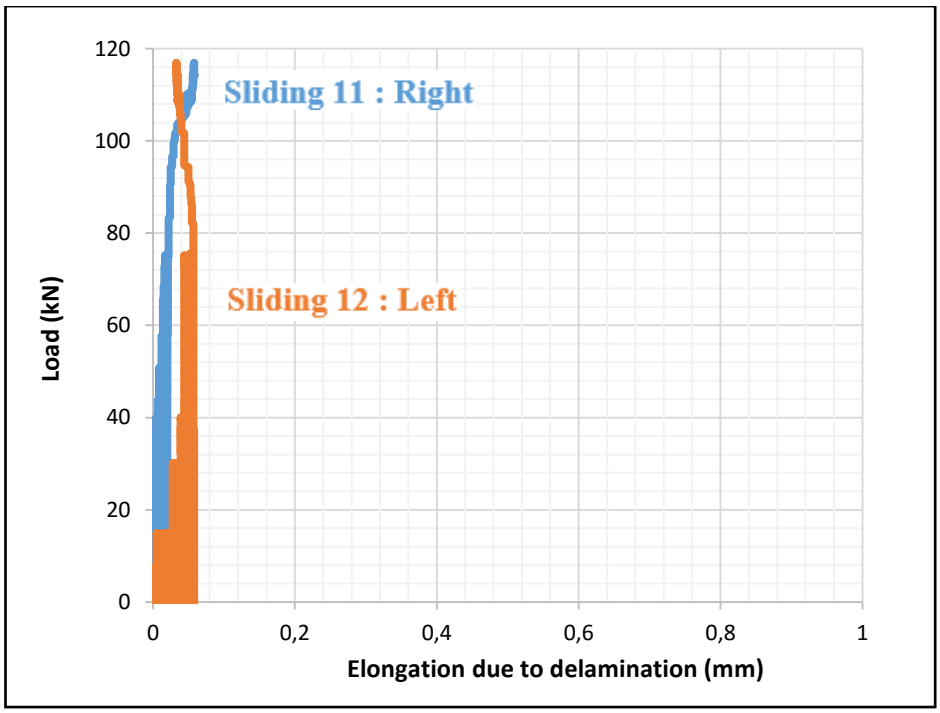

Figure 53. Graph of the load – elongation due to delamination for the second floor slab of h = 16 + 5 cm. (Source: Own design)

Finally, as for the second consolidated specimen, the interlayer delamination deflection was negligible most likely due to randomness of local efficacy of the chemical connection.

4.5 Engineering interpretation of the results

Once the results of the laboratory tests have been collected and presented in graphs with their respective comments, an engineering interpretation will be carried out.

The purpose of this analysis is twofold:

- For non – consolidated slabs, the reliability of the mock – ups as realized, in achieving the target design – anticipated capacity, will be checked.
- For consolidated slabs, the reliability of the composite action will be checked through the application of conventional "monolithic section" design approaches.

4.5.1 ULS verification

To satisfy the Ultimate Limit State, a structure must not collapse when it is subjected to the peak design load for which it was designed. A structure is deemed to satisfy the ULS criteria if all factored bending, shear and tensile or compressive stresses are below the factored resistance calculated for the section under consideration.
Whereas the Magnification Factor is used for the loads, and Reduction Factor for the resistance of members. The limit state criteria can also be set in terms of stress rather than load. Thus the structural element being analysed is shown to be safe when the factored "Magnified" loads are less than their factored "Reduced" resistance.
Complying with the design criteria of the ULS is considered as the minimum requirement (among other additional demands), to provide the proper structural safety.

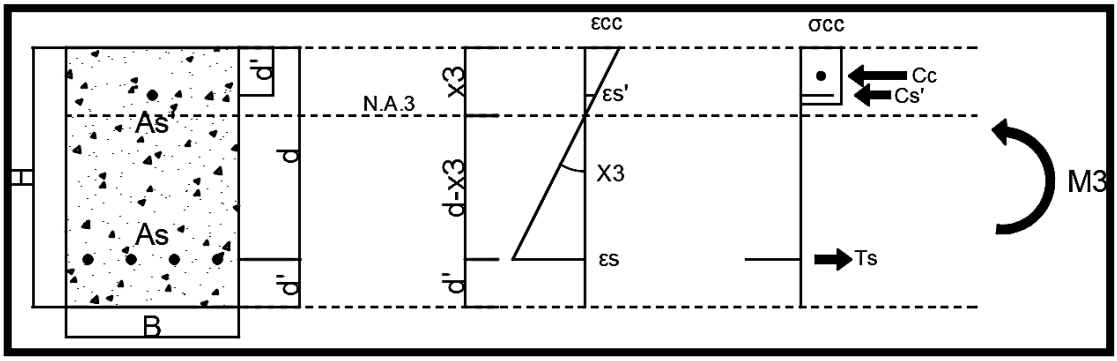

Figure 54. Design of the ULS stage of strains – stresses. (Source: Own design)

$$M_{Rd} = As * f_y * (d - 0{,}4 * x_3) \; + As' * f_y * (d' - 0{,}4 * x_3) \;\; > \;\; M_{Ed}$$

For the case at issue, the ULS considered will make reference to the bending failure of the maximum bending moment cross section, from which the Ultimate Design Load related to bending failure can be calculated as:

$$P_{Rd} = \frac{2 * MRd}{\frac{1{,}85}{2} - 0{,}25}$$

Moreover the ULS in shear should also be checked:

For the analysis of the shear action on each specimen, reference is made to a diagram as the one shown in the following figure, in which the structure is conceived as a doubly-reinforced beam, supported at the ends and subjected to two concentrated loads.

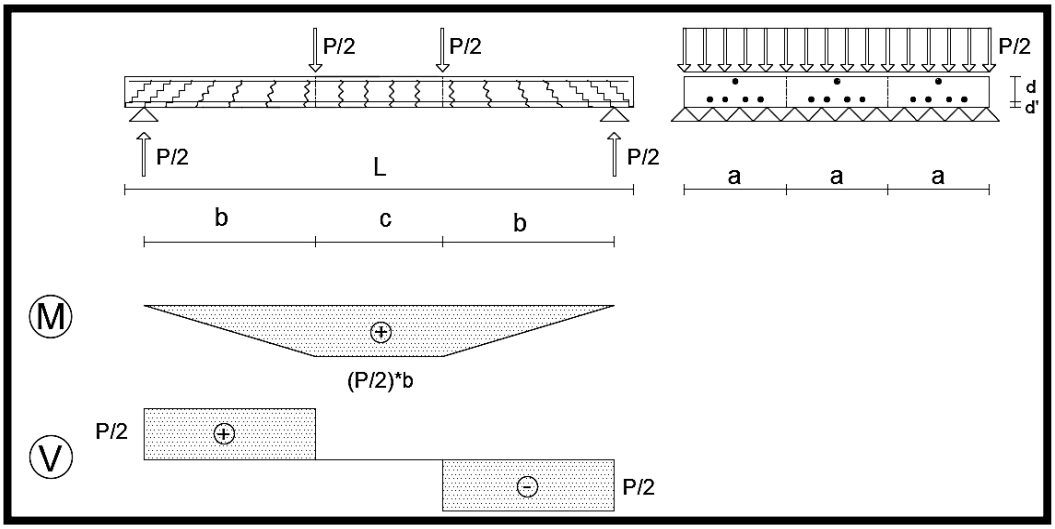

Figure 55. Design of the slab with the loads and cracks suffered by bending and shear actions. (Source: Own design)

When the load applied by the actuator is increased the appearance of some cracks can be observed at the bottom part of the specimen with vertical direction. Upon increasing the applied load, is expected that:

- In the central part of the specimen the crack will develop always in vertical direction.
- Instead, near to the supports the cracks progressively undergo an inclination up to an angle of 45º, where Vmax is reached.

The shear behaviour of a doubly-reinforced beam without transverse reinforcement can be analysed according to the "comb model". It conceives the cracked beam due to shear action as formed by a compressed area, corresponding to the rib of the comb, and the elements included between the cracks, corresponding to the comb teeth, inclined at 45 ° with respect to the rib. The teeth of the comb are crossing the lower longitudinal reinforcement (Figure 56).

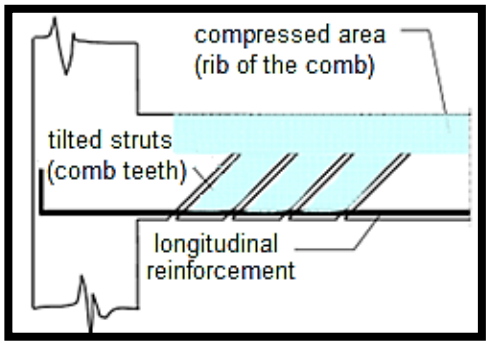

Figure 56. Diagram of the "comb model". (Source: tecnica delle costruzione)

Analysing the set of stresses acting on a single element of the comb it, can be seen that it is subjected to bending and axial force, due to the delamination force Q, generated by the variation of the bending moment. This combined bending gives rise, in the tooth, at a section (AB), to tensile stresses, which brings the concrete to failure (Figure 57).

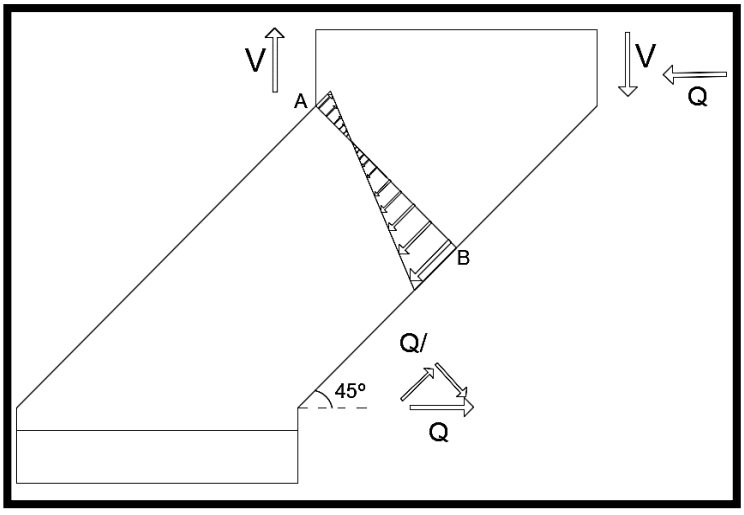

Figure 57. Diagram of the stresses of one teeth of the comb. (Source: Own design)

This model is used for the analysis of the shear action in longitudinally reinforced beams, but without stirrups, as in the case herein considered.

Can be calculated as:

$$V_{Rd} = 0{,}25 * b * d * f_{ctd}$$

According to this model, it is necessary to make some considerations on this formula, in order to make it more complete and take into account all the variables:

1. The longitudinal bars are not only subjected to tensile stress but also to a small contribution of shear action. The dowel action consists in the fact that the bar, due to the shear, exerts an extra pressure on the concrete and the concrete cover reacts exerting upward forces. When the stress reaches the tensile strength of concrete appears the first crack and the limit of the dowel action capacity is attained. The factor that takes into account the dowel action is: $(1{,}2 + 40\rho_s)$ with $\rho_s = \frac{A_s}{b*d}$
   For the consolidated floor slabs we have to consider (d + h') due to it is the distance from the tensile reinforcement to the top of the section.
2. A further contribution is provided by the aggregate interlock, or roughness of the crack opening (delamination prevented), defined as: $(1{,}6 - d)$. With d in meters.

   The equation, which incorporates all the aforementioned contributions, and is going to be used is:

$$V_{Rd} = 0{,}25 * b * d * f_{ctd} * (1{,}2 + 40\rho_s) * (1{,}6 - d)$$

The following table represents all the characteristics and the values which have been obtained on the computations of the theoretical values of all the floor slabs and shows how the laboratory tests give a good result in reference to the ULS of bending moment M_{Rd} and shear action V_{Rd}:

	NON - CONSOLIDATED SLABS		CONSOLIDATED SLABS	
	H = 0,12 m	**H = 0,16 m**	**H = 0,12+0,05 m**	**H = 0,16+0,05 m**
b (m)	**0,35**	**0,4**	**0,35**	**0,4**
d (m)	**0,1**	**0,14**	**0,1 + 0,05**	**0,14 + 0,05**
f_{ck}	**16**	**16**	**16 & 20**	**16 & 20**
f_{cd} **(MPa)**	$0.85 * \frac{16}{1,5} = 9,07$	$0.85 * \frac{16}{1,5} = 9,07$	$0.85 * \frac{16}{1,5} = 9,07$ $0.85 * \frac{20}{1,5} = 11,33$	$0.85 * \frac{16}{1,5} = 9,07$ $0.85 * \frac{20}{1,5} = 11,33$
f_{cm} **(MPa)**	$16 + 8 = 24$	$16 + 8 = 24$	$16 + 8 = 24$ $20 + 8 = 28$	$16 + 8 = 24$ $20 + 8 = 28$
As (m2)	**471,24 * 10-6**	**508,94 * 10-6**	**471,24 * 10-6**	**508,94 * 10-6**
As' (m2)	**848,2 * 10-7**	**848,2 * 10-7**	**848,2 * 10-7**	**848,2 * 10-7**
f_{yk}	**315**	**315**	**315**	**315**
f_{yd} **(MPa)**	$\frac{315}{1,15} = 273,91$	$\frac{315}{1,15} = 273,91$	$\frac{315}{1,15} = 273,91$	$\frac{315}{1,5} = 273,91$
f_{ym} **(MPa)**	$315 * 1,35 =$ $= 425,25$	$315 * 1,35 =$ $= 425,25$	$315 * 1,35 =$ $= 425,25$	$315 * 1,35 =$ $= 425,25$
ρ_s	**0,013464**	**0,009088**	**0,008976**	**0,006696579**
MRd (KN m)	**17,71**	**25,93**	**31,88**	**39,90**
PRd , M (KN)	**52,48**	**76,82**	**94,46**	**118,21**
VRd (KN)	**56,96**	**78,40**	**82,08**	**107,31**
PRd, V (KN)	**113,92**	**156,80**	**164,15**	**214,62**
PRd, Lab (KN)	**46 / 47**	**72 / 72**	**99 / 99**	**125 / 116**

Table 6. Results of the theoretical solution for the ULS of MRd and VRd, V. (Source: Own design)

For the non – consolidated slabs, as it can be observed from the Table 6, the values of the PRd, M and PRd, V are really different so, as it was explained before, the failure was reached in the central part due to bending which was the expected failure.

On the other hand, for the consolidated slabs, the first cracks appeared also in the central part due to bending but, after the delamination between the existing floor and the topping, the shear failure became critical as it can be observed from Table 6, where the values of the PRd, M of the consolidated slabs and PRd, V of the non – consolidated ones are closer.

Herein the graphs will be presented of load vs vertical deflection with the introduction of the P_{cr}, P_y and P_{ult} to compare the experimental results with the theoretical ones:

	H = 12 cm	H = 16 cm	H = 12 + 5 cm	H = 16 + 5 cm
Pcr (KN) (fctm)	8,21	15,92	16,79	26,90
Py (KN) (fcm-fym)	52,28	75,03	90,71	116,33
Pmax, M (KN) (fcd-fyd)	33,73	52,31	60,05	81,20
Pmax, M (KN) (fck-fyk)	38,77	60,79	69,91	93,94
Pmax, M (KN) (fcm-fym)	53,32	76,82	94,46	118,21
PLab (KN)	46 / 47	72 / 72	99 / 99	125 / 116

Table 7. Values of the loads depending on the stage and the stresses. (Source: Own design)

A good reliability of the design prediction appears. This means, in the case of consolidated slabs, that the connection between the topping and the subgrade, as due to the employed resin, is effective so that a composite "monolithic" section assumption can be used in the design.

This is also supported by the fact that delamination always occurred close to the failure and hence the employed chemical connector is effective in guaranteeing the monolithic composite action of the section up to the development of its full flexural capacity.

NON - CONSOLIDATED FLOOR SLAB. H= 12 cm

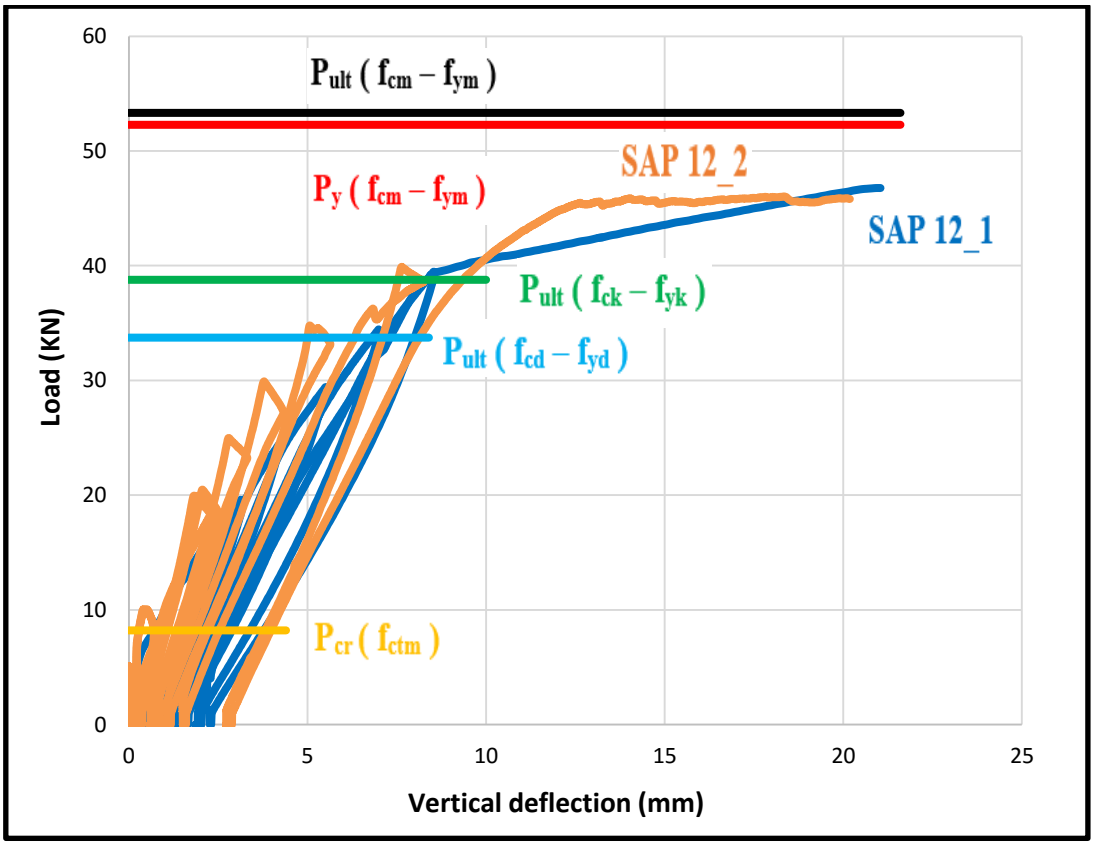

Figure 58. Diagram Load vs Deflection with characteristic loads 1. (Source: Own design)

NON - CONSOLIDATED FLOOR SLAB. H= 16 cm

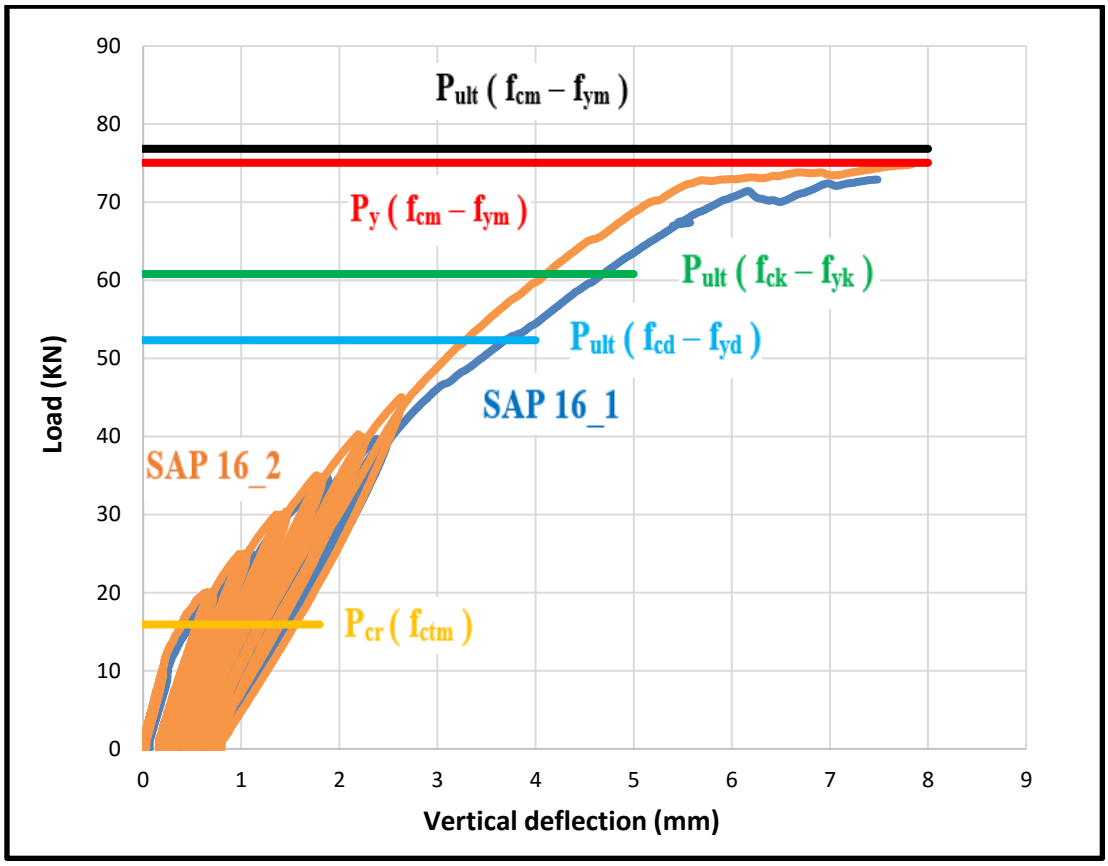

Figure 59. Diagram Load vs Deflection with characteristic loads 2. (Source: Own design)

CONSOLIDATED FLOOR SLAB. H= 12 + 5 cm

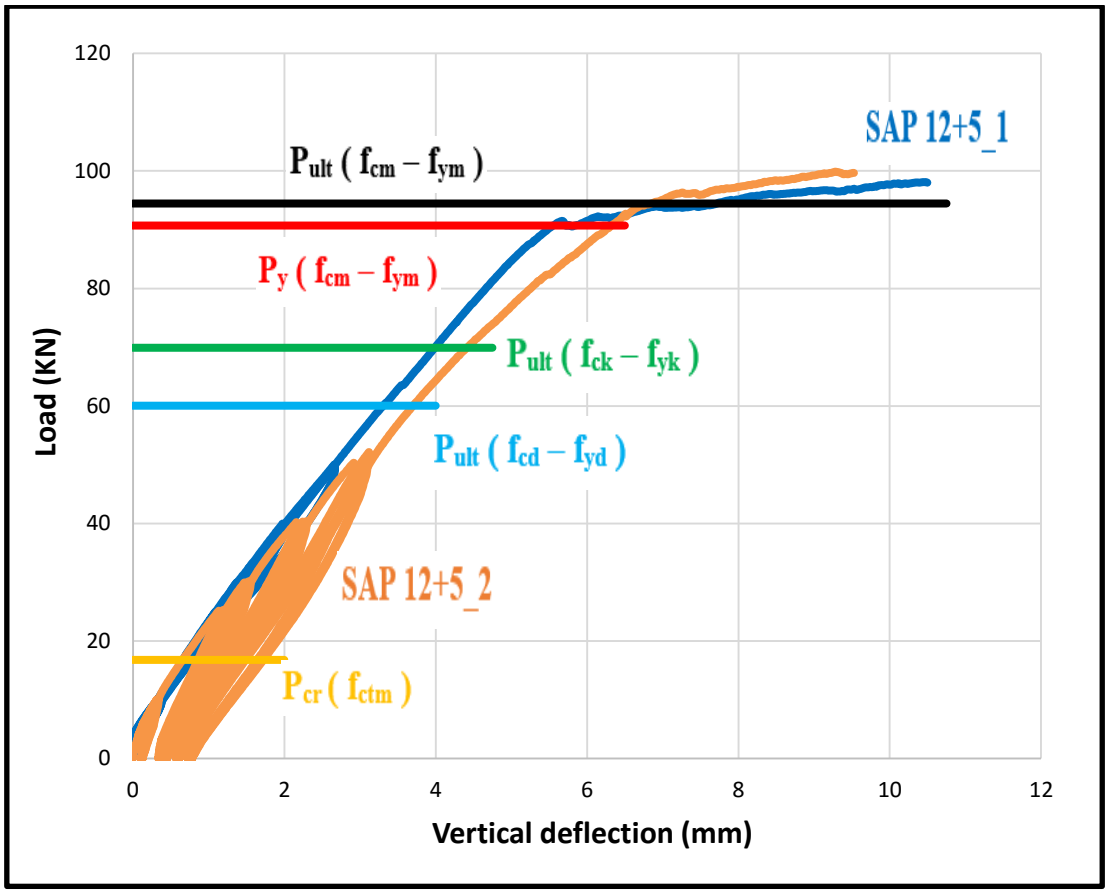

Figure 60. Diagram Load vs Deflection with characteristic loads 3. (Source: Own design)

CONSOLIDATED FLOOR SLAB. H= 16 + 5 cm

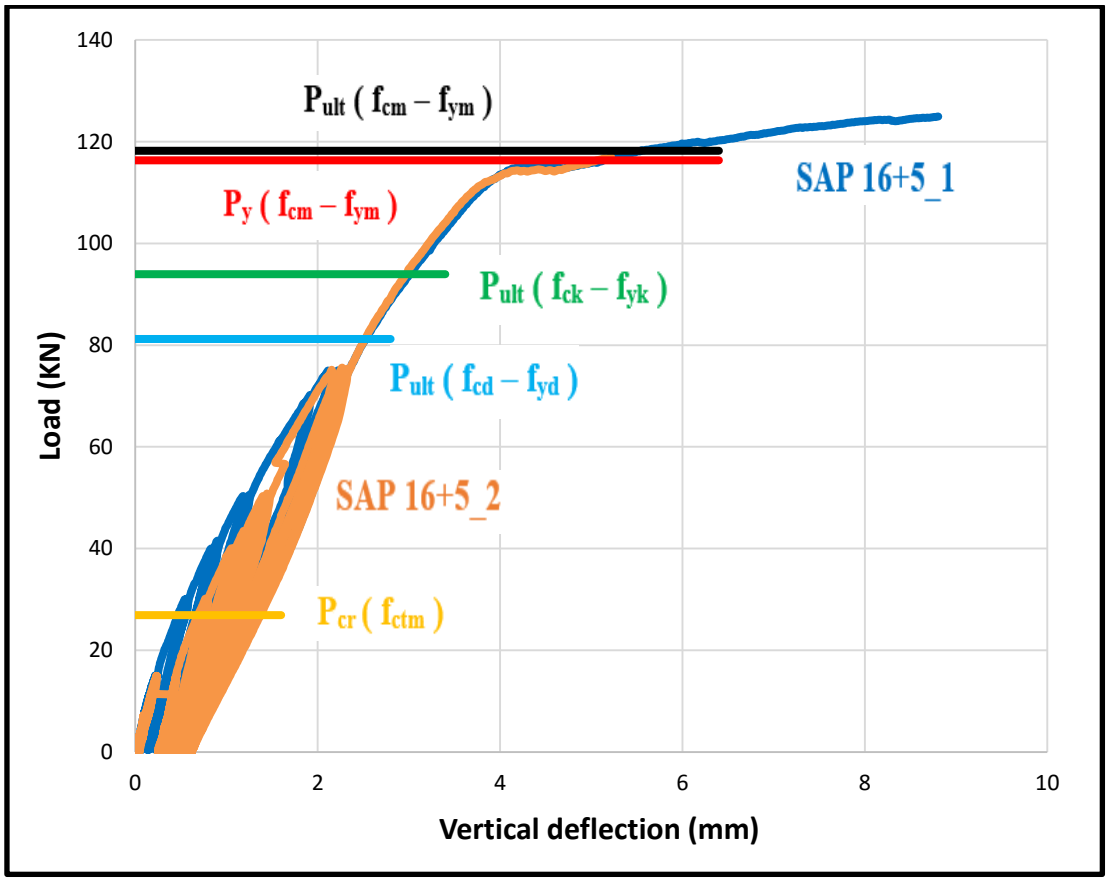

Figure 61. Diagram Load vs Deflection with characteristic loads 4. (Source: Own design)

4.5.2 Tangential action (Jourawski theory)

In this section the shear action will be studied and therefore the shear stresses acting on the floor slabs, using the theory of the Jourawski, which allows to predict the distribution of the shear stresses along the total height of the cross section.

The purpose of this computation is to check whether the level of shear stress obtained at the interface at the onset of delamination is compliant with the strength of the epoxy as measured.

A simplification of the cross section will be done to simplify the computations as it can be observed in Figures 62 and 63, considering also the slab as a simply supported beam with the contribution of the shear in the specimen due to reactions which are equal to P/2 in order to check the values of the tangential effects along the cross section for the different slabs.

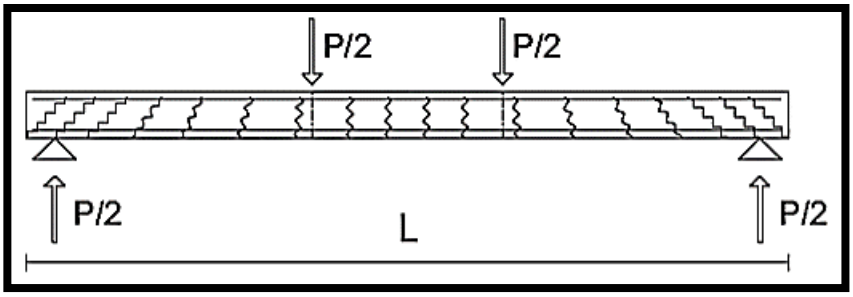

Figure 62. Design of the simply supported model used for the design. (Source: Own design)

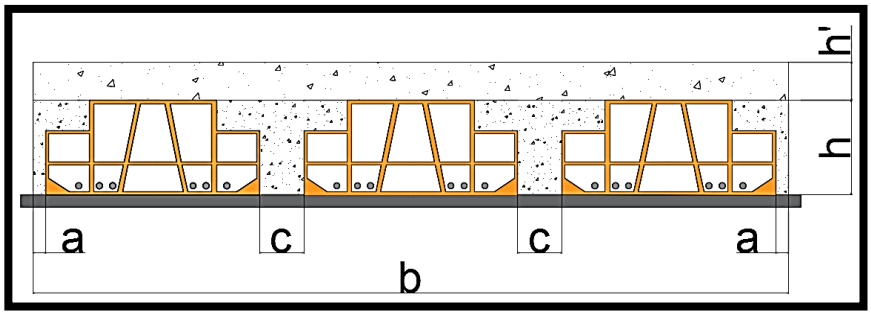

Figure 63. Design of the cross section of the consolidated floor slab. (Source: Own design)

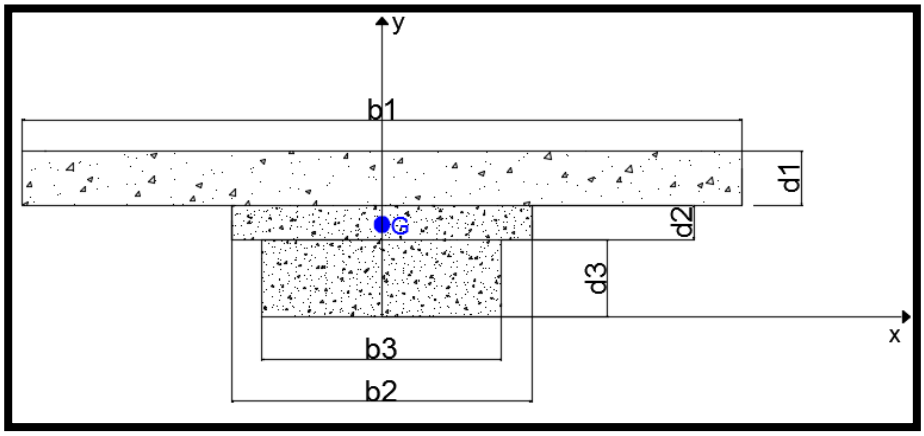

Figure 64. Design of the cross section of the consolidated floor slab used for the design. (Source: Own design)

It is possible to compute the tangential stresses using the Jourawski's formula:

$$\tau = \frac{V\ S'i}{bi\ Ii}$$

First of all, the centre of gravity of the whole section has been computed, using a reference system in which the x axis coincides with the lower edge of the section and the y axis with the corresponding axis of symmetry.

Then is computed the product between the i-th area and its centre of gravity as:

$$A_i * y_{Gi} = (b_1 * d_1) * y_{G1} + (b_2 * d_2) * y_{G2} + (b_3 * d_3) * y_{G3}$$

The total area is:

$$A_{tot} = (b_1 * d_1) + (b_2 * d_2) + (b_3 * d_3)$$

And the centre of gravity:

$$y_G = \sum_{i=1}^{n} \frac{A_i * y_{Gi}}{A_{tot}}$$

The following step is to compute the inertia. The values of the inertia corresponding to the ULS computed for the diagram of moment – curvature of the following section will be used, being the value for the floor slab of h = 12 + 5 cm, I = $3*10^{-4}$ m^4 and for the h = 16 + 5 cm, I = $5{,}89*10^{-4}$ m^4.

Once the centre of gravity has been computed and also the inertia of the whole section, the value of S'_i should be obtained, which is the static moment of the portion of cross section which is under a horizontal line created if the cross section is crossed from bottom to top. Four different stages are going to be defined, coinciding with the four lines Si in the Figure 65.

Once all the necessary values to obtain the tangential stresses will be computed, seven points will be the characteristic points to obtain the diagram of stresses (as it can be se seen also in Figure 65), being the important values to check those corresponding to the connection between the existing floor and the topping where the resin was placed:

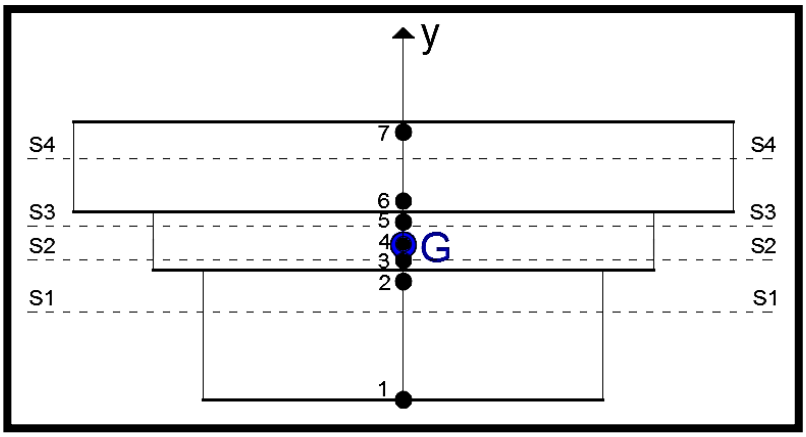

Figure 65. Position of the 4 stages and the 7 points of interest (Source: Own design)

The S'_i values are calculated as follows:

$$S1 = (b3 * y1) * \left(yg - \frac{y1}{2}\right)$$

$$with\ y1 = 0\ to\ y1 = d3$$

$$S2 = S1\ (y1 = d3) + (b2 * y2) * \left(yg - \frac{y2}{2}\right)$$

$$with\ y2 = 0\ to\ y2 = (yg - d3)$$

$$S3 = S2\left(y2 = (yg - d3)\right) + (b2 * y3) * \left(d3 + d2 - \frac{y3}{2} - yg\right)$$

$$with\ y3 = 0\ to\ y3 = (d3 + d2 - yg)$$

$$S4 = S3\ (y3 = (d3 + d2 - yg)) + (b1 * y4) * \left(d3 + d2 + d1 - \frac{y4}{2} - yg\right)$$

$$with\ y4 = 0\ to\ y4 = (d3 + d2 + d1 - yg)$$

For the computation of the tangential stress with the Jourawski's formula it is considered a value of shear action equal to: $V = \frac{P_{ULS}}{2}$, which will vary for the specimens:

- V 12 + 5 _ 1 = 99 KN / 2 = 49,5 KN
- V 12 + 5 _ 2 = 99 KN / 2 = 49,5 KN
- V 16 + 5 _ 1 = 126 KN / 2 = 62,5 KN
- V 16 + 5 _ 2 = 116 KN / 2 = 58 KN

Finally, the graph is then designed taking into account the condition in which the value of S'_i is equal to 0 at the ends of the cross section.

FLOOR SLAB Nº 1. CONSOLIDATED. H= 12 + 5 cm

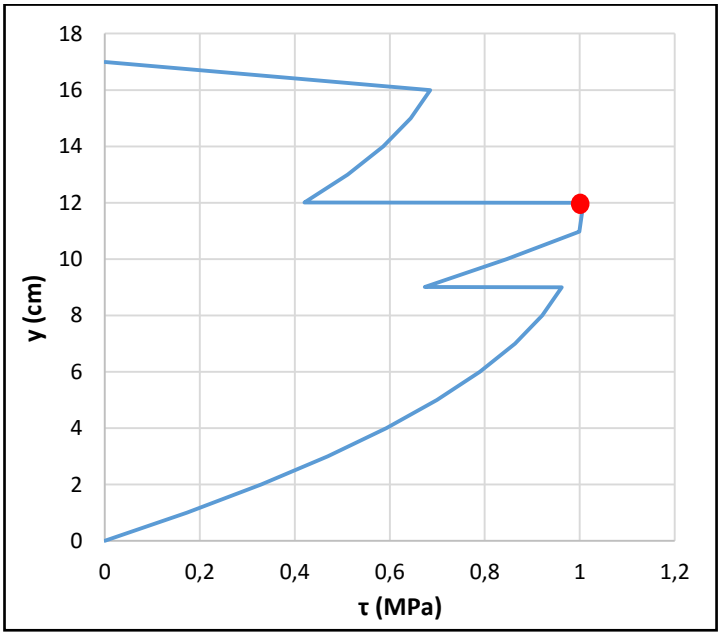

Figure 66. Distribution of tangential stresses for the first slab of h = 12 + 5 cm (Source: Own design)

FLOOR SLAB Nº 2. CONSOLIDATED. H= 12 + 5 cm

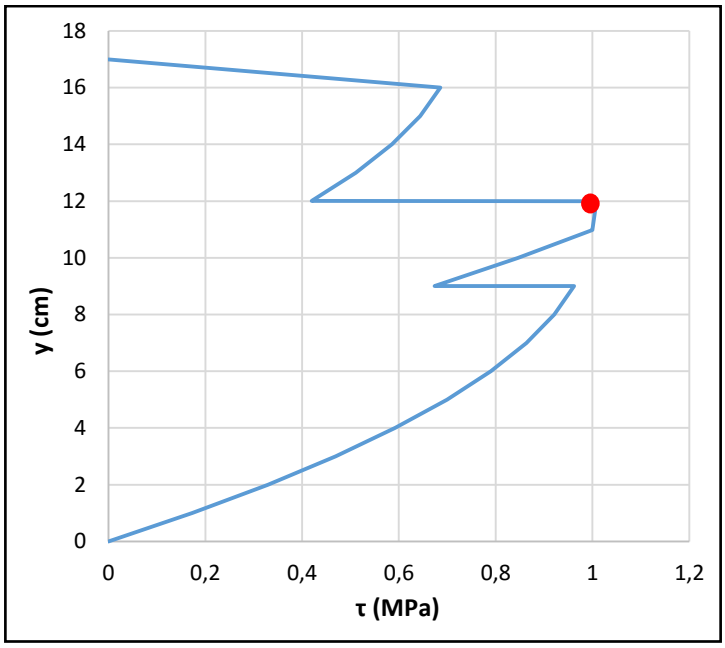

Figure 67. Distribution of tangential stresses for the second slab of h = 12 + 5 cm (Source: Own design)

FLOOR SLAB Nº 1. CONSOLIDATED. H= 16 + 5 cm

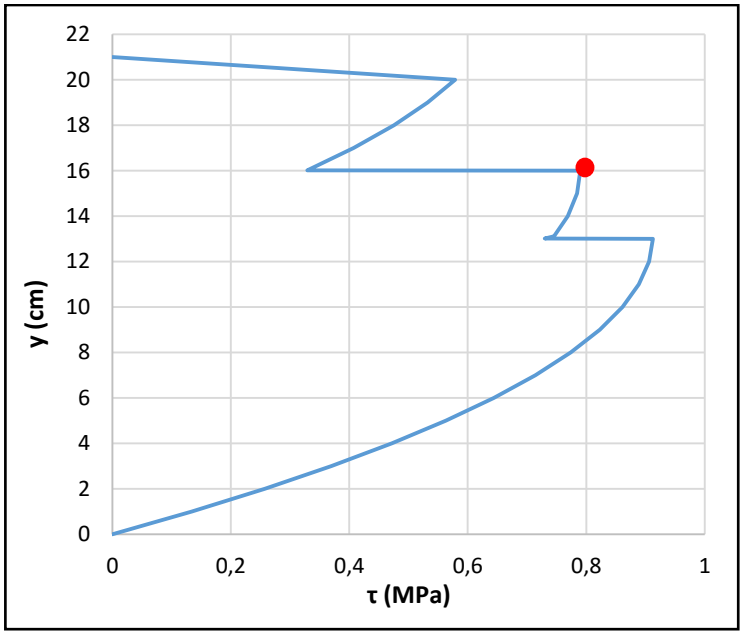

Figure 68. Distribution of tangential stresses for the first slab of h = 16 + 5 cm (Source: Own design)

FLOOR SLAB Nº 2. CONSOLIDATED. H= 16 + 5 cm

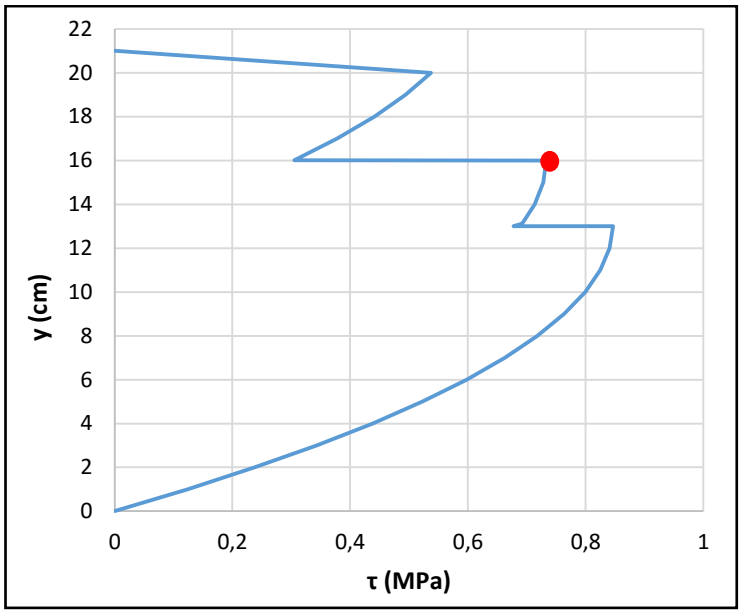

Figure 69. Distribution of tangential stresses for the second slab of h = 16 + 5 cm (Source: Own design)

It can be observed from all the graphs a similar distribution of the values of the tangential stresses when the static moment S'i vary from bottom to top, having a maximum value for the h = 12 + 5 cm where the resin is located and for the h = 16 + 5 cm in the variation of section at y = d3.

It can also be appreciated how, for a value of y = (d3 + d2) cm which corresponds to the connection of the normal and lightweight concrete (red point), a similar value of the shear resistance is obtained as for the value related with the resin resistance of the previous project explained in the section 3.2.2 (Table 1 and Figure 15).

The average tangential strength of the experimental project showed that: the larger the "glued surface", the lower the strength; so this is coherent with the results obtained in this investigation in which τ is 1 MPa for the h = 12 + 5 cm and around 0,75 MPa for the h = 16 + 5.

This is coherent with the strength values of the resin, experimentally determined and reported in section 3, also considering an unavoidable size effect inborn in the transition to full – scale mock – ups.

4.6 Diagram of Bending Moment – Curvature

In order to complete the engineering interpretation of the experimental tests, the construction of moment – curvature diagrams of typical cross sections has been performed as hereafter detailed.

4.6.1 Stage I. L-el behaviour in tension and compression until concrete cracks in tension. L-el contribution of the reinforcement

If the cross section of the middle span in which an external moment is applied is analysed, this section deforms complying with the Bernoulli's hypothesis with a linear strain diagram. In order to maintain the internal equilibrium of the section, this deformation is related to internal stresses.

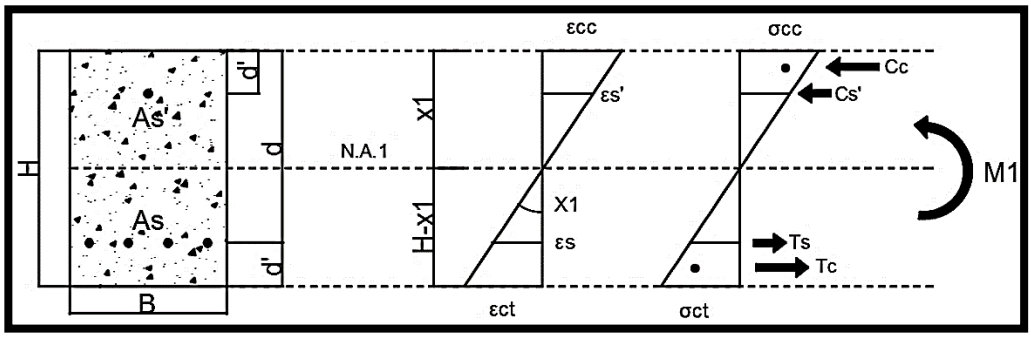

Figure 70. Design of the first stage of strains – stresses. (Source: Own design)

Before and after the deformation this section remains totally straight. In this case, as the external bending moment has a small value, the contribution of the concrete in tension has to be taken into account.

With reference to the standards, this tensile contribution has a maximum of:

$$f_{ctm,fl} = max\left\{(1{,}6 - \frac{h\,(mm)}{1000} * 0.3 * {f_{ck}}^{\frac{2}{3}};\ 0.3 * {f_{ck}}^{\frac{2}{3}}\right\}$$

So, until the maximum computed tensile stress will be lower than this value, the crack will not appear. For this stage, the details of the whole section of concrete and the contribution of the reinforcement can be used.

First of all the distance of the N.A.$_1$ from the more compressed fibre x_1 can be computed as:

$$x_1 = \frac{b * \mathrm{h} * \frac{\mathrm{h}}{2} + \alpha_E * \mathrm{As} * \mathrm{d} + \alpha_E * \mathrm{As}' * \mathrm{d}'}{\mathrm{b} * \mathrm{h} + \alpha_E * \mathrm{As} + \alpha_E * \mathrm{As}'}$$

Being α_E the ratio between the Young Modulus of the steel and the Young Modulus of the concrete.
From this point and using ε_{ct} computed with the linear elastic relation, the other strains can be solved by relation of triangles and also the stress resultants:

$$\sigma_{ct} = fctm, fl \qquad \varepsilon_{ct} = \frac{fctm, fl}{Ec}$$

$$\sigma_{cc} = Ec * \varepsilon_{cc} \qquad \varepsilon_{cc} = \frac{\varepsilon_{ct}}{(h - x_1)} * (x_1)$$

$$\sigma_s = Es * \varepsilon_s \qquad \varepsilon_s = \frac{\varepsilon_{ct}}{(h - x_1)} * (d - x_1)$$

$$\sigma_s{}' = Es * \varepsilon_s{}' \qquad \varepsilon_s{}' = \frac{\varepsilon_{ct}}{(h - x_1)} * (x_1 - d')$$

$$So \quad C_{cc} = \frac{1}{2} * \sigma_{cc} * x_1 * b \qquad T_c = \frac{1}{2} * \sigma_{ct} * (h - x_1) * b$$

$$And \quad C_{s\prime} = As' * \sigma s' \qquad T_s = As * \sigma_s$$

In order to apply the Mohr's theorem the inertia and the bending moment should be computed as:

$$I_1\ (m^4) = \frac{b * {x_1}^3}{3} + \frac{b * (h - x_1)^3}{3} + \alpha_E * As * (d - x_1)^2 + \alpha_E * As' * (x_1 - d')^2$$

$$M_1(KN\ m) = M_{cr} = T_c * \left(\frac{2}{3} * (h - x_1)\right) + T_s * (d - x_1) + C_{cc} * \left(\frac{2}{3} * x_1\right) + C_{s\prime} * (x_1 - d')$$

The curvature of the uncracked section under the cracking moment can be written as:

$$\chi_1 = \frac{M_1}{Ec * I_1} \left(\frac{1}{m}\right)$$

From the diagram of strains it can observed also that the curvature can be computed as the ratio between the maximum strain and the distance between this value and the neutral axis:

$$\chi_1 = \frac{\varepsilon_{ct}}{x_1}\left(\frac{1}{m}\right)$$

This point represents the limit of the first linear elastic branch of the moment curvature diagram. On the other hand, the corresponding "cracking load" can be calculated as:

$$P_1(KN) = P_{cr} = \frac{2 * M_1(KN\ m)}{0{,}675\ (m)}$$

4.6.2 Stage Ia. L-el behaviour in compression just after the crack of concrete in tension. L-el contribution of the reinforcement

After the first stage a second representative part of the moment – curvature diagram can be defined, in which, for the same value of the bending moment, the cracked section assumption is used. As the concrete is cracked in tension, a variation on the height of concrete should be taken into account, reducing the value of the inertia and therefore increasing the curvature.

From the stage II, the distance of the N.A.$_2$ from the more compressed fibre x_2 can be computed as:

$$As * \alpha_E = \frac{1}{2} * \frac{b * {x_2}^2}{d - x_2} + As' * \alpha_E * \frac{x_2 - d'}{d - x_2}$$

The new values of the inertia and curvature are:

$$I_{1a}\ (m^4) = \frac{b * {x_2}^3}{3} + \alpha_E * As * (d - x_2)^2 + \alpha_E * As' * (x_2 - d')^2$$

$$\chi_{1a} = \frac{M_1}{Ec * I_{1a}}\left(\frac{1}{m}\right)$$

4.6.3 Stage II. L-el behaviour in compression and concrete cracked in tension. Yielding of the reinforcement in tension

After the tensile strain and strength limits of concrete have been reached, concrete cracks and the portion of the cross section below the neutral axis does not any longer contribute to the cross section resistance.

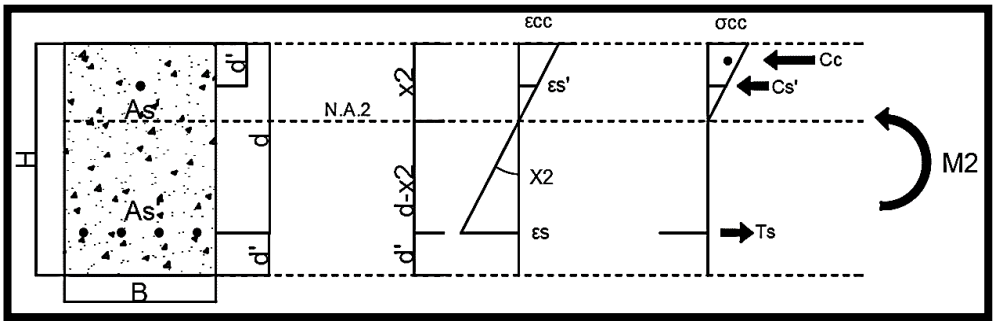

Figure 71. Design of the second stage of strains – stresses. (Source: Own design)

Onward, a second stage of the moment - curvature diagram is followed, which will end with the yielding of steel $\sigma_s = f_y$. Along this branch, the compressed concrete may show a linear elastic behaviour or may enter into its non - linear behaviour.

From Figure 71 can be observed the tensile and compressive strength areas are different but still has to be guaranteed the horizontal equilibrium of the resultant forces.

With regard to the stresses, the tensile part corresponds to a resultant force $Ts = fy * A_s$, applied at d from the top; and for the compressive part, a linear distribution of stresses in concrete is first of all hypothesized.

In this stage two limits were checked, one for the steel and another one for concrete, and both were fulfilled:

$$\varepsilon_s \leq \varepsilon_y = \frac{\mathrm{f}_y}{\mathrm{Es}} \qquad \varepsilon_{cc} \leq \frac{0{,}45 * \mathrm{f}_c}{\mathrm{Ec}}$$

- For the concrete stresses: fc could be equal to: $f_{ck}, f_{cd} = 0{,}85 * \frac{f_{ck}}{1{,}5}$ or $f_{cm} = f_{ck} + 8$, depending on the use.
- For the steel stresses: f_y could be equal to: $f_{yk}, f_{yd} = \frac{fyk}{1{,}15}$ or $f_{ym} = 1{,}35 * f_{yk}$, depending on the use.

Under the assumption of a linear elastic behaviour of compressed concrete, the equilibrium equation will be written as follows:

$$As * (Es * \varepsilon_s) = \frac{1}{2} * (Ec * \varepsilon_{cc}) * b * x_2 + As' * (Es * \varepsilon_s{}')$$

$$As * (Es * \varepsilon_s) = \frac{1}{2} * Ec * \left(\frac{\varepsilon_s}{d - x_2} * x_2\right) * b * x_2 + As' * Es * \left(\frac{\varepsilon_s}{d - x_2} * (x_2 - d')\right)$$

$$As * \alpha_E = \frac{1}{2} * \frac{b * {x_2}^2}{d - x_2} + As' * \alpha_E * \frac{x_2 - d'}{d - x_2}$$

The stress resultants can be computed as:

$$\sigma_s = \mathrm{f}_y \qquad \varepsilon_s = \ \varepsilon_y = \frac{\mathrm{f}_y}{\mathrm{Es}}$$

$$\sigma_{cc} = Ec * \varepsilon_{cc} \qquad \varepsilon_{cc} = \frac{\varepsilon_s}{(d - x_2)} * (x_2)$$

$$\sigma_s{}' = Es * \varepsilon_s{}' \qquad \varepsilon_s{}' = \frac{\varepsilon_s}{(d - x_2)} * (x_2 - d')$$

$$\text{So} \quad C_c = \tfrac{1}{2} * Ec * \varepsilon_{cc} * x_2 * b$$

$$And \quad C_{s\prime} = As' * \varepsilon_s{}' * Es \qquad T_s = \ As * \mathrm{f}_y$$

In order to apply the Mohr's theorem, the new values of inertia and bending moment should be calculated as:

$$I_2\ (m^4) = \frac{b * {x_2}^3}{3} + \alpha_E * As * (d - x_2)^2 + \alpha_E * As' * (x_2 - d')^2$$

$$M_2(KN\ m) = M_y = T_s * \left(d - \frac{x_2}{3}\right) - C_{s\prime} * \left(d' - \frac{x_2}{3}\right)$$

As for the first stage the curvature can be computed using the Mohr's analogy but now with a reduced inertia I_2 and a higher value of the moment applied My so a higher curvature will be obtained:

$$\chi_2 = \frac{M_2}{Ec * I_2}\left(\frac{1}{m}\right)$$

From the diagram of strains can be seen also that the curvature can be computed as the tangent between the maximum strain of the tensile reinforcement and the distance between this value and the neutral axis:

$$\chi_2 = \frac{\varepsilon_s}{(d - x_2)} \left(\frac{1}{m}\right)$$

The yielding load can be calculated as:

$$P_2(KN) = P_y = \frac{2 * M_2(KN\ m)}{0{,}675\ (m)}$$

4.6.4 Stage III. Ultimate strength of concrete to pure bending

Finally the third stage corresponds to the ultimate limit state in which concrete cannot bear more load and has reached its ultimate strain in compression. This limit correspond to a value of the strain of concrete in compression due to pure bending of: $\varepsilon_{cc} = \varepsilon_{cu} = 3{,}5‰$.

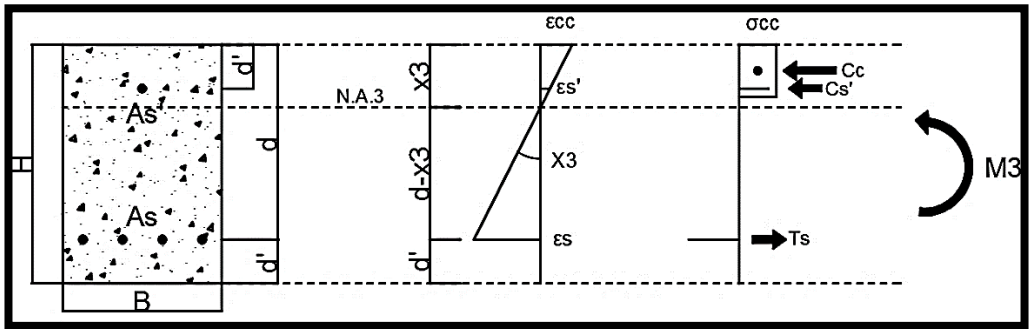

Figure 72. Design of the last stage of strains – stresses. (Source: Own design)

The values of the strains can be computed by triangular relations and also the resultants of the stresses, but now a different distribution of the compressive diagram of concrete should be used. In this case, a rectangular section of concrete with height: $0{,}8 * x_3$.

- For the concrete stresses: fc could be equal to: f_{ck}, $f_{cd} = 0{,}85 * \frac{f_{ck}}{1{,}5}$ or $f_{cm} = f_{ck} + 8$, depending on the use.
- For the steel stresses: f_y could be equal to: f_{yk}, $f_{yd} = \frac{fyk}{1{,}15}$ or $f_{ym} = 1{,}35 * f_{yk}$, depending on the use.

The value of the stress resultant of the concrete in compression is:

$$\sigma_{cc} = fc \qquad \varepsilon_{cc} = \varepsilon_{cu}$$

$$\text{So} \quad C_c = 0{,}8 * x_3 * f_c * b$$

While the values of the stress resultants of the reinforcement are:

$$\sigma_s = fy \qquad \varepsilon_s = \frac{\varepsilon_{cu}}{(x_3)} * (d - x_3)$$

$$\sigma_s{}' = Es * \varepsilon_s{}' \qquad \varepsilon_s{}' = \frac{\varepsilon_{cu}}{(x_3)} * (x_3 - d')$$

$$\text{So} \quad C_s{}' = As' * \varepsilon_s{}' * Es \qquad T_s = As * f_y$$

With those values the distance from the uppermost compressed fibre to the neutral axis x_3 can be computed as:

$$x_3 * 0{,}8 * f_c * \mathrm{b} = As * f_y + As' * \varepsilon_s{}'(x_3) * Es$$

As for this stage there is no more linear elastic behaviour, the Mohr's analogy cannot be used to compute the curvature so the strain diagram needs to be used:

$$\chi_3 = \frac{\varepsilon_{cu}}{x_3}\left(\frac{1}{m}\right)$$

Finally, the value of the bending moment can be calculated as before, using the values of x_3 and the new stress resultants:

$$M_3(KN\ m) = M_{ult} = T_s * (d - 0{,}4 * x_3) - C_s{}' * (d' - 0{,}4 * x_3)$$

The ultimate load can be finally computed as:

$$P_3(KN) = P_{ult} = \frac{2 * M_3(KN\ m)}{0{,}675\ (m)}$$

4.6.5 Effect of the consolidation in the computation of moment – curvature diagram

In order to introduce the effect of the consolidation in the computation of the moment – curvature diagram the same steps as before should be used with the diagrams of strains and stresses but with a new contribution which corresponds to the LWAC which provide the consolidation of the structure:

For the topping, some changes should be applied due to is used a LWAC:

- $E' = 22000 * \left(\frac{f_{cm'}}{10}\right)^{0,3} * \left(\frac{\rho}{2200}\right)^{2}, being\ \rho = 1400$

And also that the limit strain at the ultimate state should be multiplied by a reduction factor which will be:

- $\varepsilon_{cu}' = 0{,}0035 * \left(\frac{\rho}{2200}\right), being\ \rho = 1400$

Hereafter are going to be introduced the stages with their respective diagrams and modifications taking into account the new contributions due to the topping:

Stage I. L-el behaviour in tension and compression until concrete cracks in tension. L-el contribution of the reinforcement

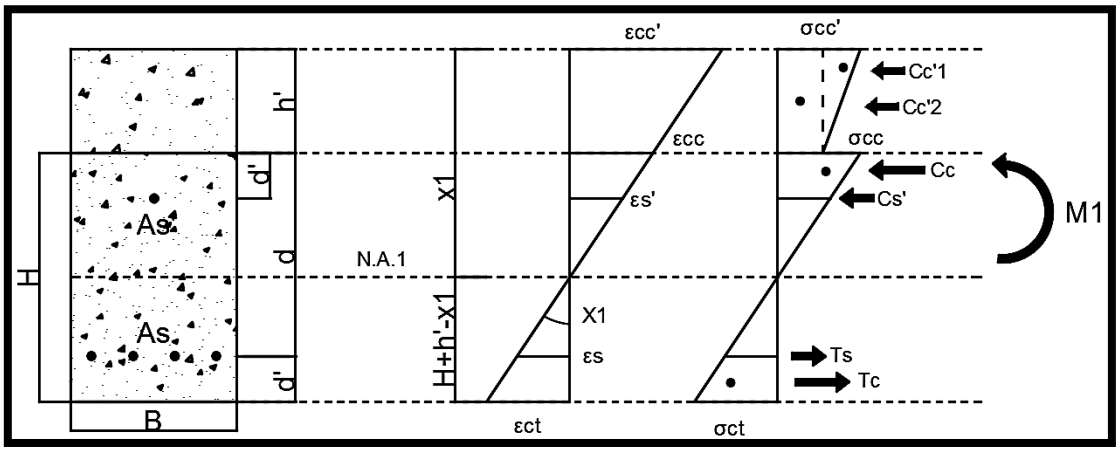

Figure 73. Design of the first stage of strains – stresses for the consolidated slab floor. (Source: Own design)

First of all the distance of the N.A.$_1$ from the more compressed fibre x_1 can be computed as:

$$x_1 = \frac{b * \mathrm{h} * (\frac{\mathrm{h}}{2} + \mathrm{h}') + \alpha_{C-C'} * \mathrm{b}' * \mathrm{h}' * \left(\frac{\mathrm{h}'}{2}\right) + \alpha_E * \mathrm{As} * (\mathrm{d} + \mathrm{h}') + \alpha_E * \mathrm{As}' * (\mathrm{d}' + \mathrm{h}')}{\mathrm{b} * \mathrm{h} + \alpha_{C-C'} * \mathrm{b}' * \mathrm{h}' + \alpha_E * \mathrm{As} + \alpha_E * \mathrm{As}'}$$

Being α_E the ratio between the Young Modulus of the steel and the Young Modulus of the concrete and $\alpha_{C-C}{}'$, the ratio between the Young Modulus of the LWAC and the Young Modulus of the normal concrete.

From this point and using ε_{ct} computed with the linear elastic relation, the other strains can be solved by relation of triangles and also the stress resultants:

$$f_{ctm,fl} = max\left\{(1{,}6 - \frac{h\,(mm)}{1000} * 0.3 * {f_{ck}}^{\frac{2}{3}};\ 0.3 * {f_{ck}}^{\frac{2}{3}}\right\}$$

$$\sigma_{ct} = fctm, fl \qquad \varepsilon_{ct} = \frac{fctm, fl}{Ec}$$

$$\sigma_{cc} = Ec * \varepsilon_{cc} \qquad \varepsilon_{cc} = \frac{\varepsilon_{ct}}{(h + h' - x_1)} * (x_1 - h')$$

$$\sigma_{cc\prime 1} = Ec' * \varepsilon_{cc\prime} \qquad \varepsilon_{cc\prime} = \frac{\varepsilon_{ct}}{(h + h' - x_1)} * (x_1)$$

$$\sigma_{cc\prime 2} = Ec' * \varepsilon_{cc} \qquad \varepsilon_{cc} = \frac{\varepsilon_{ct}}{(h + h' - x_1)} * (x_1 - h')$$

$$\sigma_s = Es * \varepsilon_s \qquad \varepsilon_s = \frac{\varepsilon_{ct}}{(h + h' - x_1)} * (d + h' - x_1)$$

$$\sigma_s{}' = Es * \varepsilon_s{}' \qquad \varepsilon_s{}' = \frac{\varepsilon_{ct}}{(h + h' - x_1)} * (h' - d' - x_1)$$

$$So \quad C_{cc} = \frac{1}{2} * \sigma_{cc} * (x_1 - \mathrm{h}') * b \qquad T_c = \frac{1}{2} * \sigma_{ct} * (h + h' - x_1) * b$$

$$C_{cc\prime 1} = \frac{1}{2} * (\sigma_{cc'1} - \sigma_{cc'2}) * \mathrm{h}' * b' \qquad C_{cc'2} = \sigma_{cc} * \mathrm{h}' * b'$$

$$And \quad C_{s\prime} = As' * \sigma s' \qquad T_s = As * \sigma_s$$

In order to apply the Mohr's theorem the inertia and the bending moment should be computed as:

$$I_1\,(m^4) = \alpha_{C-C'} * \frac{b' * \mathrm{h}'^3}{12} + (\mathrm{b}' * \mathrm{h}') * \left(x_1 - \frac{\mathrm{h}'}{2}\right)^2 + \frac{b * \mathrm{h}^3}{12} + (\mathrm{b} * \mathrm{h}) * \left(\frac{\mathrm{h}}{2} + h' - x_1\right)^2$$
$$+ \alpha_E * As * (d + h' - x_1)^2 + \alpha_E * As' * (h' + d' - x_1)^2$$

$$M_1(KN\,m) = M_{cr} = T_c * \left(\frac{2}{3} * (h + h' - x_1)\right) + T_s * (d + h' - x_1) + T_{s'} * (\mathrm{h}' + \mathrm{d}' - x_1)$$
$$+ C_{cc} * \left(\frac{2}{3} * (x_1 - h')\right) + C_{cc2} * \left(x_1 - \frac{\mathrm{h}'}{2}\right) + C_{cc1} * \left(\frac{2}{3} * (x_1 - h')\right)$$

The curvature of the uncracked section under the cracking moment can be written as:

$$\chi_1 = \frac{M_1}{Ec * I_1}\left(\frac{1}{m}\right)$$

From the diagram of strains it can observed also that the curvature can be computed as the ratio between the maximum strain and the distance between this value and the neutral axis:

$$\chi_1 = \frac{\varepsilon_{ct}}{h + h' - x_1}\left(\frac{1}{m}\right)$$

This point represents the limit of the first linear elastic branch of the moment curvature diagram. On the other hand, the corresponding "cracking load" can be calculated as:

$$P_1(KN) = P_{cr} = \frac{2 * M_1(KN\,m)}{0{,}675\ (m)}$$

Stage Ia. L-el behaviour in compression just after the crack of concrete in tension. L-el contribution of the reinforcement

From the stage II, the distance of the N.A.$_2$ from the more compressed fibre x_2 can be computed as:

$$As * \alpha_{c'-s} = \frac{1}{2} * \frac{b' * {x_2}^2}{d + h' - x_2} + As' * \alpha_{c'-s} * \frac{h' + d' - x_2}{d + h' - x_2}$$

The new values of the inertia and curvature are:

$$I_{1a}\ (m^4) = \frac{b' * {x_2}^3}{3} + \alpha_{c'-s} * As * (d + h' - x_2)^2 + \alpha_{c'-s} * As' * (\mathrm{h}' + \mathrm{d}' - x_2)^2$$

$$\chi_{1a} = \frac{M_1}{Ec * I_{1a}} \left(\frac{1}{m}\right)$$

Being $\alpha'_{C\prime-S}$ the ratio between the Young Modulus of the steel and the Young Modulus of the LWAC.

Stage II. L-el behaviour in compression and concrete cracked in tension. Yielding of the reinforcement

A further assumption is made: the neutral axis is within the thickness of the topping slab.

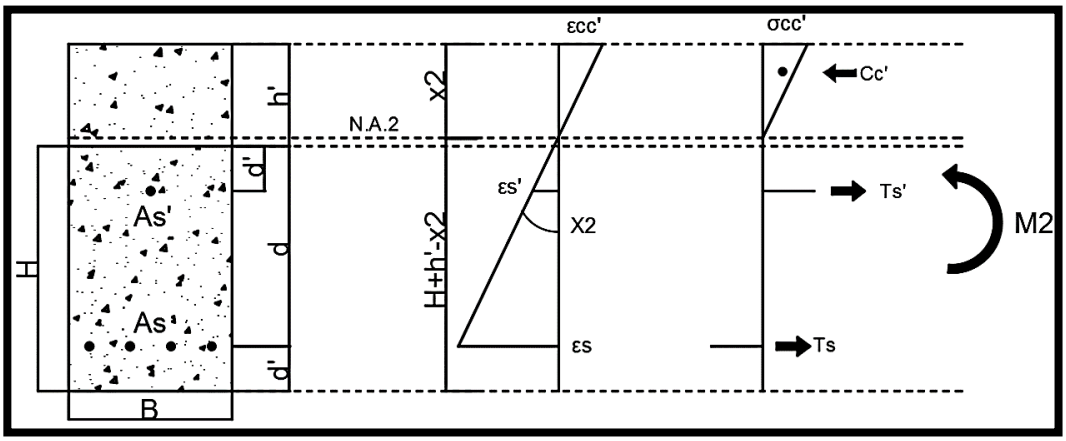

Figure 74. Design of the second stage of strains – stresses for the consolidated slab floor. (Source: Own design)

Onward, a second stage of the moment - curvature diagram is followed, which will end with the yielding of steel $\sigma_s = f_y$. Along this branch, the compressed LWAC may show a linear elastic behaviour or may enter into its non - linear behaviour.

In this stage two limits were checked, one for the steel and another one for concrete, and both were fulfilled:

$$\varepsilon_s \leq \varepsilon_y = \frac{\mathrm{f}_y}{\mathrm{Es}} \qquad \varepsilon_{cc} \leq \frac{0{,}45 * \mathrm{f}_c}{\mathrm{Ec}}$$

- For the concrete stresses: fc could be equal to: $f_{ck}, f_{cd} = 0{,}85 * \frac{f_{ck}}{1{,}5}$ or $f_{cm} = f_{ck} + 8$, depending on the use.
- For the steel stresses: f_y could be equal to: $f_{yk}, f_{yd} = \frac{fyk}{1{,}15}$ or $f_{ym} = 1{,}35 * f_{yk}$, depending on the use.

Under the assumption of a linear elastic behaviour of compressed LWAC concrete, the equilibrium equation will be written as follows:

$$As * \alpha_{c'-s} = \frac{1}{2} * \frac{b' * {x_2}^2}{d + h' - x_2} + As' * \alpha_{c'-s} * \frac{h' + d' - x_2}{d + h' - x_2}$$

The stress resultants can be computed as:

$$\sigma_s = \mathrm{f}_y \qquad \varepsilon_s = \varepsilon_y = \frac{\mathrm{f}_y}{\mathrm{Es}}$$

$$\sigma_{cc\prime} = Ec' * \varepsilon_{cc\prime} \qquad \varepsilon_{cc} = \frac{\varepsilon_s}{(d + h' - x_2)} * (x_2)$$

$$\sigma_s{}' = \mathrm{f}_y \qquad \varepsilon_s{}' = \frac{\varepsilon_s}{(d + h' - x_2)} * (h' + d' - x_2)$$

$$\text{So} \quad C_{c\prime} = \tfrac{1}{2} * Ec' * \varepsilon_{cc}{}' * x_2 * b'$$

$$And \quad T_s = As * \mathrm{f}_y \qquad T_s{}' = As' * \mathrm{f}_y$$

In order to apply the Mohr's theorem, the new values of inertia and bending moment should be calculated as:

$$I_2\ (m^4) = \frac{b' * {x_2}^3}{3} + \alpha_{c'-s} * As * (d + h' - x_2)^2 + \alpha_{c'-s} * As' * (\mathrm{h}' + \mathrm{d}' - x_2)^2$$

$$M_2(KN\ m) = M_y = T_s * \left(d + h' - \frac{x_2}{3}\right) - T_{s\prime} * \left(h' + d' - \frac{x_2}{3}\right)$$

As for the first stage the curvature can be computed using the Mohr's analogy but now with a reduced inertia I_2 and a higher value of the moment applied My so a higher curvature will be obtained:

$$\chi_2 = \frac{M_2}{Ec * I_2}\left(\frac{1}{m}\right)$$

From the diagram of strains can be seen also that the curvature can be computed as the tangent between the maximum strain of the tensile reinforcement and the distance between this value and the neutral axis:

$$\chi_2 = \frac{\varepsilon_s}{(d + h' - x_2)}\left(\frac{1}{m}\right)$$

The yielding load can be calculated as:

$$P_2(KN) = P_y = \frac{2 * M_2(KN\ m)}{0{,}675\ (m)}$$

Stage III. Ultimate strength of concrete to pure bending

Finally the third stage corresponds to the ultimate limit state in which concrete cannot bear more load and has reached its ultimate strain in compression. This limit correspond to a value of the strain of concrete in compression due to pure bending of:

$$\varepsilon_{cc\prime} = 0{,}0035 * \left(\frac{\rho}{2200}\right), being\ \rho = 1400$$

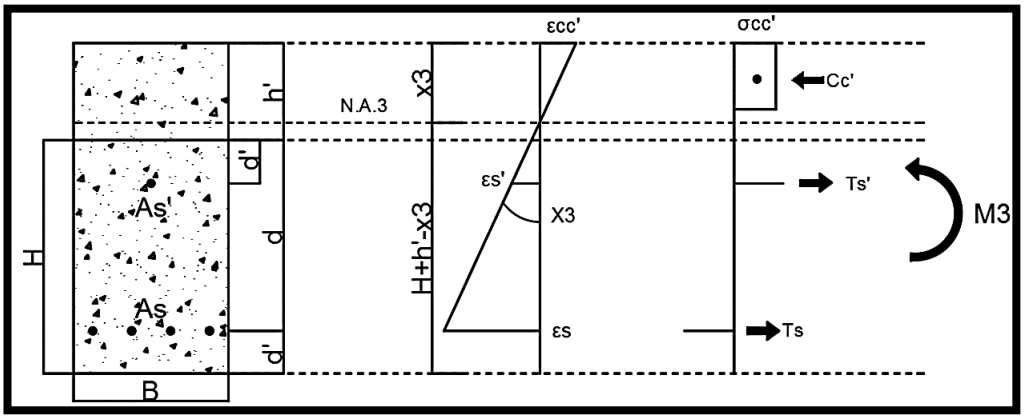

Figure 75. Design of the last stage of strains – stresses for the consolidated slab floor. (Source: Own design)

The values of the strains can be computed by triangular relations and also the resultants of the stresses, but now a different distribution of the compressive diagram of concrete should be used. In this case, a rectangular section of LWAC with height: $0{,}8 * x_3$.

- For the concrete stresses: fc could be equal to: $f_{ck,LWAC}$, $f_{cd,LWAC} = 0{,}85 * \frac{f_{ck,LWAC}}{1{,}5}$ or $f_{cm} = f_{ck,LWAC} + 8$, depending on the use.
- For the steel stresses: f_y could be equal to: f_{yk}, $f_{yd} = \frac{fyk}{1{,}15}$ or $f_{ym} = 1{,}35 * f_{yk}$, depending on the use.

The value of the stress resultant of the concrete in compression is:

$$\sigma_{cc\prime} = fc' \qquad \varepsilon_{cc}{}' = 0{,}0035 * \left(\frac{\rho}{2200}\right), being\ \rho = 1400$$

$$\text{So}\quad C_c = 0{,}8 * x_3 * f_c{}' * b\text{'}$$

While the values of the stress resultants of the reinforcement are:

$$\sigma_s = fy \qquad \varepsilon_s = \frac{\varepsilon_{cc}{}'}{(x_3)} * (d + h' - x_3)$$

$$\sigma_s{}' = fy \qquad \varepsilon_s{}' = \frac{\varepsilon_{cc}{}'}{(x_3)} * (h' + d' - x_3)$$

$$\text{So} \quad T_s = As * f_y \qquad T_s{}' = As' * f_y$$

With those values the distance from the uppermost compressed fibre to the neutral axis x_3 can be computed as:

$$x_3 * 0{,}8 * f_c{}' * \mathrm{b}' = As * f_y + As' * f_y$$

As for this stage there is no more linear elastic behaviour, the Mohr's analogy cannot be used to compute the curvature so the strain diagram needs to be used:

$$\chi_3 = \frac{\varepsilon_{cc}{}'}{x_3} \left(\frac{1}{m}\right)$$

Finally, the value of the bending moment can be calculated as before, using the values of x3 and the new stress resultants:

$$M_3(KN\ m) = M_{ult} = T_s * (d + h' - 0{,}4 * x_3) + T_s{}' * (h' + d' - 0{,}4 * x_3)$$

The ultimate load can be finally computed as:

$$P_3(KN) = P_{ult} = \frac{2 * M_3(KN\ m)}{0{,}675\ (m)}$$

4.6.6 Results of the test. Diagram moment – curvature

The Moment – Curvature diagrams for the different examined cross sections are shown hereafter and reflect the aforementioned assumptions.

FLOOR SLABS Nº 1 & 2. NON - CONSOLIDATED. H= 12 cm

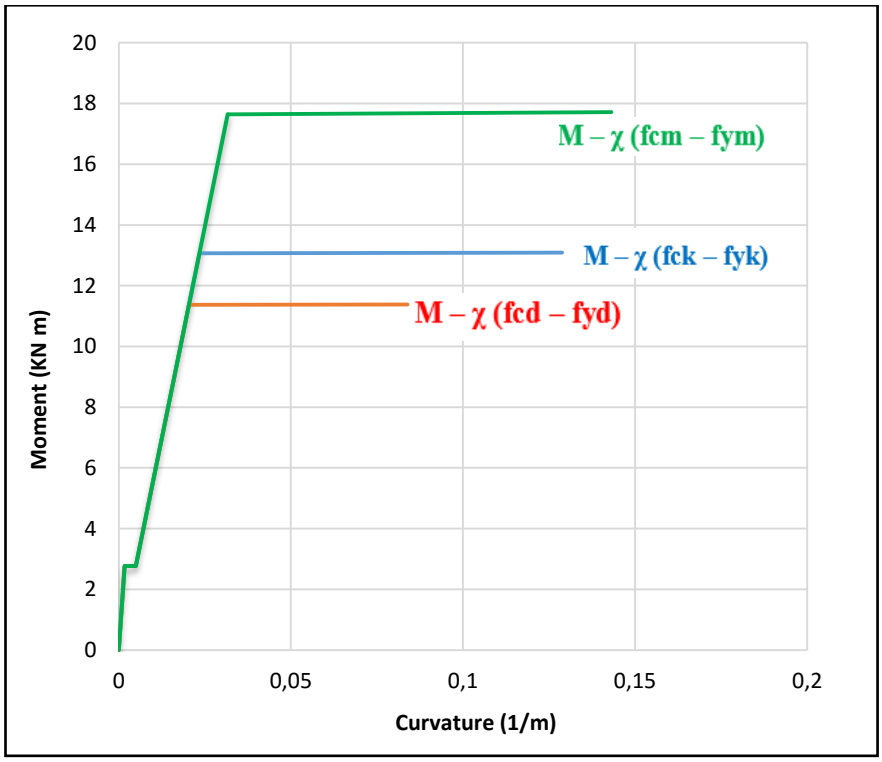

Figure 76. Diagram of moment – curvature for the non - consolidated slab of H = 12 cm (Source: Own design)

FLOOR SLABS Nº 3 & 4. NON - CONSOLIDATED. H= 16 cm

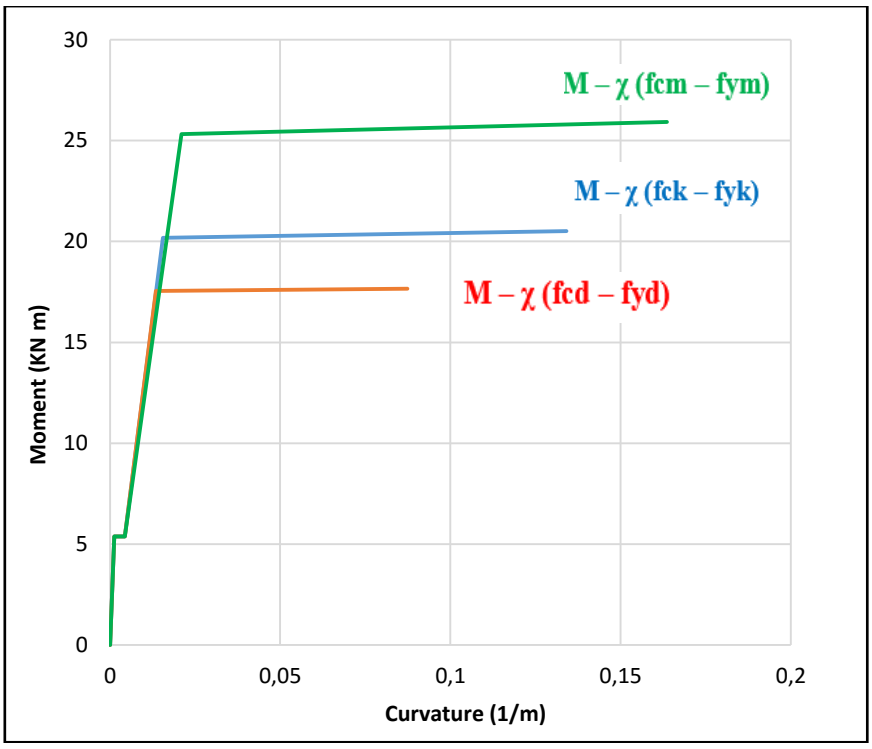

Figure 77. Diagram of moment – curvature for the non - consolidated slab of H = 16 cm (Source: Own design)

FLOOR SLABS Nº 1 & 2. CONSOLIDATED. H= 12 + 5 cm

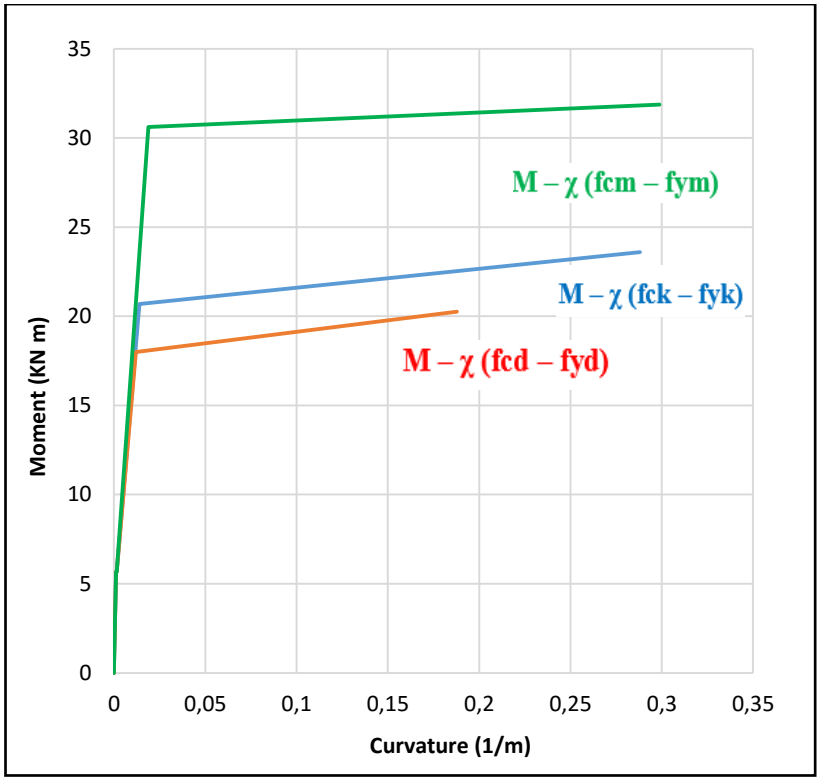

Figure 78. Diagram of moment – curvature for the consolidated slab of H = 12 + 5 cm (Source: Own design)

FLOOR SLABS Nº 3 & 4. CONSOLIDATED. H= 0,16 + 0,05 m

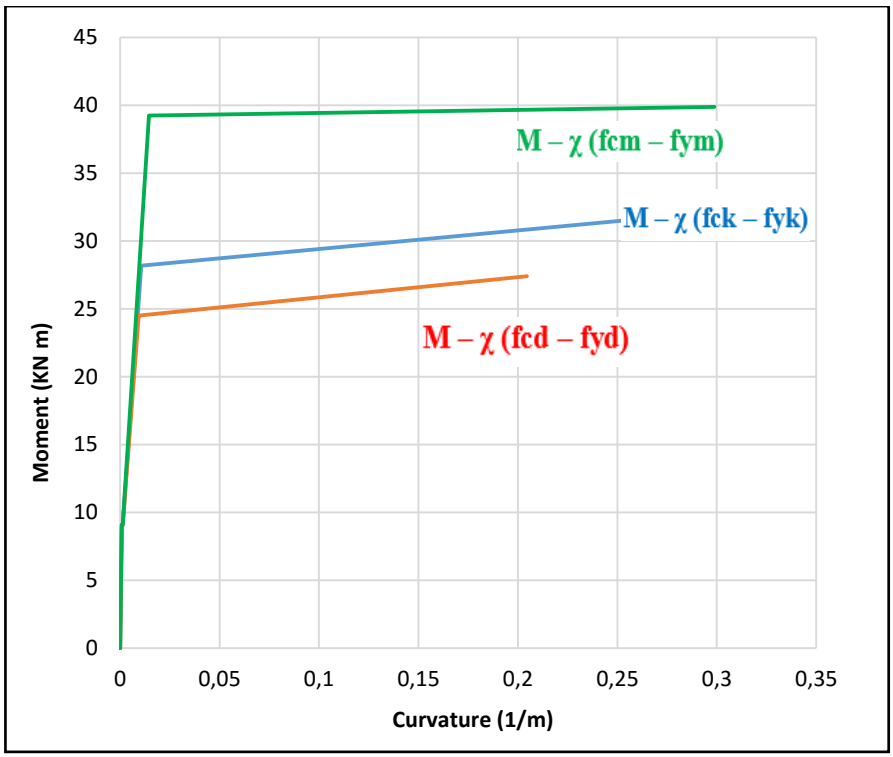

Figure 79. Diagram of moment – curvature for the consolidated slab of H = 16 + 5 cm (Source: Own design)

5

CONCLUSIONS - COMMENTS

This document has analysed the benefits, from a structural point, of the composite cooperating topping slab technique applied to floor slabs.
The analysis was based on eight loading test specimens on beam and block floor slabs (which dimensions were 2 m x 1,2 m and variable height), of whom the first four were non – consolidated and the others consolidated with the under investigation technique.

The non – consolidated floor slabs reached the failure due to bending as also confirmed by theoretical predictions.

The first two specimens of h = 12 cm had a higher ductility than the second pair of slabs of h = 16 cm, which reached failure just after the yielding. This is due to the steel reinforcement ratio $\rho_s = \frac{A_s}{b*d}$ is higher for the specimens of h = 12 cm, so they experimented a better contribution of the reinforcement, leading to a better ductility.

For the consolidated floor slabs, instead, the employed retrofitting technique provided good results, increasing the resistance of the consolidated floor slabs by about 100 % for the 12 cm high slabs and by nearly 70 % for the 16 cm high.

In those specimens, in correspondence of the maximum load, started a mechanism of delamination and failure. The shear failure was developed initially at 45º and then with a horizontal propagation following the perimeter of the original slab which was the only part of the composite section that actually resisted those stresses.

It can be noted that the ultimate load due to bending PRd, M of the consolidated specimens and the ultimate load due to shear PRd, V for the non – consolidated slabs differ by about 10%, thus making the two failure mechanisms to compete with each other.

For the consolidated slabs of h = 12 + 5 cm, the increase of bearing capacity to bending at mid span ensure that they become competitive against failure due to bending at mid span or due to shear at the supports.

Also for the consolidated slabs of h = 16 + 5 cm delamination occurs and some cracks due to shear failure appear but, the prevailing failure is always due to bending at mid span. However the resistance to shear is in general higher and therefore the relative deflection are lower.

The resin is therefore effective due to, when the delamination starts, in the area closer to the supports and consequently, the resistance to shear failure, it is only withstand by the original slab, while at mid span, the specimen works as a composite section. The employed chemical resin is effective in guaranteeing monolithic action of the composite cross section up to the development of its full flexural capacity.

Hereafter, are going to be introduced some diagrams in which it is shown the variation of the applied bending moment when the total length of the floor slab increases, assuming a load due to finishing's of 2 KN/ m^2, 2 KN/ m^2 due to partitions and 3 KN/m^2 due to variable loads with respect to the experimental results, the characteristic bending moment M_k (computed from the moment - curvature diagram with f_{ck} and f_{yk}) and the design bending moments M_d (computed from the moment - curvature diagram with f_{cd} and f_{yd}). These clearly highlight the benefits of the consolidation.

For the Serviceability Limit State (SLS), the maximum bending moment is computed as:

$$g_{k1} = 2{,}00\,\frac{kN}{m^2} \qquad Finishing$$

$$g_{k2} = 2{,}00\,\frac{kN}{m^2} \qquad Partitions$$

$$q_k = 3{,}00\,\frac{kN}{m^2} \qquad Variable\ load$$

The SLS moment applied is equal to:

$$M_{SLS} = \frac{(g_{k1} + g_{k2} + q_k) * L^2}{8}$$

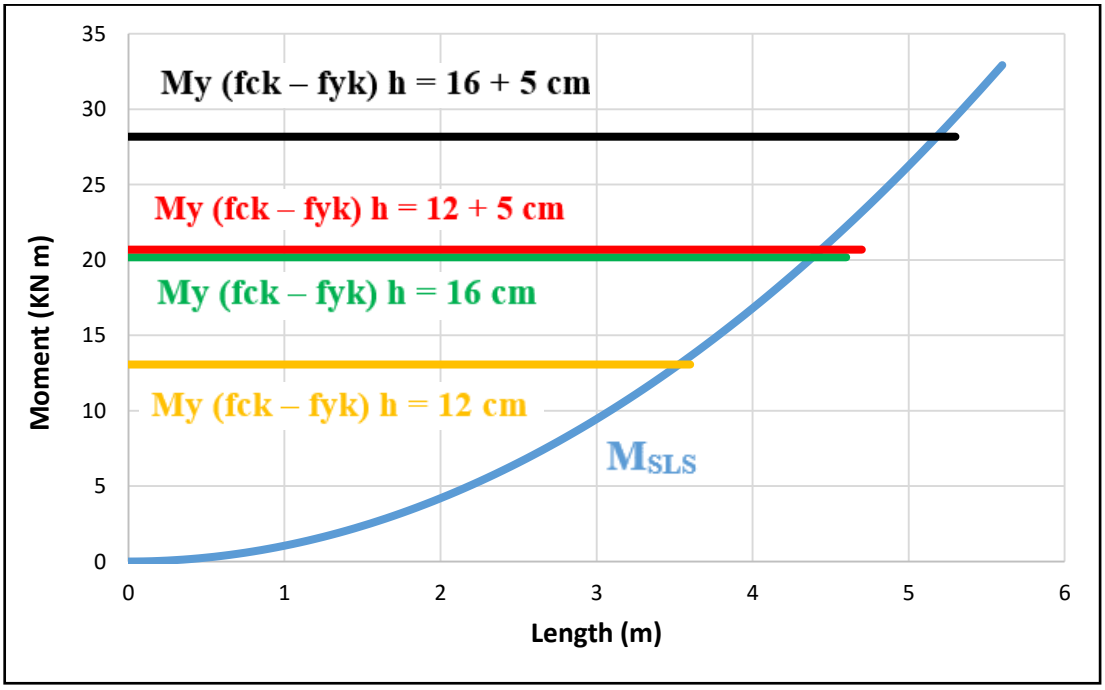

Figure 80. Diagram of SLS moment with respect to the ultimate moment of fck-fyk of each specimen (Source: Own design)

For the Ultimate Limit State (ULS) the maximum bending moment is computed as:

$$g_{k1} = 2{,}00\,\frac{kN}{m^2} \qquad g_{d1} = g_{k1} * 1{,}35 \qquad Finishings$$

$$g_{k2} = 2{,}00\,\frac{kN}{m^2} \qquad g_{d2} = g_{k2} * 1{,}5 \qquad Partitions$$

$$q_k = 3{,}00\,\frac{kN}{m^2} \qquad q_d = q_k * 1{,}5 \qquad Variable\ load$$

The SLS moment applied is equal to:

$$M_{SLU} = \frac{(g_{d1} + g_{d2} + q_d) * L^2}{8}$$

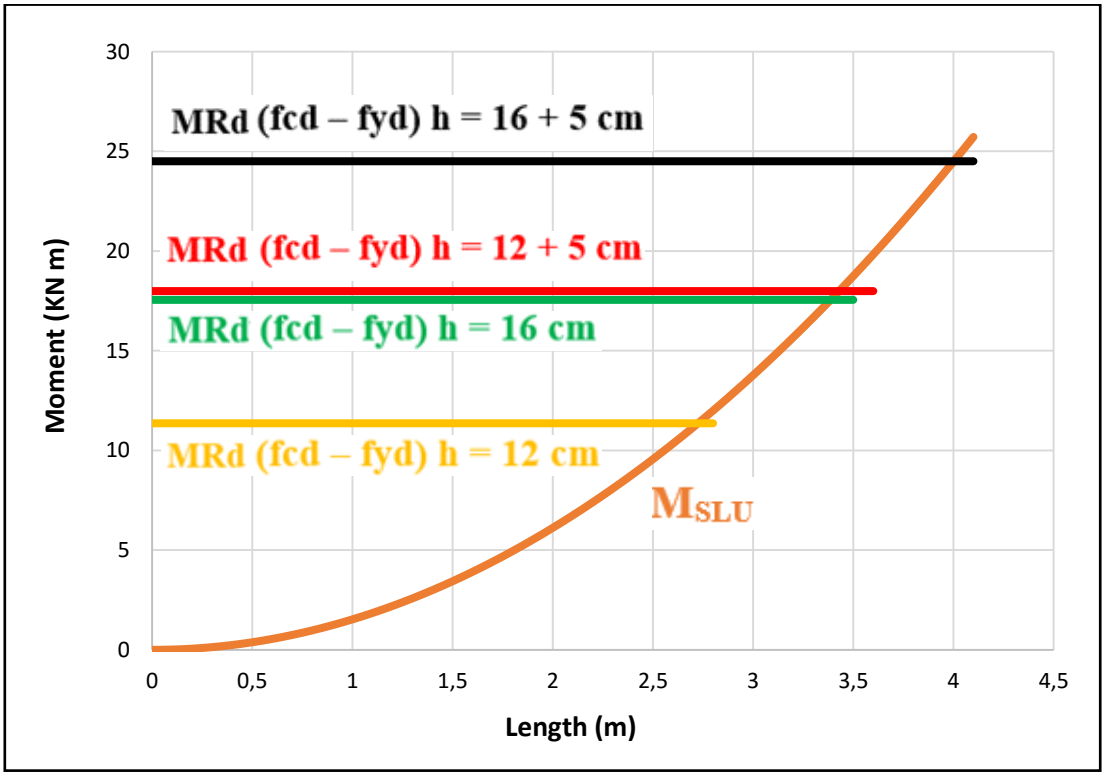

Figure 81. Diagram of SLU moment with respect to the ultimate moment of fcd-fyd of each specimen (Source: Own design)

And finally a comparison with the experimental results obtained from the laboratory is shown for both SLS and ULS, introducing the values of f_{cm} - f_{ym} computed for the My whose values are similar to the Mu:

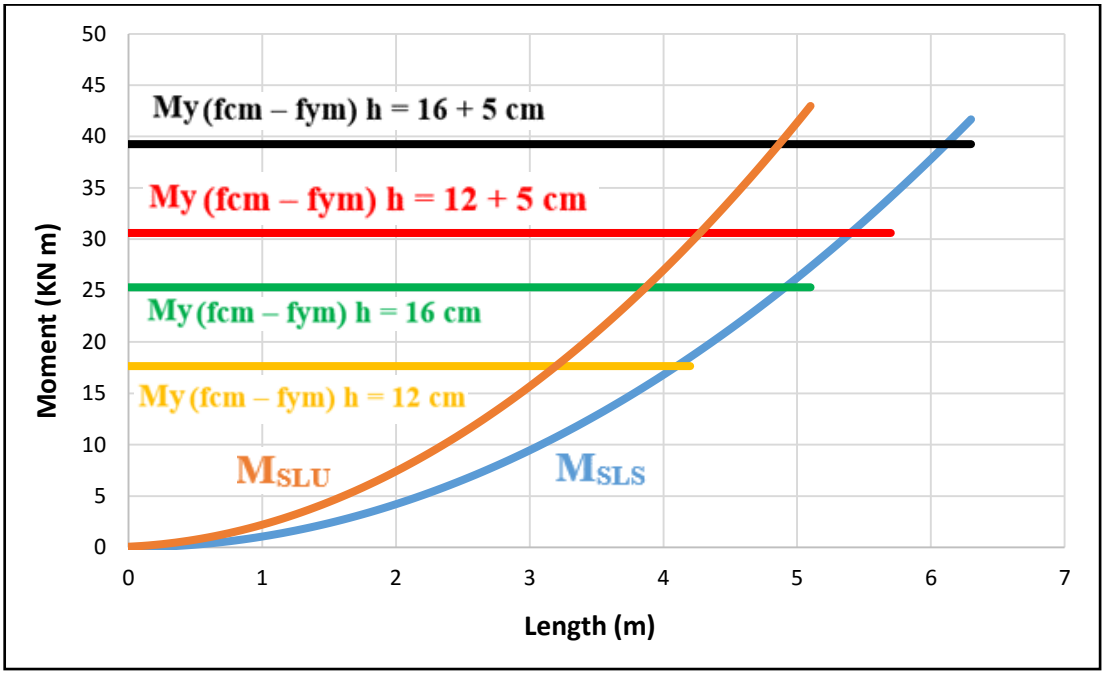

Figure 82. Diagram of SLS and ULS moment with respect to the ultimate moment of fcm-fym of each specimen (Source: Own design)

On the basis of these results, with the hypothesis that the slab must carry the loads described above and with a width of b = 1.2 m, the maximum lenght.

h (cm)	Lmax SLS (fck - fyk)	Lmax SLU (fcd - fyd)	Lmax SLS Lab results	Lmax SLU Lab results
12	3,5 m	2,7 m	4,1 m	3,3 m
16	4,3 m	3,4 m	4,9 m	3,9 m
12 + 5	4,4 m	3,5 m	5,4 m	4,2 m
16 + 5	5,2 m	4,3 m	6,1 m	4,9 m

Table 8. Maximum length provided by the relation SLS / SLU and h (Source: Own design)

APPENDIX A. PHOTO REPORT

Hereafter will be introduced some images of the laboratory test in order to complete the photo report and give a better idea of how the tests were performed:

FLOOR SLAB Nº 1. NON - CONSOLIDATED. H= 12 cm

Figure 83. Disposition of the first specimen of h = 12 cm. (Source: Laboratory image)

FLOOR SLAB Nº 2. NON - CONSOLIDATED. H= 12 cm

Figure 84. Failure of the second specimen of h = 12 cm. (Source: Laboratory image)

Figure 85. Lateral failure of the second specimen of h = 12 cm. (Source: Laboratory image)

Figure 86. Top failure of the second specimen of h = 12 cm. (Source: Laboratory image)

FLOOR SLAB Nº 1. NON - CONSOLIDATED. H= 16 cm

Figure 87. Disposition of the first specimen of h = 16 cm. (Source: Laboratory image)

FLOOR SLAB Nº 2. NON - CONSOLIDATED. H= 16 cm

Figure 88. Failure of the second specimen of h = 16 cm. (Source: Laboratory image)

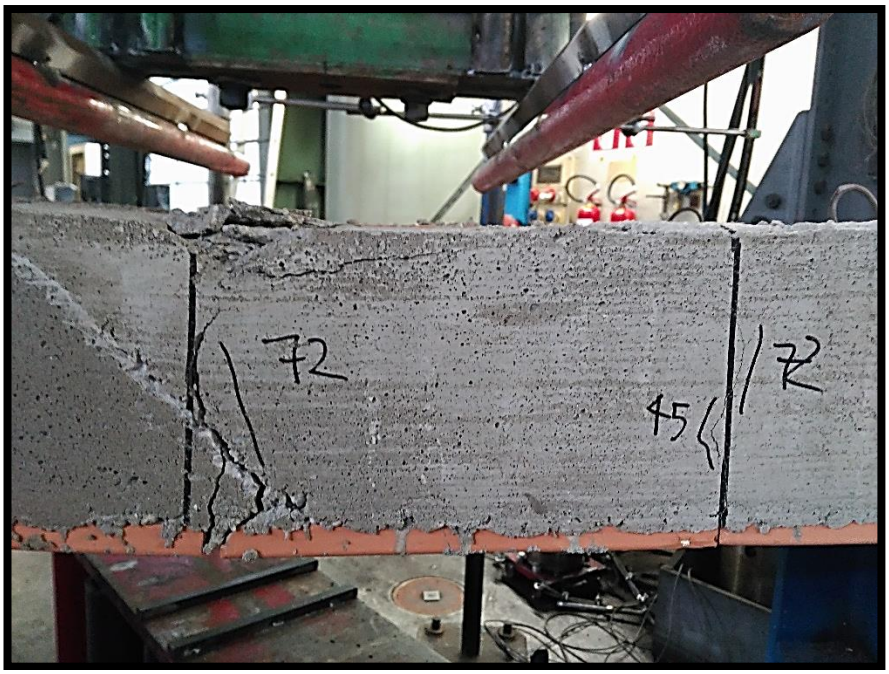

Figure 89. Lateral failure of the second specimen of h = 16 cm. (Source: Laboratory image)

FLOOR SLAB Nº 1. CONSOLIDATED. H= 12 + 5 cm

Figure 90. Disposition of the first specimen of h = 17 cm. (Source: Laboratory image)

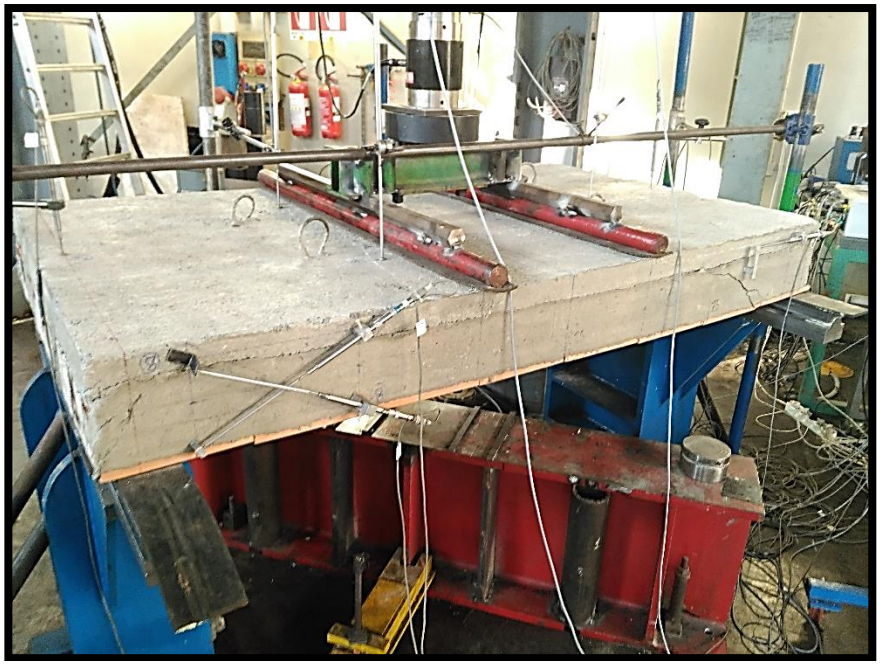

Figure 91. Failure of the first specimen of h = 17 cm. (Source: Laboratory image)

FLOOR SLAB Nº 2. CONSOLIDATED. H= 12 + 5 cm

Figure 92. Disposition of the second specimen of h = 17 cm. (Source: Laboratory image)

FLOOR SLAB Nº 1. CONSOLIDATED. H= 16 + 5 cm

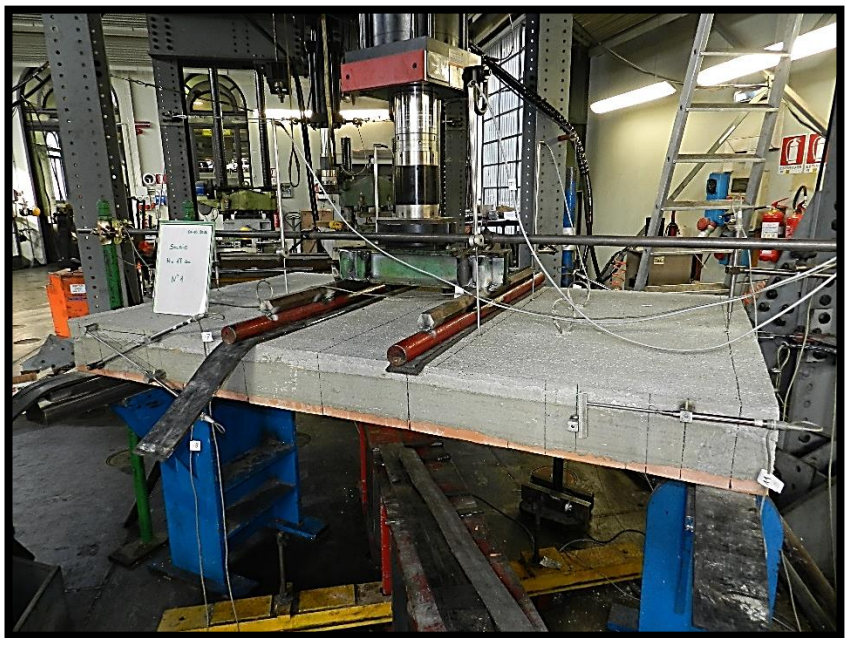

Figure 93. Disposition of the first specimen of h = 21 cm. (Source: Laboratory image)

Figure 94. Failure of the first specimen of h = 21 cm. (Source: Laboratory image)

Figure 95. Bottom failure of the first specimen of h = 12 cm. (Source: Laboratory image)

FLOOR SLAB Nº 2. CONSOLIDATED. H= 16 + 5 cm

Figure 96. Disposition of the second specimen of h = 21 cm. (Source: Laboratory image)

APPENDIX B. 3D SKETCHUP DESIGN

Finally in this last appendix will be presented the 3D design of the tests performed in the laboratory. To do this have been used the program Sketch up which allows to create textures of the materials creating a render similar to the reality.

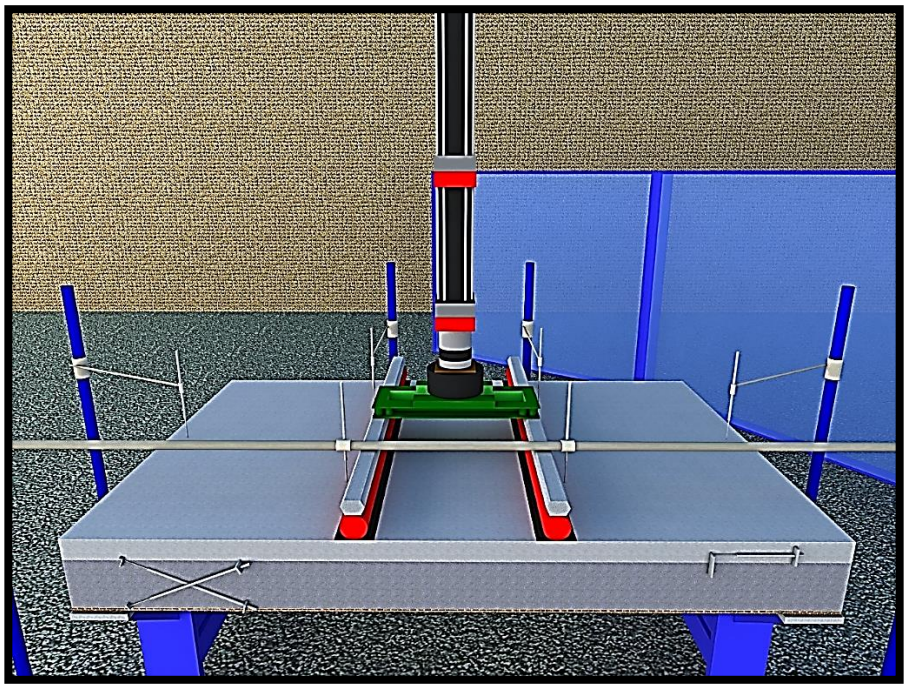

Figure 97. Design of the floor slab frontal view. (Source: Own design)

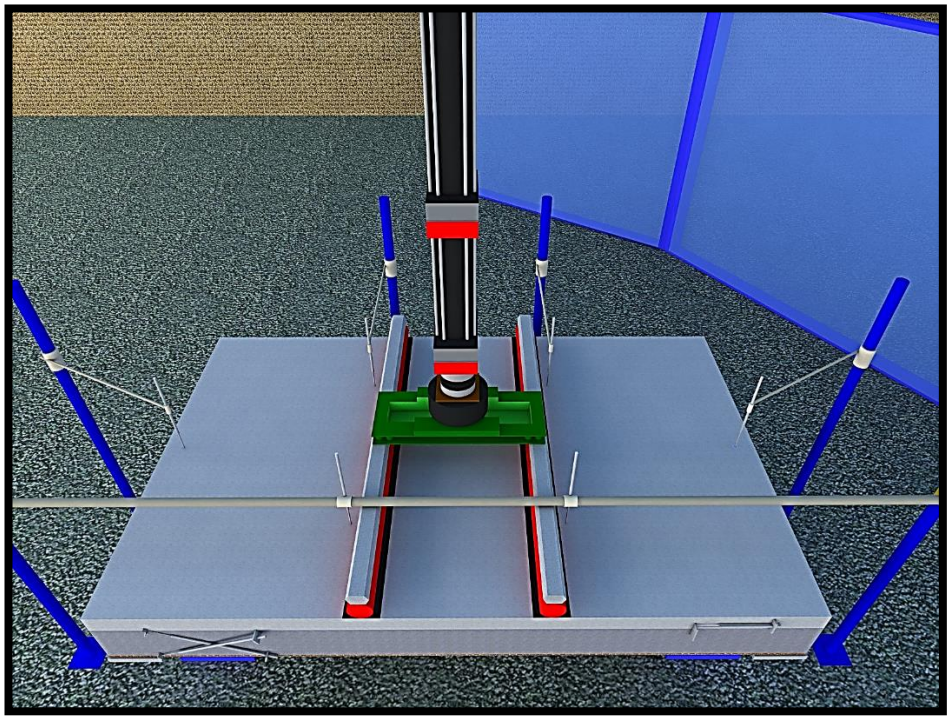

Figure 98. Design of the floor slab top view. (Source: Own design)

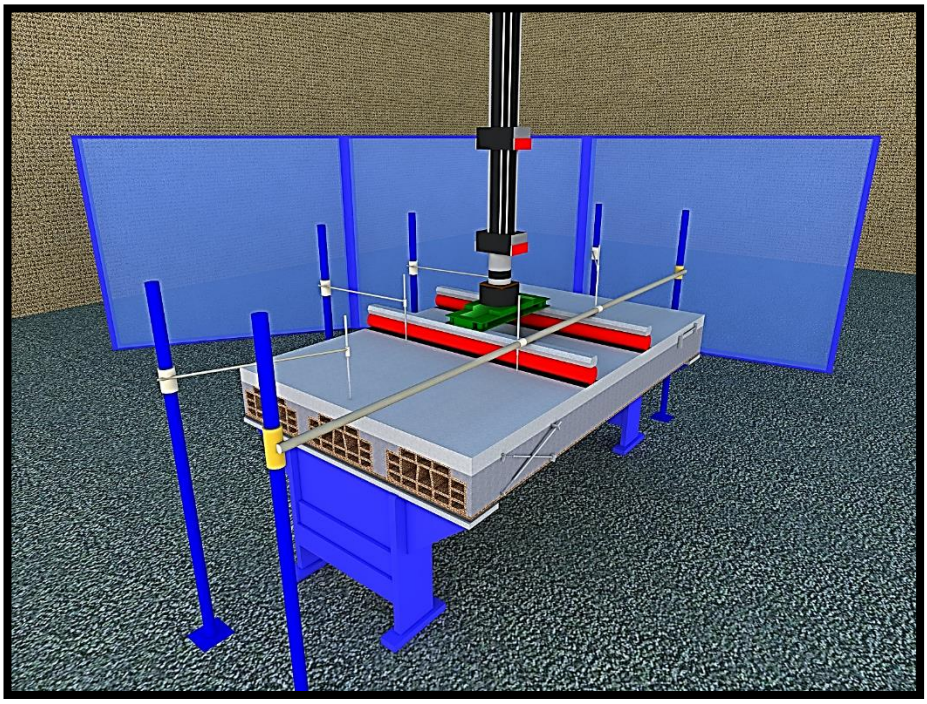

Figure 99. Design of the floor slab lateral view 1. (Source: Own design)

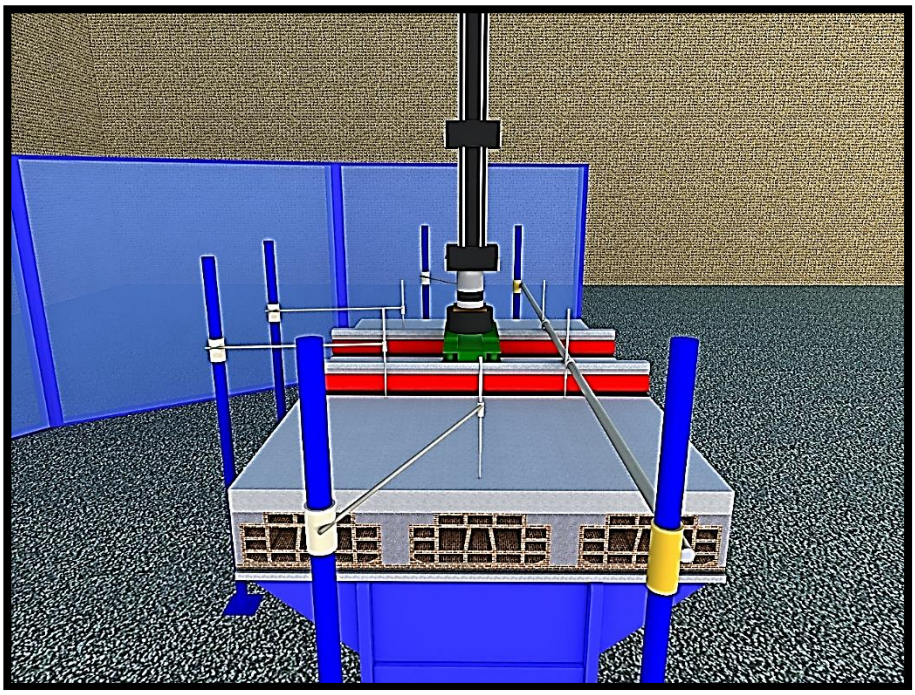

Figure 100. Design of the floor slab lateral view 2. (Source: Own design)

BIBLIOGRAPHY

Leca Laterlite S.p.A. *Consolidamento e rinforzo dei solai, Guida tecnica per il recupero statico e la riqualificazioni dei divisori orizzontali nel patrimonio edilizio esistente* (2015). Milano

Prof. Ing. Liberato Ferrara, Dr. Ing. Patrick Bamonte. *Caratterizzazione del comportamento di resine epossidiche per il consolidamento di solai in latero-cemento*. Milano, Politecnico di Milano

Norma Europea Sperimentale ENV 1992-1-1. *Eurocode 2 – Design of concrete structures.*